CONSTRAINTS ON THE LOW-MASS IMF IN YOUNG SUPER-STAR CLUSTERS IN STARBURST GALAXIES

by

Julia Jennifer Greissl

A Dissertation Submitted to the Faculty of the

DEPARTMENT OF ASTRONOMY

In Partial Fulfillment of the Requirements
For the Degree of

DOCTOR OF PHILOSOPHY

In the Graduate College

THE UNIVERSITY OF ARIZONA

2010

THE UNIVERSITY OF ARIZONA
GRADUATE COLLEGE

As members of the Dissertation Committee, we certify that we have read the dissertation prepared by Julia Jennifer Greissl
entitled Constraints on the Low-Mass IMF in Young Super-Star Clusters in Starburst Galaxies
and recommend that it be accepted as fulfilling the dissertation requirement for the Degree of Doctor of Philosophy.

Date: 8/4/2010
Michael Meyer

Date: 8/4/2010
Marcia Rieke

Date: 8/4/2010
Robert Blum

Date: 8/4/2010
Daniel Eisenstein

Date: 8/4/2010
Yancy Shirley

Final approval and acceptance of this dissertation is contingent upon the candidate's submission of the final copies of the dissertation to the Graduate College.
I hereby certify that I have read this dissertation prepared under my direction and recommend that it be accepted as fulfilling the dissertation requirement.

Date: 8/4/2010
Dissertation Director: Michael Meyer

Date: 8/4/2010
Dissertation Director: Marcia Rieke

STATEMENT BY AUTHOR

This dissertation has been submitted in partial fulfillment of requirements for an advanced degree at the University of Arizona and is deposited in the University Library to be made available to borrowers under rules of the Library.

SIGNED: Julia Jennifer Greissl

ACKNOWLEDGEMENTS

There are many people who deserve acknowledgement for their assistance during my grad school career. I would like to begin by thanking my advisor Michael Meyer. Michael, thank you for putting up with my unorthodox approach to a grad school career. Thanks also for your guidance in framing this project and for encouraging me to stick with it when the going got tough. Thanks to all my collaborators who helped this project and others get off the ground: Morten Andersen, Bruce Wilking, Robert Blum, Micol Christopher, Nick Scoville, Glenn Schneider and anyone else who I might have left out.

Thanks to my committee Robert Blum, Daniel Eistenstein, Marcia Rieke and Yancy Shirley for all the suggestions and encouragement and for not complaining about that early morning thesis defense!

Thanks to all those friends and colleagues at Steward Observatory who kept grad school fun and who were great sounding boards for research related chatter: Wayne, Richard, Moire, Kristian, Eric, Amy and Matt. Also to all the people behind the scenes, who make Steward Observatory run so smoothly but who do not always get the credit they deserve. In particular thanks to Michelle Cournoyer who makes everything work.

To Mandy and Nicole, thanks for innumerable dinners and discussions and games of Mario Kart. Also, thanks for letting me crash on your couches. To all the folks up in Seattle: Ryan, Ralph, Ayeh, Serge, Sandor, Trista, Greg, thanks for taking my mind of Astronomy when it was needed.

To my family for all their unconditional love and support and their encouragement for me to be myself - my father, who told me stories about Archimedes when I was little and who ignited my passion for science, my brother, for his ability to make me smile even when I don't want to, Anneliese, for showing me what inner strength really means, and my grandmother, for being everything a grandma should be and more.

And finally to V, who needs no words.

DEDICATION

To my mother.

Inge Greissl (1946 – 2001)

TABLE OF CONTENTS

TABLE OF CONTENTS – *Continued*

TABLE OF CONTENTS – *Continued*

LIST OF FIGURES

LIST OF FIGURES – *Continued*

LIST OF FIGURES – *Continued*

LIST OF TABLES

ABSTRACT

As evidence for variations in the initial mass function (IMF) in nearby star forming regions remains elusive we are forced to expand our search to more extreme regions of star formation. Starburst galaxies, which contain massive young clusters have in the past been reported to have IMFs different than that characterizing the field star IMF. In this thesis we use high signal-to-noise near-infrared spectra to place constraints on the shape of the IMF in extreme regions of extragalactic star formation and also try to understand the star formation history in these regions. Through high signal-to-noise near-infrared spectra it is possible to directly detect low-mass PMS stars in unresolved young super-star clusters, using absorption features that trace cool stars. Combining Starburst99 and available PMS tracks it is then possible to constrain the IMF in young super-star clusters using a combination of absorption lines each tracing different ranges of stellar masses and comparing observed spectra to models. Our technique can provide a direct test of the universality of the IMF compared to the Milky Way.

We have obtained high signal-to-noise H- and K-band spectra of two young super-star clusters in the starburst galaxies NGC 4039/39 and NGC 253 in order to constrain the low-mass IMF and star formation history in the clusters. The cluster

in NGC 4038/39 shows signs of youth such as thermal radio emission and strong hydrogen emission lines as well as late-type absorption lines indicative of cool stars. The strength and ratio of these absorption lines cannot be reproduced through either late-type pre-main sequence stars or red supergiants alone. We interpret the spectrum as a superposition of two star clusters of different ages over the physical region of 90 pc our spectrum represents. One cluster is young ($\leq$ 3 Myr) and is responsible for part of the late-type absorption features, which are due to PMS stars in the cluster, and the hydrogen emission lines. The second cluster is older (6 Myr - 18 Myr) and is needed to reproduce the overall depth of the late-type absorption features in the spectrum. While the superposition of clusters does not allow us to place stringent constraints on the IMF there is no evidence of a low-mass cutoff in the cluster and the IMF is consistent with a Chabrier and Kroupa IMF typical of the field.

The cluster in NGC 253 shows the same signs of youth as the cluster in NGC 4038/39 and sits in front of a background population of older stars. The background population has an age of $\approx$ 12 Myr and thus contains red supergiants. After carefully subtracting this background we model the spectrum of the young cluster. We find that its IMF is consistent with a Chabrier and Kroupa IMF with a best-fit power-law slope of 1.0 in linear units. Slopes of 0.0 - 1.5 are also formally consistent with the cluster spectrum. We conclude that there is no strong evidence for an unusual IMF or a lack of low-mass stars ($\leq$ 1 $M_{\odot}$) in either of these galaxies.

CHAPTER 1

INTRODUCTION: SUPER-STAR CLUSTERS AND THE IMF IN EXTREME ENVIRONMENTS

1.1 The IMF: Background and Definitions

The Initial Mass Function (IMF) and its origin remain one of the most important problems in Astronomy. Measuring the shape of the IMF allows us to understand the unresolved light from distant galaxies and discerning what physical parameters control its shape helps us understand the process of star formation. Understanding its origin would help us create a predictive theory of star formation if variations with initial conditions exist and if no variations are present any theory of star formation must be able to explain this absence satisfactorily. Since so many fields in Astronomy and Astrophysics deal with aggregate populations of stars it is indeed hard to find a problem which does not require an assumption about the shape of the IMF.

The IMF is generally represented by either a broken power-law or a lognormal form. The power-law can be formally expressed as:

$$\phi(m) = \frac{dN}{dm} \propto m^{-\alpha}$$

where ϕ is the number of single stars in the mass interval m + dm. This power-law IMF is generally measured to have a slope of $\alpha \approx 2.35$ above 0.5 $M_{\odot}$ and flattens out

below 0.5 $M_{\odot}$ to a slope of $\alpha \approx 1.3$ (Salpeter (1955); Kroupa (2001)). For the rest of this document we will refer to any IMF with a single power-law slope of $\alpha = 2.35$ as a "Salpeter IMF" and a broken power-law IMF with the slopes given above as a "Kroupa IMF". Below the hydrogen burning limit (0.08 $M_{\odot}$) the slope of the IMF appears to flatten and may even turn over in linear units (Andersen et al., 2008). These results are well matched by the lognormal IMF given by Chabrier (2003) (see also Miller and Scalo (1979)). In this case:

$$\phi(logm) = \frac{dN}{dlogm} \propto exp(\frac{-(logm - logm_c)^2}{2\sigma^2}), m \leq 0.7 M_{\odot}$$

where m_c is the mean mass ($m_c = 0.22\ M_{\odot}$) and σ is the square root of the variance. Above 0.7 $M_{\odot}$ Chabrier (2003) extends his lognormal IMF into a power-law form with a Salpeter slope. Both forms of the IMF therefore have a characteristic mass at or below 1 $M_{\odot}$. For the power-law IMF this is the IMF breakpoint where the slope flattens, for the lognormal IMF this is where the IMF moves from a power-law Salpeter-like slope to a lognormal representation.

1.2 Theoretical Expectations for the Shape of the IMF

Theoretical models of star formation are generally successful at reproducing the overall shape of the IMF. In particular when many different physical processes are invoked to determine stellar masses a log-normal IMF shape is relatively easy to generate given the central limit theorem (Adams and Fatuzzo, 1996). More recent observational evidence points to the fact that the core mass function (CMF) of star-

less cores which have yet to form into stars is of a very similar functional form as the stellar IMF. The measured CMF has a similar shape as that measured for the IMF but shifted up in mass by a factor of a few. This evidence may indicate that stellar masses are set early in the star formation process, though understanding the fragmentation of cores into binaries and the dependence of this process on mass as well as the resulting companion mass ratio distribution is important to be able to understand how the CMF transforms into the IMF. Goodwin et al. (2008) showed that allowing cores to fragment and dynamically evolve the binary fraction to resemble the current field star population can reproduce the evolution of the CMF into the IMF. The IMF of Chabrier (2003) has a different mean mass depending on whether unresolved binaries are taken into account and corrected for (0.22 vs. 0.79 $M_{\odot}$) so it is important to know whether one is measuring a resolved binary or a system IMF.

And yet most theoretical models predict some dependence of the functional form of the IMF on conditions in the parent cloud. The presence of a characteristic mass of the IMF suggests that there is some fundamental physical process in star formation which results in a characteristic stellar mass of $\leq 1\ M_{\odot}$ (Larson, 2005). In addition to this characteristic mass the minimum mass at which an object can form through gravitational collapse, often associated with the minimum mass for fragmentation as well as a maximum stellar mass are also important values which may yield insights into the process of star formation and may depend on initial conditions. However

there are some theoretical arguments by which an IMF may be constructed that is insensitive to initial conditions. If star formation is completely self regulating, for example through termination of accretion through stellar feedback then one would expect no change in the IMF with initial conditions (Adams and Fatuzzo (1996)).

There are several methodologies which have been suggested as the cause for a characteristic IMF mass such as turbulent star formation (e.g. Mac Low and Klessen (2004)) and magnetic fields (Shu et al., 2004) as well as fragmentation (Larson, 2005). However all of these physical processes have some dependence on external conditions in the cloud such as the thermal Jeans mass ($M_J \propto T^{3/2}/\sqrt{\rho}$) and the magnetic field strengths in star forming regions. If the characteristic stellar mass is indeed connected to the thermal Jeans mass in the star forming cloud it is possible that changes in environmental conditions such as the radiation environment (which could increase the temperatures in star forming molecular clouds and thus increase the Jeans mass) of star forming regions could change overall IMF properties.

Metallicity is a particularly tempting variable in a search for IMF variations since there may be a critical value of the metallicity below which a cluster produces predominantly massive stars (Omukai et al., 2005). The critical value at which this change to a normal IMF occurs remains under debate with estimates ranging from 10^{-2} $Z_\odot$ to values as low as $10^{-5.5}$ $Z_\odot$ (Tumlinson, 2007). Indeed the strongest claim for a non-uniform IMF comes from the earliest stars formed in the universe which are thought to have been extremely massive ($\geq$ 1000 $M_\odot$) (e.g. Abel et al.

(2002)) due to a lack of metals to cool collapsing clouds. The fact that no low-mass Population III stars which should have survived to the present day have been discovered strengthens this argument.

1.3 IMF Measurements in the Milky Way and Nearby Galaxies

Beyond measurements of the overall shape of the IMF in the field, such as those given Section 1.1, the main focus of observational IMF studies is to understand whether changes in the environmental conditions of star formation cause the shape of the IMF to vary. For this purpose, extensive efforts have been undertaken to search for such variations (e.g. Hillenbrand (1997); Carpenter et al. (1997); Luhman et al. (1998)), in particular on the low-mass end where nearby star forming regions are well populated enough that stochastic effects due low number counts are minimized. Studies of young star clusters have shown the IMF above 0.1 $M_{\odot}$ to be universal within 1 kpc (Meyer et al., 2000). These results have come mostly through extinction limited surveys of nearby open clusters as well as nearby young star clusters and associations. In these clusters objects can be surveyed to below the hydrogen burning, with stellar masses determined either spectroscopically or photometrically in conjunction with theoretical models, from which an IMF can then be generated.

Below the hydrogen burning limit the picture is less clear. In the past there have been some claims of IMF variations in particular in the Taurus molecular

cloud (Briceño et al., 2002). More complete results indicate that the deficiency in brown dwarfs in Taurus compared to clusters such as the Orion Nebula are not as strong as previously reported (Luhman et al. (2009); Rebull et al. (2010)), but the discrepancy appears to remain statistically significant. The Orion Nebula which is often used as a template for nearby star forming regions has an IMF which is consistent with the field down below the hydrogen burning limit. There have been similar reports of IMFs which are inconsistent with a normal Chabrier IMF in older open clusters. However the best studied open cluster, the Pleiades, has an IMF consistent with the field star IMF down to 30 M_{Jup} (Moraux et al., 2003). Indeed most measurements of discrepancies in the IMF slope are plagued by small sample statistics in particular at high stellar masses and in the brown dwarf regime.

In more extreme regions of star formation in the Milky Way such as the Galactic Center, NGC 3603 or Westerlund 1 it is currently impossible to get a direct census of objects below the IMF breakpoint and IMF measurements have mostly been confined to above 1 $M_{\odot}$. Much focus has been on measuring the IMF slope above 1 $M_{\odot}$ in these regions, in particular those close to the Galactic center. The Arches cluster which is located at a projected distance of ≈ 25 pc from the Galactic center had in the past been measured to have an IMF slope significantly flatter than a Salpeter slope of $\alpha = 2.35$ (Figer et al., 1999). However more complete samples have corrected this value to be consistent with a Salpeter IMF (e.g. (Espinoza et al., 2009)). In objects close to galactic nuclei mass segregation may play an important role even

at young ages as clusters are subject to strong dynamical effects ((Bastian et al., 2010)). Westerlund I, the most massive young cluster in the Milky Way discovered to date, appears to have an IMF consistent with a Salpeter IMF (Brandner et al., 2008), while NGC 3603 has been measured to have a logarithmic IMF slope of $\Gamma = 0.9 \pm 0.15$ ($\Gamma = \alpha$ -1) marginally consistent with a Salpeter slope of $\Gamma = 1.35$. Intriguingly all of the clusters mentioned above show evidence of mass segregation, which if primordial rather than due to dynamical evolution would be evidence of IMF variations over small spatial scales.

Beyond the Milky Way the best studied star forming region is 30 Doradus with its massive young central region of R 136 in the Large Magellanic Cloud. This cluster is of particular interest because of its mass ($\approx 2.2 \times 10^4$ $M_\odot$ within a 4.7 pc radius (Hunter et al., 1995)) and low metallicity ($\leq 1/2$ solar) (Smith, 1999). Results by Sirianni et al. (2000) using optical imaging data had previously suggested that the IMF above 2 $M_\odot$ was flatter than a Salpeter slope. However again updated results by Andersen et al. (2009) find that the IMF down to 1 $M_\odot$ can be matched by a Salpeter slope, though a caveat to take into consideration here is that the regions studied do not overlap.

1.4 The IMF in Extreme Regions of Star Formation: Starbursts and Super-Star Clusters

1.4.1 Super-Star Clusters

The advent of the Hubble Space Telescope (HST) as well as more recently adaptive optics observations from the ground have made it possible to study in detail nearby starburst galaxies with star-formation rates orders of magnitude higher than the Milky Way (e.g. M82, Henize 2-10, NGC 5253). The HST was the first observatory to provide the kind of resolution needed to study individual star clusters in distant galaxies. Prior to this only a small number of studies of star clusters systems in other galaxies had been undertaken.

Many starburst galaxies are now known to host massive (10^5 - 10^6 $M_\odot$) young super-star clusters (SSC). The discovery of regions of star formation with masses similar to those of observed globular clusters has changed our understanding of the process of star cluster formation as a whole. SSC are seen as likely progenitors to globular clusters and have extended our view of star formation to an extreme regime of densities (perhaps up to 10^5 $M_\odot/\mathrm{pc}^3$ in cluster cores (Portegies Zwart et al., 2010)) an order of magnitude larger than more quiescent star forming regions in the Milky Way (Bastian et al., 2010).

Though SSC were first observed in starburst galaxies, massive star clusters appear to be present in many different classes of galaxies from spirals to dwarf galaxies.

However, the number and maximum cluster mass seem to be related directly to the star formation rate (SFR) in a galaxy (Larsen, 2002) with maximum cluster masses reaching up to a few 10^7 $M_\odot$ (McCrady, 2005) while the cluster mass function is thought to peak at around 10^5 $M_\odot$. Mergers such as the Antennae (Whitmore et al., 1999) and NGC 3256 (Zepf et al., 1999) host a particularly large population of SSC of a wide range of ages. These young massive clusters often dominate the ultra-violet and near-infrared emission of their host galaxies. Thus understanding their properties is necessary for any analysis of the light of unresolved distant galaxies.

Though we refer to young SSC as clusters in this work it is not clear that the objects we refer to are actually bound. Young SSC have a high "infant mortality" (Fall, 2006) of upwards of 50 % and many are disrupted within the first 10 Myr of their lifespan. Through this process SSC feed the field star population of their host galaxies. Studies of M51 (Bastian et al., 2005) and NGC 4038/39 (Bastian et al., 2005) have shown that more than 70% of young SSC may be disrupted after an age of 10 Myr. For the sake of this thesis we will continue to refer to the objects we study as clusters with no implication that they are gravitationally bound. Despite this high mortality rate of SSC, massive star clusters of ages of several hundred Myr exist which are bound.

1.4.2 The Importance of Super-Star Clusters to our Understanding of Star Formation

SSC play an important role in the star forming process of many galaxies. Because they are so massive even one SSC produces as much stellar material as a hundred Orion Nebula Clusters. In merging systems which are forming many SSC at the same time, they dominate the current star forming process. SSC represent an extreme form of star formation which cannot be studied in the Milky Way with perhaps the exception of the Arches cluster near the Galactic center or the young massive cluster Westerlund 1. The closest analogue is R136 in the star forming region 30 Doradus in the LMC with a mass of $10^{4.5}$ $M_{\odot}$ (Massey and Hunter, 1998) and an age of ≈ 3 Myr (Andersen et al., 2009). SSC often form in the intense radiation environment of nuclear starbursts and interacting galaxies. Because they are so massive they can be studied out to great distances allowing us to explore star formation environments radically different than that observed locally, such as the low-metallicity starburst SBS 0335-052 ($Z=Z_{\odot}/40$ (Izotov et al., 1990)) which hosts several SSC which have been studied in great detail (see for example: Hunt et al. (2001); Thompson et al. (2006)). In addition because of their great mass they influence a large region of surrounding space through photoionization, supernovae and stellar winds (Gallagher and Smith, 2004).

It is unclear whether SSC follow a single formation mechanism. It has been proposed by Gallagher and Smith (2004) that SSC can form through two differ-

ent mechanisms in quiescent spiral galaxies and more active mergers and dwarf starbursts. They argue that different processes, such as high ISM pressures and interaction between star forming regions, become important in starbursts which are not seen in the giant HII regions of spiral galaxies. However there is also evidence that SSC in all environments can be modeled with a single cluster mass function as long as the star formation history of the host galaxy is well understood (Bastian, 2008), which supports a single formation mechanism. Dwarf galaxies which are often quoted as having exceptional cluster mass functions are then special cases because star formation histories in these galaxies proceeds in a highly bursty manner. This would imply that star formation in mergers and starbursts functions in the same manner as more quiescent regions and only the level of scale is different.

1.4.3 The Connection between Super-Star Clusters and Globular Clusters

SSC clusters are thought to mirror a mode of star-formation that was ubiquitous in the early universe (Leitherer, 2001) as evidenced by the fact that star formation rates of galaxies at high redshift are very similar to those in local starbursts (Steidel et al., 1996). The large number of old globular clusters we observe in the Galaxy, which resemble SSC in their masses and radii (Zhang et al., 2001) provide additional support that the formation of massive star clusters was common in the early universe. Thus, studying local SSC can provide insight into star formation at high redshift. If SSC are indeed the present-day equivalent of globular clusters then

their high infant mortality must mean that such massive star forming regions must have formed with a high frequency in the early Universe (Johnson, 2005), given the abundance of globular clusters in the Galaxy as well as nearby galaxies such as M51.

Globular clusters have been observed in many galaxies outside the Milky Way and are generally more common in massive elliptical galaxies than spiral galaxies. Elliptical galaxies often host a globular cluster population which is bi-modal in color, a metal-poor blue population and a more metal-rich red population. This is often explained as due to the build up of the galaxy through a violent merger process which formed the red population and the blue population as being due to a primordial population. This supports the theory of SSC as proto-globular clusters, since mergers produce a particularly large number of SSC.

The challenge remains to explain the discrepancy between the luminosity and mass functions of young clusters, which are power laws, and old globular clusters, which follow lognormal distributions (Harris, 1991), though it may be possible to explain this evolution theoretically ((Fall and Zhang, 2001); (Baumgardt et al., 2008); (Vesperini and Zepf, 2003)). Methods invoked to evolve the mass function involve either dynamical evolution, gas expulsion or stellar mass loss all of which lead to preferential disruption of low-mass clusters. If the SSC we see today are indeed precursors to an eventual globular cluster population studying the properties of SSC clusters will help us understand formation mechanisms as well as globular cluster evolution and ultimately the star formation history of the Universe.

In addition to old GC systems many galaxies are also known to host an albeit much smaller population of intermediate age GC systems (ages $\leq$ 6 Gyr). The LMC for example has a significant population of clusters at an age of 3 Gyr, though a lack of clusters between 4 - 12 Gyr, and the SMC contains a similar though somewhat older population. The GC populations of both galaxies seem to indicate a bursty star formation history (Brodie and Strader, 2006). NGC 1316, an intermediate age merger remnant contains the best studied intermediate age GC population to date (Goudfrooij et al., 2007). These clusters have a power law luminosity function as opposed to the lognormal distributions of older GC systems. The presence of this system gives credence to the creation of large GC populations in galaxy mergers and may give further support to the evidence that the red population of GCs formed in major mergers.

In light of the high infant mortality for young SSCs mentioned above and the presence of large populations of GCs formed in older starburst events in galaxies the question remains what influence young massive star clusters have on the field star populations of their host galaxies. If a significant fraction of SSC are disrupted at an early age and if this was a dominant phase of star formation in the early universe we could expect metal-poor field star populations of galaxies to have received a significant infusion from dissipating massive star clusters. If the mass function of these primordial SSC was a similar power-law to the one we observe today, clusters smaller than 10^5 $M_\odot$ contain a roughly equal amount of stellar mass as those more

massive than 10^5 $M_\odot$. If we assume that this power-law then evolved into the lognormal function we observe today, meaning that smaller clusters get disrupted preferentially, clusters less massive than 10^5 $M_\odot$ actually contributed more mass to the field than massive young SSC and the same may be true today.

1.4.4 Search for IMF Variations in Starburst Galaxies and Super-Star Clusters

As compelling evidence for IMF variations in the Milky Way and neighboring galaxies remains elusive we are forced to expand the search for IMF variations to more extreme regions of star formation. Super-star clusters represent ideal objects to search for IMF variations with initial conditions such as metallicity and formation environment.

Massive young clusters have been of particular interest in the search for IMF variations. Since individual objects cannot be probed in SSC and starburst galaxies historically IMF measurements have relied on integrated properties of these clusters or galaxies. Particular focus has been on the prototypical starburst galaxy M82. Rieke et al. (1993) modeled numerous properties affected by the shape of the IMF in M82, such as K-band luminosity and UV fluxes. They found that to match observed quantities they required M82 to have fewer low-mass stars than predicted by a Miller and Scalo (1979) IMF. It is important to point out that this Miller and Scalo (1979) IMF produces an overabundance of low-mass stars compared the a Chabrier (2003) IMF and the best-fit IMF derived is actually more similar to a

Chabrier (2003) or Kroupa (2001) IMF integrated over the whole stellar mass range, though still slightly overabundant in high-mass stars. Similar results were reported by Engelbracht et al. (1998) for NGC 253 and Alonso-Herrero et al. (2001) for NGC 1614. However Satyapal et al. (1997) found that M82 was fainter than previously assumed bringing measurements in line with a Kroupa or Chabrier IMF.

It is possible to measure mass-to-light ratios directly for SSC with ages $\leq$ 40 Myr and many clusters have been found to have anomalous mass-to-light ratios compared to those expected for a Kroupa/Chabrier IMF (e.g. NGC 1705-1 (Smith and Gallagher, 2001), NGC 1569-B (Anders et al., 2004b)), at a given age. This has often been interpreted as variations in the mass function. The dynamical mass measurements required to construct mass-to-light ratios assume that clusters are in virial equilibrium however. Goodwin and Bastian (2006) have shown that this assumption can be faulty in young clusters due to the effects of gas expulsion. Support for this theory is provided by the fact that the mass-to-light ratio variations disappear for clusters with ages of a few hundred Myr. Thus assuming virial equilibrium could cause the mass of the cluster to be overestimated which leads to an estimate for a mass function overabundant in low-mass stars in contrast to IMF measurements overabundant in high-mass stars in starbursts as described in the previous paragraph. The mass-to-light ratio of M82-F however, a massive cluster in the prototypical starburst M82 with an age of 40-60 Myr, remains inconsistent with a Kroupa (2001) IMF (McCrady et al., 2005) and M82-F remains the best candidate

for an unusual IMF in a SSC.

Both cluster mass-to-light ratios and especially models of whole starburst galaxies are at best an indirect way to determine the IMF because the entire mass range of the IMF is treated as one mass bin. A more direct method of detecting stellar populations in unresolved SSC is needed to provide confirmation of the shape of their IMF.

1.5 Targets in this Study

This thesis focuses on a method to constrain the low-mass stellar content in young SSC using late-type absorption features in the near-infrared, explained in detail in Chapter 2. Young clusters are not easily studied at optical wavelengths as they suffer high amounts of extinction. Thus infrared studies are ideal to survey the low-mass stellar population of the very youngest objects. These clusters are usually unresolved even with the highest resolution available today, and broadband photometry can only provide limited information. High signal-to-noise integrated spectra can be an important tool in understanding the populations of unresolved star clusters.

This study focuses in particular on SSC in two targets: NGC 4038/39, "the Antennae" and NGC 253 a spiral galaxy with a nuclear starburst. These targets were chosen from a larger sample of starburst galaxies where young super-star cluster populations exist and which are close enough that study of individual clusters is possible. We chose to focus on these two targets because they both represent

extremes in some way. The Antennae is the nearest major merger and as such contains a large population of very massive clusters. It is also perhaps the best-studied merger system which means that a wealth of literature exists. NGC 253 on the other hand is nearby starburst galaxy with an extremely active starburst region in its nucleus. Its proximity makes is considerably easier to study individual clusters in detail than in the Antennae. The proximity of the star clusters in NGC 253 to its nucleus allows for interesting parallels between clusters in the Milky Way which are close to the center of the Galaxy and the corresponding SSC in NGC 253. Since the central Galactic clusters remain a source of intense study of star formation properties under extreme radiation and dynamical environments, NGC 253 provides an interesting contrast. The targets and their cluster populations are describe in more detail in Chapters 3 and 4.

1.6 Thesis Outline

This thesis is organized as follows. Chapter 2 focuses on the modeling of young integrated pre-main sequence SSC in the near-infrared. We detail the combination of Starburst99 for main sequence and post-main sequence evolution in combination with appropriate pre-main sequence tracks and stellar libraries. In addition to the modeling we present results of an analysis of two massive young clusters in the starbursts NGC 4038/39 (the Antennae) and NGC 253. Chapter 3 describes in detail the observations, reductions and analysis of one massive star cluster in the Antennae,

while Chapter 4 describes observations, reduction and analysis of a massive SSC in NGC 253. In Chapter 5 we summarize our results and discuss the implications for IMF measurements and star formation histories of young SSC. We also discuss future avenues of study.

CHAPTER 2

POPULATION SYNTHESIS MODELS OF YOUNG SUPER-STAR CLUSTERS IN THE NEAR-INFRARED

In recent years it has become possible to study the properties of individual unresolved star clusters in distant galaxies. Since we will never resolve all but the clusters in the closest galaxies into their individual stellar members it is critical to be able to understand their aggregate properties. For this purpose population synthesis models which simulate whole star clusters or galaxies over a variety of ages have been created. These models can cover a wide range of physical parameters which makes it possible to compare and contrast the models to real datasets and to infer the underlying properties of the stellar population, such as mass, age and metallicity.

While population synthesis models of star clusters at optical and ultraviolet wavelengths have reached a high degree of sophistication (e.g. Bruzual and Charlot (2003); Leitherer et al. (1999)) less focus has been placed on modeling SSC spectra in the near-infrared accurately. With the upcoming launch of JWST however it is critical that we understand the predictive possibilities and limitations near-infrared population synthesis can offer for the study of extragalactic massive star clusters. Lançon et al. (2008) used near-infrared population synthesis models to attempt to place age constraints on massive young star clusters in M82 dominated by red su-

pergiant populations older than 6 Myr, to compare and contrast results with those obtained by optical studies. They found that while they were able to reproduce the observed spectra well with their models, assumptions required in various evolutionary tracks could have a large effect on their age determinations.

In this work we focus on modeling clusters younger than 6 Myr with the dual goals of exploring the star formation history of the clusters and constraining the low-mass IMF in the clusters directly. The near-infrared flux of star clusters is dominated by red supergiants after $\approx$ 6 Myr and up to 100 Myr. In clusters younger than 6 Myr however, no red supergiants exist and near-infrared emission is dominated by a broad stellar mass range.

We model the spectra of young super-star clusters in the near-infrared incorporating the fact that at an age of $\leq$ 6 Myr stars less massive than $\approx$ 4 $M_{\odot}$ are still on the PMS. For objects on the PMS we use our own synthesis code combined with a set of PMS tracks (Siess et al., 2000) which is described in detail in this chapter. For any objects not on the PMS we use the STARBURST99 (S99) population synthesis models (Leitherer et al., 1999) which are designed to accurately reproduce spectrophotometric properties of starbursts and SSC but do not incorporate any PMS models. In addition to modeling the stellar component of cluster emission we also place constraints on the nebular emisssion from hot stars in the cluster which can contribute a significant portion of the total cluster flux at young ages.

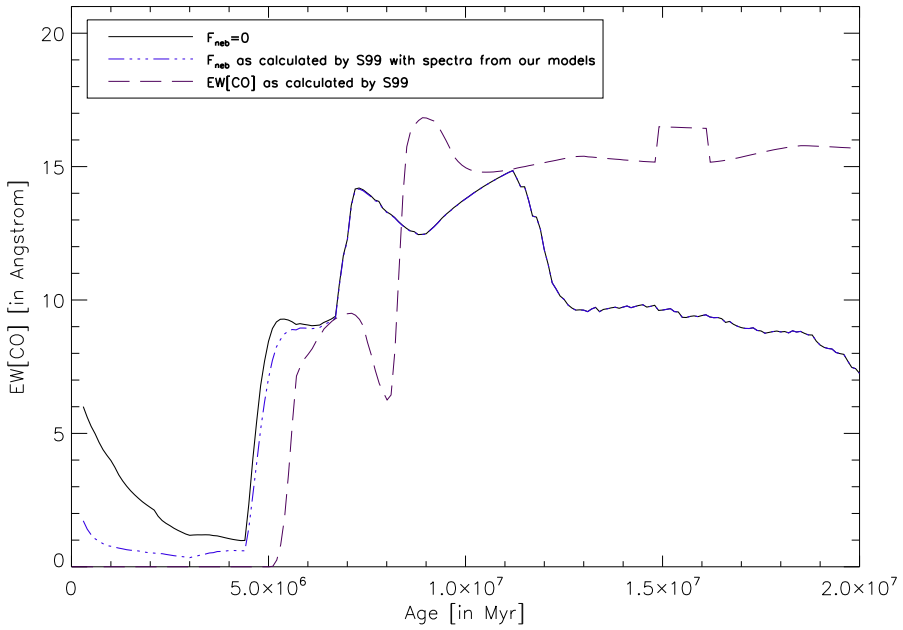

Figure 2.1 Plot of CO(2-0) equivalent width with age. The equivalent width is calculated according to the absorption and continuum bands given by Kleinmann and Hall (1986). Plotted are two models including PMS evolution and one model excluding the PMS taken from Starburst99. The model with PMS evolution with more attenuated CO bandheads includes nebular flux estimated by Starburst99, the second model has no nebular flux added. Past the age of 6 Myr red supergiants dominate the CO absorption line. In our models we have taken the number of supergiants from the results given by Starburst99. We then generate model spectra and calculate the equivalent width. The Starburst99 models generate an output of near-infrared equivalent widths independently from the output of the number of stars. This explains the differences between the equivalent width evolution of the CO(2-0) equivalent width in the plots after 6 Myr.

2.1 Stellar Component

2.1.1 Combining PMS Models and Starburst99

Starburst99 is a population synthesis code developed by Leitherer et al. (1999) to accurately predict properties of starburst galaxies over a large wavelength and age range. It is widely used to model SSC properties in the optical and ultraviolet (e.g. Tremonti et al. (2001)). S99 uses the Geneva (Schaller et al. (1992); Schaerer et al. (1993a); Schaerer et al. (1993b); Charbonnel et al. (1993); Meynet et al. (1994)) and Padova (Fagotto et al. (1994a); Fagotto et al. (1994b); Bressan et al. (1993); Girardi et al. (2000)) evolutionary models with model atmospheres by Lejeune et al. (1997,1998). The code allows for instantaneous star formation as well as a non-instantaneous, continuous burst of star formation at a range of input metallicities from 5% solar to twice solar. It also allows for multi-part power law IMFs with the preset value set to a Kroupa (2001) IMF. Cluster models can be generated with ages ranging from ≤ 1 Myr and up to 1 Gyr. S99 generates a large number of outputs for the user. Among these are the number of stars of each spectral class and type as well as a low-resolution spectrum over a large wavelength range. It is these output files in particular which we use to generate our models.

Though S99 does not have a dedicated near-infrared spectral library it does output several equivalent width measurements in the near-infrared. Most important for us among these are the two CO bandheads at 1.62 and 2.29 μm and the $Br\gamma$

emission line at 2.16 μm. Fig. 2.1 shows the evolution of the CO(2-0) 2.29 μm bandhead for S99 alone and overplotted the CO evolution including our PMS-enhanced models, described in detail in following sections, with varying input parameters. Since S99 does not take into account any PMS evolution no CO bandhead is visible in S99 models prior to 6 Myr when the first red supergiants appear. Our model CO equivalent widths due to PMS stars are strongest at the youngest ages and then decrease (though the overall equivalent width is still less than the maximum equivalent width due to supergiants by 65 %).

S99 is not optimized for very young clusters and therefore does not include PMS tracks. However for young ages low-mass stars on the PMS can contribute a significant portion of the near-infrared light. Fig. 2.2 shows the contribution of the PMS flux contribution for a 10^6 $M_\odot$ cluster in the H and K-band as a function of age. For a 1 Myr cluster, half the K-band light is generated by stars still on the PMS (for a Kroupa IMF). Therefore to model SSC spectra in the near-infrared accurately one needs to incorporate PMS tracks.

To more accurately treat these important effects we need PMS evolutionary models vs. mass and age as well as a near-infrared spectral library which includes dwarf, giant and supergiant spectra. We use the PMS models of Siess et al. (2000) to estimate PMS luminosity and evolution for young SSC. These models are available over a mass range of 0.1 - 7 $M_\odot$, ages of $\leq 10^5$ yr - a few times 10^9 yr, and for metallicities between 0.5 - 3 x solar. Hillenbrand and White (2004) report generally

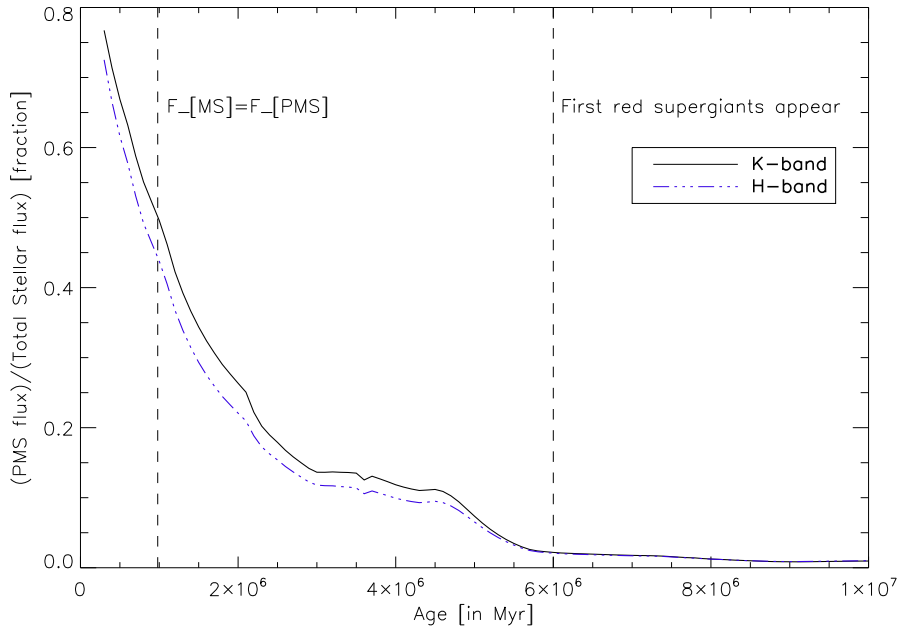

Figure 2.2 Plot of PMS flux percentage in a 10^6 $M_\odot$ cluster in the H- and K-band. The PMS flux decreases as the cluster ages both due to the fact that more massive stars evolve onto the main sequence as well as due to the fact that the low-mass stars are dimming as they contract over time.

reasonable agreement between these models and dynamically determined PMS star masses. However the Siess et al. (2000) models as well as most of the models tested underpredict stellar masses at the low-mass end of the models. The Siess et al. (2000) models cover a greater mass range than other PMS models which is beneficial for our needs since we are modeling a whole cluster simultaneously. These models are also available on a web server at: http://www-astro.ulb.ac.be/ siess/prog.html.

2.1.2 Spectral Library

There are now a wide array of spectral libraries available in the literature (e.g. Lançon and Wood (2000); Ivanov et al. (2004); also see Ivanov et al. (2004) for a more complete list) which cover a large range of spectral types and resolutions in the 1.0 - 2.5 μm region. We use the spectral libraries of Wallace and Hinkle (1997) in the K-band and Meyer et al. (1998) in the H-band since both cover a large range of spectral types at a relatively high resolution (R=3000). Both were obtained at the KPNO 4m telescope using the FTS dual-output interferometer. We also have a similar J-band library (Wallace et al., 2000) but have not done extensive work to incorporate it into our models. Both spectral libraries span a large range of spectral types (O-M) and both incorporate a range of luminosity classes from class V dwarfs all the way to class I supergiants. However they contain no pre-main sequence spectra. Fig. 2.3 shows a sample of the normalized H- and K-band spectra incorporated into our models with pertinent spectral features marked. Since the

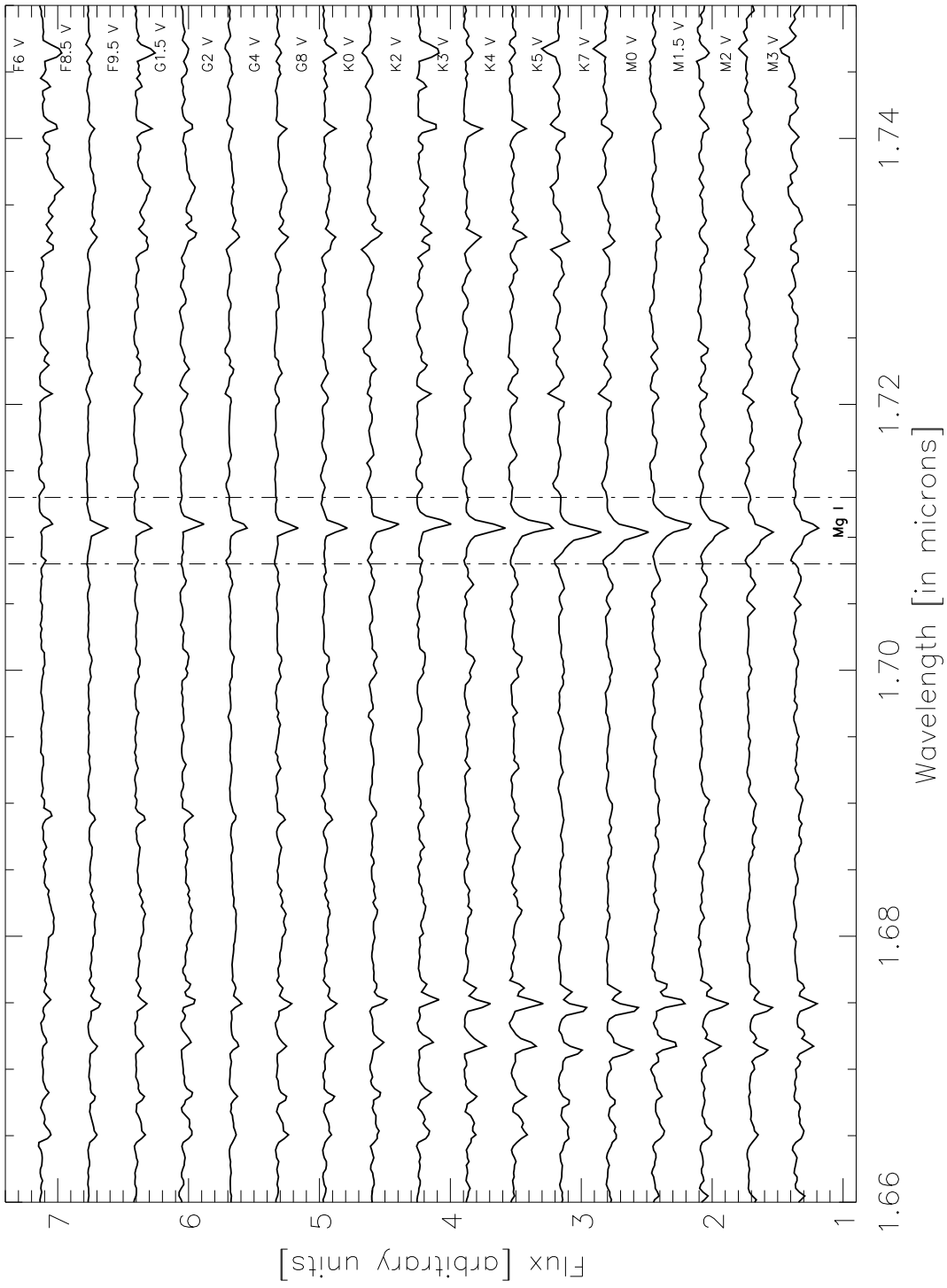
F6 V
F8.5 V
F9.5 V
G1.5 V
G2 V
G4 V
G8 V
K0 V
K2 V
K3 V
K4 V
K5 V
K7 V
M0 V
M1.5 V
M2 V
M3 V
Mg I
Flux [arbitrary units]
Wavelength [in microns]
1.66
1.68
1.70
1.72
1.74
1
2
3
4
5
6
7

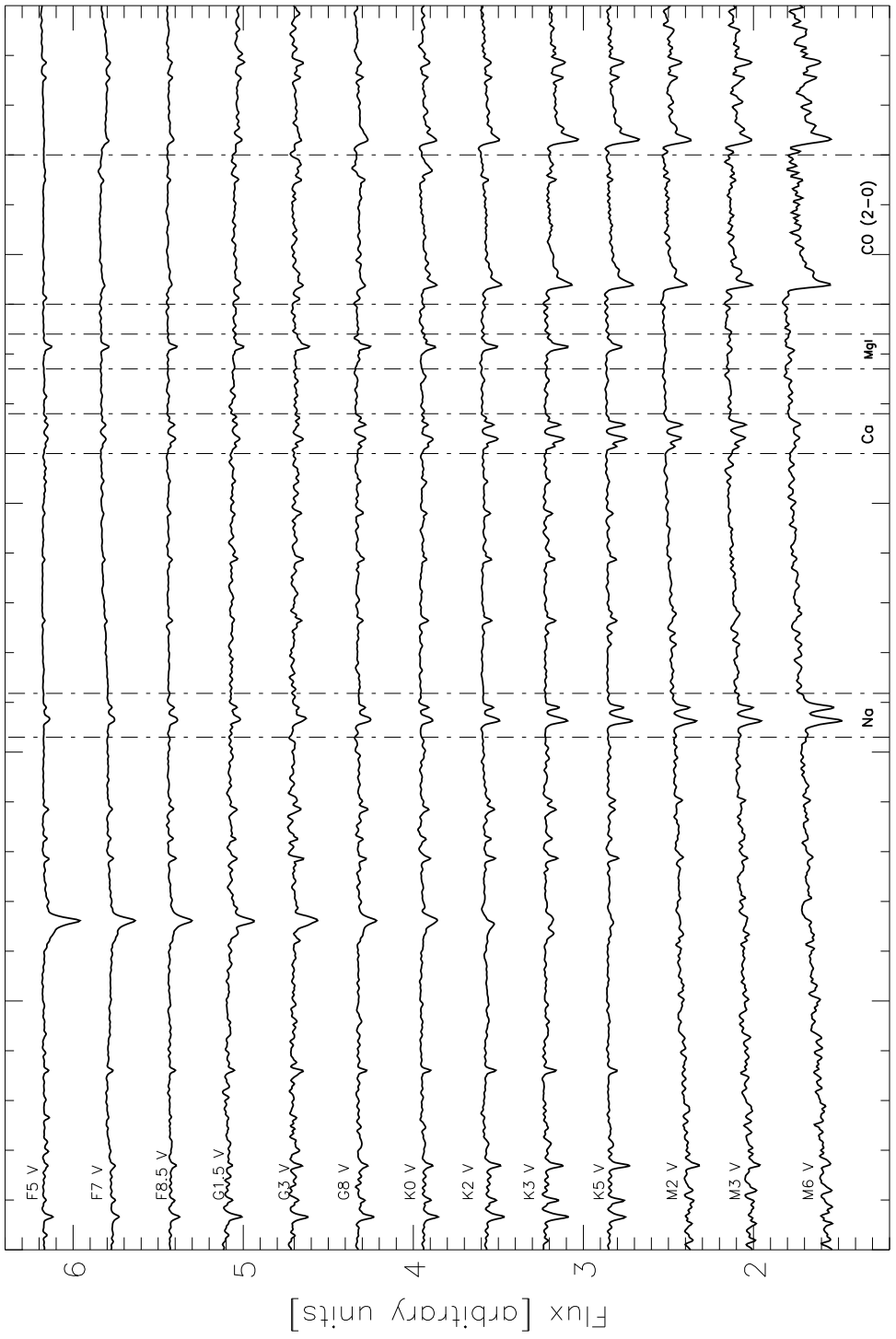

Figure 2.3 Sample of H-band and K-band stellar library. Spectral lines used in our analysis are marked.

spectral libraries contain normalized spectra we cannot reproduce the SED of the low-mass stars in the near-infrared and we thus focus our analysis on narrowband absorption lines in the spectra as opposed to Lançon et al. (2008) who focus on the overall SED of SSC spectra over the J-, H- and K-band. When more than one star of a given spectral type was available the average of these stars was incorporated into the model.

2.2 Nebular Emission

In addition to stellar light, the near-infrared spectrum also contains nebular emission due to ionizing radiation emitted by the massive stars present in high-mass clusters. S99 predicts that at very young ages up to 90 % of the near-infrared luminosity of young SSC should be emitted in free-free and free-bound emission. However for actual observations, the nebular component can also be constrained directly through thermal radio data. A large number of extragalactic clusters have been observed in the radio and it is possible to distinguish between young clusters which contain only nebular emission and other types of radio sources such as supernova remnants by the spectral index of the source. Young SSC typically have radio sources with a spectral index $\alpha \geq 0$, meaning their flux increases towards shorter wavelengths (Johnson et al., 2001).

2.2.1 Transforming Thermal Radio Flux into the Near-Infrared

We can estimate the nebular emission in a cluster in the H and K band in the following way. The number of Lyman continuum photons is related to the free-free and bound-free radio flux by the following formula (Condon, 1992):

$$Q_{\rm Lyc} \geq 6.3 \times 10^{52} \left(\frac{T_e}{10^4\ {\rm K}}\right)^{-0.45} \times \left(\frac{\nu}{\rm GHz}\right)^{0.1} \times \left(\frac{L_{thermal}}{10^{27}\ {\rm erg\ s^{-1}\ Hz^{-1}}}\right) \tag{2.1}$$

where T_e is the electron temperature. We then convert this to a thermal luminosity in the H- and K-band following:

$$L_{thermal} = \left(\frac{c}{\lambda^2}\right) \times \left(\frac{\gamma_{total}}{\alpha_B}\right) \times Q_{Lyc} \tag{2.2}$$

Here, α_B refers to the case B recombination coefficient and γ_{total} is the continuous emission coefficient. The values used were adopted from Ferland (1980). We can then compare this to measured broadband magnitudes of individual clusters.

The slope of the nebular emission in the near-infrared is $f_{neb} \propto \lambda^{-2}$. S99 assumes that every Lyman continuum photon emitted in the cluster is absorbed and reradiated into free-free or free-bound emission (case B). This results in ≈ 90 % of the flux of a 1 Myr, 10^6 $M_\odot$ cluster being emitted through nebular emission. This assumption seems to overestimate the measured free-free emission in young SSC (see Chapter 3 & 4). We attribute this to the fact that the dust surrounding the hot stars in young clusters is likely clumpy. Indebetouw et al. (2006) have found

that the near-infrared SEDs of high-mass stars can vary by orders of magnitude depending on the clumpiness of the surrounding material.

2.3 Resulting Synthesis Spectra

The final spectrum of our clusters is modeled in the following way (see also Meyer and Greissl (2005)). To determine the most massive star still on the PMS at a given age, we use the tracks of Siess et al. (2000). At ages of 1 and 3 Myr this corresponds to 7 $M_{\odot}$ and 5 $M_{\odot}$ respectively. An appropriate PMS mass-luminosity relationship for this age is then assumed according to the PMS models (Siess et al., 2000). We also adopt tables of intrinsic colors and bolometric corrections from Kenyon and Hartmann (1995). Stars above this limiting mass are modeled using S99. This includes the main sequence as well as the post-main sequence. We use S99 instantaneous burst models assuming a Salpeter (1955) IMF above the PMS cutoff combined with the evolutionary models of the Padova group. The mass of the PMS and S99 components are scaled according to the IMF used and the total mass of our simulated clusters is 10^6 $M_{\odot}$. We adopt a lower mass cutoff of 0.08 $M_{\odot}$ and an upper mass cutoff of 100 $M_{\odot}$.

Assuming an IMF and an age, all stars below the PMS cutoff in the simulated cluster are assigned a mass in a Monte Carlo way, based on the parent IMF. We then chose the appropriate standard star spectrum depending on age and mass which is converted to a temperature and bolometric luminosity. We calculate an appropri-

ate monochromatic luminosity based on the Kenyon and Hartmann (1995) tables mentioned above. The stellar spectra are scaled with the appropriate luminosity, co-added and combined with appropriately scaled main sequence and post-main sequence contributions from S99. If simulating a real cluster the spectrum is also scaled by the amount of nebular emission in the cluster. It is important to note here that stochasticity effects can play a role for any clusters with masses less than 10^5 $M_\odot$ since the upper end of the IMF is not well populated. Above that mass stochastic effects in cluster flux decrease to $\leq$ 10 % (assuming a Chabrier (2003) IMF).

2.4 Model Results and Predictions

Figure 2.4 shows H- and K-band spectra for input power-law IMFs with a varying slope below 0.5 $M_\odot$ at ages of 0.3 - 3 Myr. Above 0.5 $M_\odot$ we assume a Salpeter slope of $\alpha = 2.35$ similar to a Kroupa IMF. An "appropriate" nebular emission of 20 % is included in these spectra based on the contributions measured for our observations in Chapters 3 and 4. Changes in the IMF in these spectra can be detected because different absorption lines are prominent among different mass ranges in the simulated clusters. In particular we use the 2.29 μm CO(2-0) bandhead which is prominent in cool objects. This bandhead, the Ca triplet (2.261, 2.263 & 2.117 μm) and the Na doublet (2.206 & 2.208 μm) in the K-band are strongest in stars below 3500 K ($\leq$ 0.5 $M_\odot$). In addition we included the MgI 1.71 μm and 2.28 μm features which are

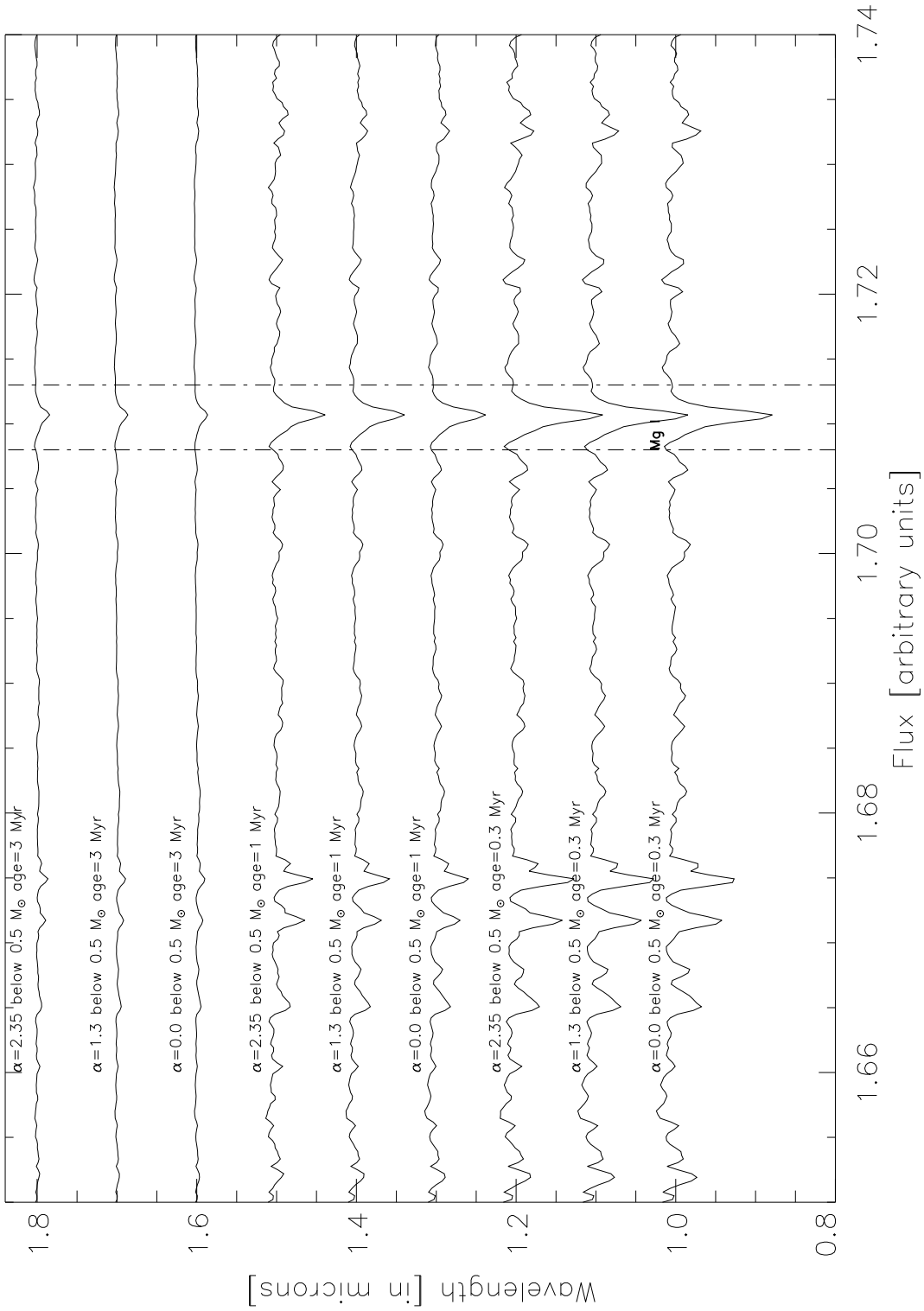
α=2.35 below 0.5 M⊙ age=3 Myr
α=1.3 below 0.5 M⊙ age=3 Myr
α=0.0 below 0.5 M⊙ age=3 Myr
α=2.35 below 0.5 M⊙ age=1 Myr
α=1.3 below 0.5 M⊙ age=1 Myr
α=0.0 below 0.5 M⊙ age=1 Myr
α=2.35 below 0.5 M⊙ age=0.3 Myr
α=1.3 below 0.5 M⊙ age=0.3 Myr
α=0.0 below 0.5 M⊙ age=0.3 Myr
Mg
Wavelength [in microns]
Flux [arbitrary units]
1.8
1.6
1.4
1.2
1.0
0.8
1.66
1.68
1.70
1.72
1.74

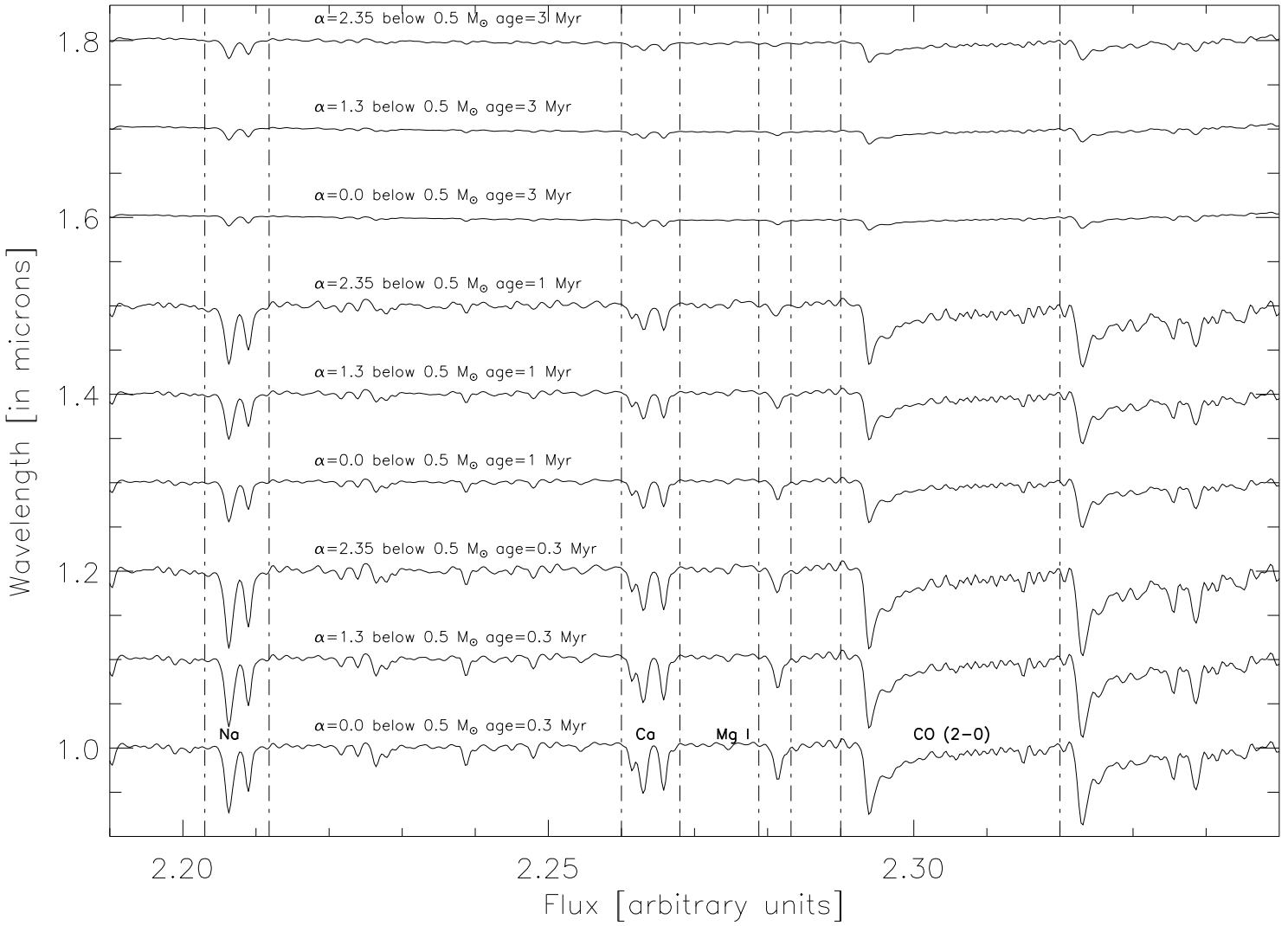

Figure 2.4 Models with different IMFs and ages as marked in the plot. Note the divergent evolution of the CO, Ca and Na bands compared with the MgI bands. For an IMF weighted more heavily towards low-mass stars the MgI line grows weaker while the other lines grow stronger. The opposite is true for an IMF weighted more towards high-mass stars.

Table 2.1. Equivalent Widths of Absorption Bands in the H- and K-band Spectra

$\alpha \leq 0.5\ M_{\odot}$	Age	EW[CO(2-0)]($\AA$)	EW[Ca I]($\AA$)	EW[Na I]($\AA$)	EW[Mg I K]($\AA$)	EW[Mg I H]($\AA$)
0.00	0.3 Myr	4.379 ± 0.231	1.523 ± 0.090	1.130 ± 0.061	0.540 ± 0.023	2.037 ± 0.152
1.30	0.3 Myr	4.781 ± 0.276	1.470 ± 0.072	1.268 ± 0.066	0.478 ± 0.042	2.013 ± 0.172
2.30	0.3 Myr	5.778 ± 0.328	1.270 ± 0.048	1.573 ± 0.061	0.287 ± 0.031	1.981 ± 0.143
0.00	1.0 Myr	2.501 ± 0.190	0.840 ± 0.041	0.745 ± 0.041	0.285 ± 0.012	1.160 ± 0.078
1.30	1.0 Myr	3.221 ± 0.195	0.782 ± 0.035	0.943 ± 0.067	0.207 ± 0.009	1.147 ± 0.094
2.30	1.0 Myr	4.370 ± 0.249	0.701 ± 0.037	1.313 ± 0.092	0.104 ± 0.008	1.023 ± 0.087
0.00	3.0 Myr	0.610 ± 0.032	0.201 ± 0.009	0.229 ± 0.012	0.044 ± 0.009	0.130 ± 0.010
1.30	3.0 Myr	0.872 ± 0.048	0.191 ± 0.008	0.259 ± 0.005	0.034 ± 0.012	0.128 ± 0.024
2.30	3.0 Myr	1.264 ± 0.101	0.180 ± 0.009	0.268 ± 0.008	0.023 ± 0.009	0.100 ± 0.009

strongest in stars between 0.5 - 1.5 $M_{\odot}$ (3500 - 7000 K).

The relative strength of the Mg (solar-type stars) line compared to the Ca, Na and CO (cooler stars) features is what allows us to place constraints on the IMF. Table 2.1 lists equivalent widths for the absorption lines given above for the spectra shown in Figure 2.4. The errors on the equivalent widths are due variations in the estimates for the continuum for each line. Note for example the evolution of the ratio of EW[CO(2-0)]/EW[Mg I K] which illustrates our ability to differentiate between different power-law IMFs. For a slope of 0.0 at an age of 0.3 Myr (below 0.5 $M_{\odot}$) this ratio is equal to 8.109 ± 0.55 while the ratio increases to 20.118 ± 2.45 for a slope of 2.3 at 0.3 Myr.

To estimate what kind of changes in the IMF we can detect with our models we

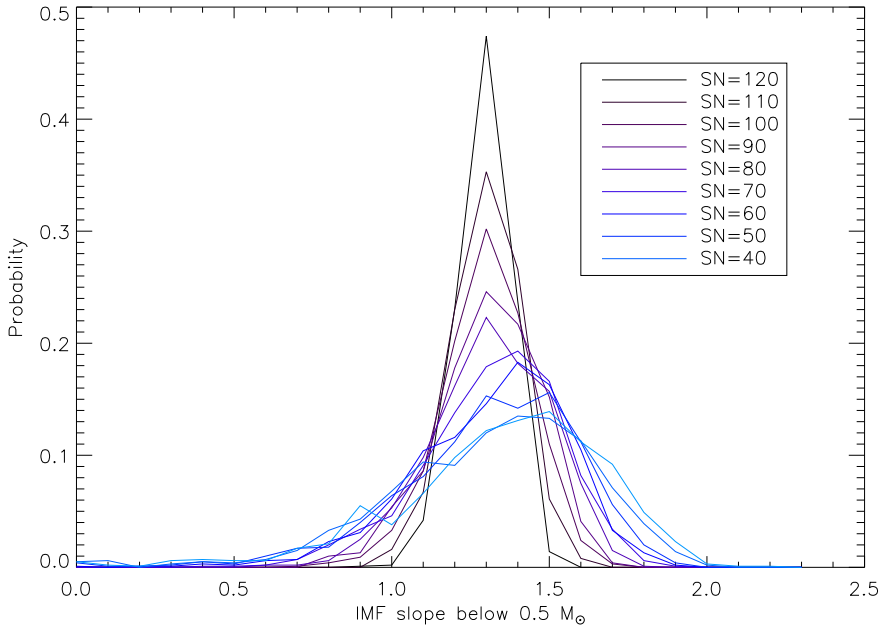

Figure 2.5 Range and frequency of slopes returned as best fits for an initial model with a slope of 1.3 below 0.5 $M_{\odot}$ at a resolution of 3000 and with a variety of noise levels added to simulate data with a given signal-to-noise level. As the signal-to-noise decreases the range of slopes inferred from the data increases from roughly 0.5 dex at signal-to-noise of 120 to 1.7 dex at signal-to-noise of 40. Both H- and K-band lines are included in these simulations.

created a set of Monte Carlo simulations. We added a random noise spectrum to a model with known parameters ($\alpha = 1.3$ below 0.5 $M_{\odot}$ and $\alpha = 2.35$ above at an age of 0.3 Myr) to simulate a real spectrum at a specific signal-to-noise level. We then repeated this procedure 10000 times generating a separate spectrum each time and then compared each realization to a suite of models with known parameters. These models were chosen to have a large range of slopes (0.0 - 2.35 below 0.5 $M_{\odot}$ in increments of 0.1) and ages (0.1 Myr - 3 Myr in 0.1 Myr increments). For each of the 10000 realizations we determined the best-fit model by determining the fit with the lowest $\chi^2 = \sum_{i=0}^{n}(d_i - m_i)/\sigma_i^2$ compared to the model suite for the absorption lines in the H- and K-band as mentioned above. Here d_i refers to the ith data pixel and m_i refers to the corresponding model point and σ_i^2 is the signal-to-noise value at the ith pixel which in this case is determined by the amount of noise added to to each spectral realization. The range in slopes returned for the best-fit models can then tell us what IMF constraints are possible for simulated data with a specific signal-to-noise level.

We created models for signal-to-noise ranges between 40 and 120. See Figure 2.5 for results of the range of best-fit slopes for a resolution of 3000 which is the inherent resolution of our spectral library. Assuming an approximately gaussian distribution of best-fit IMF slopes in Figure 2.5 we consider any slopes outside of a 99% probability ruled out. For example for a signal-to-noise level of 100 slopes below 0.8 and above 1.7 are ruled out according to this assumption. This indicates

that we should be able to detect IMF variations of $\approx \pm 0.4$ dex for data with signal-to-noise levels of 100. For realizations with a signal-to-noise of 40 this decreases to $\pm$ 0.85 dex. See Table 2.2 for more details.

We also attempted to understand the differences between model constraints when both H- and K-band spectra were used and when K-band spectra alone were used. Since the MgI line in the K-band is weaker than the line in the H-band using just K-band spectra makes it harder to detect IMF variations for the same signal-to-noise level data. We found that using K-band data alone somewhat degraded the IMF slope variations that were detectable. Since the observational challenge is most likely conclusively detecting the MgI line in the K-band particularly for data with lower signal-to-noise levels it is still advisable to obtain both H- and K-band data for a cluster if possible. In addition we performed these simulations for spectra with downgraded resolutions of 1000 and 300. We found that data with resolutions of 3000 and 1000 generated very similar results indicating that there is no penalty for obtaining data at a somewhat lower resolution requiring less time intensive observations. This results are not surprising since the bands we use in our analysis are rather broad. However spectra of resolutions of 300 made it harder to detect IMF variations. This indicates that a resolution of around 1000 is an ideal resolution to perform these kinds of observations with the bands we have chosen for our analysis since there is no trade-off in IMF variations detectable and since the lower resolution requires less observing time.

Table 2.2. IMF constraints for given model parameters

S/N	Resolution	K-band / H-band	IMF constraint
120	3000/1000	both	0.25 dex
120	3000	K-band only	0.25 dex
110	3000/1000	both	0.3 dex
110	3000	K-band only	0.35 dex
100	3000/1000	both	0.4 dex
100	3000	K-band only	0.4 dex
90	3000/1000	both	0.45 dex
90	3000	K-band only	0.5 dex
80	3000/1000	both	0.5 dex
80	3000	K-band only	0.55 dex
70	3000/1000	both	0.6 dex
70	3000	K-band only	0.65 dex
60	3000/1000	both	0.65 dex
60	3000	K-band only	0.75 dex
50	3000/1000	both	0.8 dex
50	3000	K-band only	0.8 dex
40	3000/1000	both	0.85 dex
40	3000	K-band only	0.85 dex

To determine these constraints we chose a model with a young age and thus strong absorption bands. Any older clusters or clusters with a flatter IMF and thus weaker absorption bands would make it more difficult to determine IMF variations and would broaden the slopes allowed and thus the ranges of slopes given in Table 2.2 are likely lower limits.

Observing the youngest clusters is critical since PMS absorption lines attenuate quickly after an age of 1 Myr (see Figure 2.2). By 3 Myr PMS stars contribute less than 20 % of the near-infrared flux of a cluster and the absorption lines we use for our analysis have decreased in strength by roughly 70 % compared to a 1 Myr cluster assuming the nebular contribution listed above. For clusters older than 4 Myr the absorption lines decrease to less than 1 % in depth and are thus not detectable in spectra with a S/N of even 100. Thus there is a narrow window in age at which our technique is applicable. Determining exact ages of SSC through broadband SEDs and the presence of thermal radio emission as well as spectroscopy which can detect emission lines remains challenging especially at young ages. Anders et al. (2004a) find that ages of SSC can be constrained to a factor of 3 based on broadband SEDs which include at least one near-infrared bandpass as well as either U or B colors. The additional possibility of combining broadband SEDs with radio data should make it feasible to rule out objects older than a few Myr.

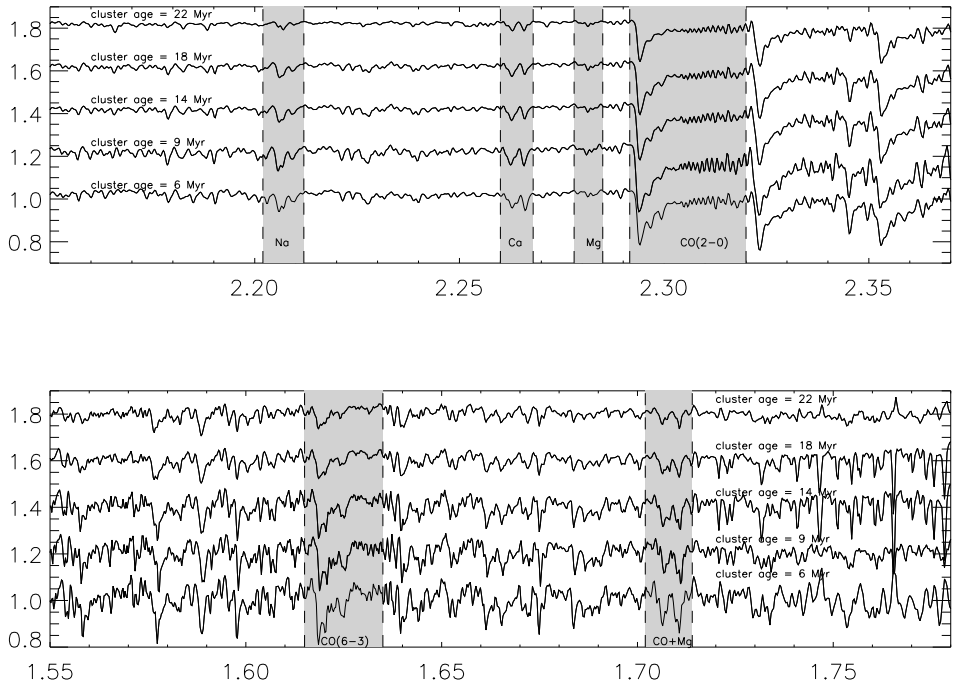

Figure 2.6 H- and K-band spectra for 10^6 $M_\odot$ clusters with ages between 6 and 22 Myr. The CO lines in the H- and K-band are particularly sensitive to age. At the earlier ages the spectra are dominated by one or two spectral types of supergiants while older ages feature a blend or a larger number of spectral types.

2.4.1 Generating Older Cluster Spectra

Though we had initially intended to only generate PMS models our model is also able to generate near-IR H- and K-band spectra of older clusters. In this case we only use the S99 outputs and convert them to a near-infrared spectrum. We use the S99 output of the numbers of stars at a given spectral type ranging from dwarfs to supergiants. We then chose an appropriate stellar spectrum from our library which contains a similarly fine grid of supergiants and dwarfs for each spectral type. Similarly to the PMS models the spectra are then scaled with an appropriate luminosity and co-added. See Fig. 2.6 for a set of spectra of 10^6 $M_\odot$ clusters of ages between 6 Myr and 22 Myr. It is important to note that it remains challenging to accurately predict the evolution of red supergiants in particular for low metallicities (Levesque, 2010). Thus it is likely that the limitations of this model are due to the accuracy of the output of supergiant spectral types of S99. The evolution of binaries for example, which is not included in S99 can influence the frequency of red supergiants in a cluster.

2.5 Discussion

The main strength of this technique in determining the IMF in massive star clusters lies in its ability to determine the IMF for low-mass star directly. Recent results by van Dokkum and Conroy (2010) employ a similar technique to ours to constrain the IMF in elliptical galaxies and derive a best-fit IMF steeper than Salpeter. Other

methods such as that employed by Tremonti et al. (2001) in unresolved massive clusters only trace their massive stellar content though this study does not quote specific ranges for their IMF results. Results for mass-to-light ratio measurements are generally not sensitive to changes in the IMF slope of smaller than 1 - 1.5 dex. For extragalactic measurements where actual star counts are possible such as the LMC or in more distant clusters in the Milky Way errors on slope determinations for the IMF are generally smaller than 0.4 dex. Thus depending on the quality of the data that can be obtained out method is somewhere in between these sensitivities.

There are a number of physical phenomena which affect young SSC which are currently not included in our model. Below we describe these issues in more detail and explain how each may affect the outputs of our model and our ability to constrain the resulting IMF. The effects are listed in order of magnitude, though the effect of using field dwarfs to represent PMS stars and of not including dust emission is likely similar in scale.

While we have made no assumptions about age in Figure 2.5, instead allowing for a broad range of ages in the models, we do assume that our model correctly predicts the depth of the absorption features used in our analysis with regard to age. If however spectra of clusters with ages of 1 Myr really were better represented by models with ages of 0.3 Myr this could cause us to assign an IMF to the cluster with a flatter power-law slope. We have attempted to address this issue in the subsequent chapters by varying the ages assumed for our data and comparing the

IMF results and discuss this issue in more detail. It is also possible that the star clusters we observe have populations with an inherent spread of ages. In some nearby star forming regions such as the Orion Nebula young stars exist of a variety of ages although these age spreads are generally smaller than 30% (Hillenbrand et al., 2008). If distant star clusters have similar age spreads by modeling these clusters with a single age we may be degrading our ability to detect IMF variations. However, if we can correctly predict the mean age we are still on average modeling the strength of late type absorption lines correctly. In this case our model overpredicts the accuracy of our IMF estimate.

Both S99 and the Siess et al. (2000) evolutionary tracks can generate models with subsolar and supersolar metallicities. In our models we have used a spectral library composed of main sequence stars with solar metallicity to model young PMS stars. Since the strength of absorption lines depends on metallicity (with their strength decreasing for decreasing metallicity and vice versa) generating models with metallicities other than solar would cause us to overpredict ($Z \leq Z_{\odot}$) or underpredict ($Z \geq Z_{\odot}$) the equivalent widths of late-type absorption lines. The library by Ivanov et al. (2004) contains a larger range of metallicities and may present an acceptable substitute to use in this case though the greatest range in metallicities in this library is for their sample of giants and supergiants rather than dwarfs. In addition the number of main sequence stars included is smaller than the one we use here. This may cause issues with the spectral binning of the stars. Model spectra are available of

a variety of metallicities and could also be used to expand our models to metallicities other than solar. However, model atmospheres at present struggle to reproduce accurately the properties of PMS stars (Doppmann et al., 2003) and thus spectral standards remain an attractive option to model SSC in the near-infrared.

Since our library is comprised of main sequence stars as opposed to PMS stars we underpredict the strength of the CO feature which is surface gravity sensitive. This could lead us to assign an erroneously flat IMF slope to real observations though PMS are generally found to lie closer to field dwarfs than giants in surface gravity (Gorlova et al., 2003).

Dust emission from circumstellar disks in young stars or the HII regions in which SSC are embedded contributes another source of uncertainty in particularly toward the red end of the K-band. This excess continuum emission weakens absorption lines towards longer wavelengths and thus may cause us to underestimate the strength of absorption lines in the K-band compared to the H-band as well as the strength of the CO line compared to the other lines in the K-band. This would cause us to assign an IMF that is erroneously steep. In star forming regions such as Taurus the disk fraction is only around 50% (Luhman et al., 2010) however, and the disk emission is generally small compared to that of the star. Compared to the free-free and free-bound emission which we discuss in Section 2.2 this effect is thus likely small. In addition Ando et al. (2002) found the extended thermal emission in the HII region M17 was dominated by free-free and free-bound emission. We do not directly

consider extinction in our IMF determinations and do not have an independent way of determining it with our datasets in subsequent chapters. Our IMF results should not be affected by strongly by issues of extinction. We do account for extinction when determining cluster masses in a coarse way since any cluster mass calculated without taking extinction into account will underestimate the real mass of a cluster.

CHAPTER 3

STAR FORMATION HISTORY OF A YOUNG SUPER-STAR CLUSTER IN NGC 4038/39: DIRECT DETECTION OF LOW MASS PRE-MAIN SEQUENCE STARS

The contents of this chapter were previously published in Greissl et al. (2010).

We now apply the models discussed in the previous chapter to modeling a young cluster in NGC 4038/39. As mentioned in Chapter 1, the Antennae (NGC 4038/9) are the nearest (distance = 19.2 Mpc, 1" $\approx$ 90 pc, Whitmore et al. (1999)) pair of merging spiral galaxies. The galaxies are the earliest and closest merger in the Toomre (1977) sample of prototypical mergers and contain an extremely rich population of up to a thousand young star clusters formed by the merger process. These clusters have been the target of a multitude of studies at different wavebands (e.g. Whitmore et al. (1999); Neff and Ulvestad (2000); Brandl et al. (2005)). Whitmore and Schweizer (1995) identified a large population of SSC in the optical using HST WFPC2 images. These clusters appear to belong to four distinct populations. The youngest group of clusters has ages of $\leq$ 20 Myr while older populations of $\approx$ 100 Myr and 500 Myr also exist in addition to the pre-merger cluster population of the two individual galaxies. The older (500 Myr) population

may be associated with the previous encounter of the two galaxies (Whitmore et al., 1999).

The faintest and reddest of the young clusters are revealed to be bright near-infrared and mid-infrared emitters and comprise the youngest clusters (Snijders et al. (2006); Wang et al. (2004); Brandl et al. (2005)) which are primarily located in the dust overlap region (Whitmore et al., 1999). Radio images by Neff and Ulvestad (2000), which detect sources with purely nebular emission (i.e. $\alpha_{4cm-6cm} \geq$ -0.4) due to massive stars in the clusters, provide additional evidence for the youth of these objects. Sources with non-thermal radio emission likely contain supernova remnants and are thus older. An extensive spectroscopic study of the Antennae in the near-infrared and the optical has been undertaken by Christopher (2008) who found that many objects contained simultaneous hydrogen emission features as well as CO bandheads which are indicative of late-type stars. They interpreted this as indication that star formation in these clusters in the Antennae may have occurred over a burst of 5 Myr duration. Our study focuses on one cluster in their sample, the object designated cluster 89/90 in Whitmore and Schweizer (1995) an extremely red object in the visible which is revealed as a massive young cluster in the near-infrared.

Cluster 89/90, the cluster targeted in this study, was first surveyed by Whitmore and Schweizer (1995) using WFPC2 on the HST. It is the brightest near-infrared cluster in NGC 4038/9 as well as the second brightest thermal radio source at 4 and 6 cm. In addition Snijders et al. (2006) observed the cluster in the mid-infrared and

found strong NeII 12.8 and NeIII 15.5 μm emission as well as PAH emission at 11.25 μm. These features are an indication of the presence of hot stars (Mirabel et al., 1998). See Table 1 for a list of broadband magnitudes for cluster 89/90 obtained from archival data.

In the following sections we present a H- and K-band spectrum of cluster 89/90 and model its underlying population. Section 3.2 details the observations and data reduction. Section 3.3 gives an overview of the method used to model the spectrum of the cluster. The analysis of the spectrum, which constrains the population of the cluster, is presented in section 3.4. Section 3.5 contains the results of the analysis, as well as its limitations. Section 3.6 places our analysis in the context of previous work.

3.1 Observations and Data Reduction

H- and K-band spectra of cluster 89/90 were obtained with NIRSPEC (McLean et al., 1998) on Keck in February 2003 using the 42" slit with a scale of 0.144"/pixel. The spectrum was observed as part of a larger dataset of Antennae clusters which are described in detail in Christopher (2008). For the H-band spectra we used the N5 filter, covering 1.54-1.83 μm. The K-band spectrum was obtained with the N7 filter covering 2.05-2.47 μm. The K-band seeing during the observations was $\approx$ 0.5" and stable throughout the night; accordingly the 0.57" wide slit was used in both bands. The spectra were obtained with a total integration time of 900 s (3

x 300s) in both the H- and the K-band at an airmass of ≈ 1.3. The object was offset along the slit in successive frames to allow for sky subtraction. Since SSC can often have a wealth of small-scale structure we were careful to make sure the sky subtracted images contained no significant galactic background contamination. After sky subtraction the background had no identifiable shape and the noise in the background was dominated by instrumental noise. We did not see detectable CO absorption outside of our cluster in the spectrum which would have affected our analysis. Calibration data were obtained including a flatfield and appropriate dark frame as well as neon and argon arc lamp spectra to use for wavelength calibration. To correct for telluric absorption we used a G2V star in the H-band and an A0V star in the K-band. To ensure the best telluric correction we observed the standard stars within 0.05 airmasses of the target. Flatfielding and cosmic ray removal were performed on each spectrum using standard IDL procedures.

NIRSPEC spectra have spatial and spectral distortions that must be removed during the reduction process. The spatial distortion corrections were calculated by measuring the position of the brightest calibrator spectra at multiple positions in the slit. The traces of these sources were fit with polynomials to determine the spatial distortion correction. This routine was modified from the REDSPEC[1] package written by Lisa Prato. For wavelength calibration, we used an argon arc lamp in the H-band and a neon arc lamp in the K-band.

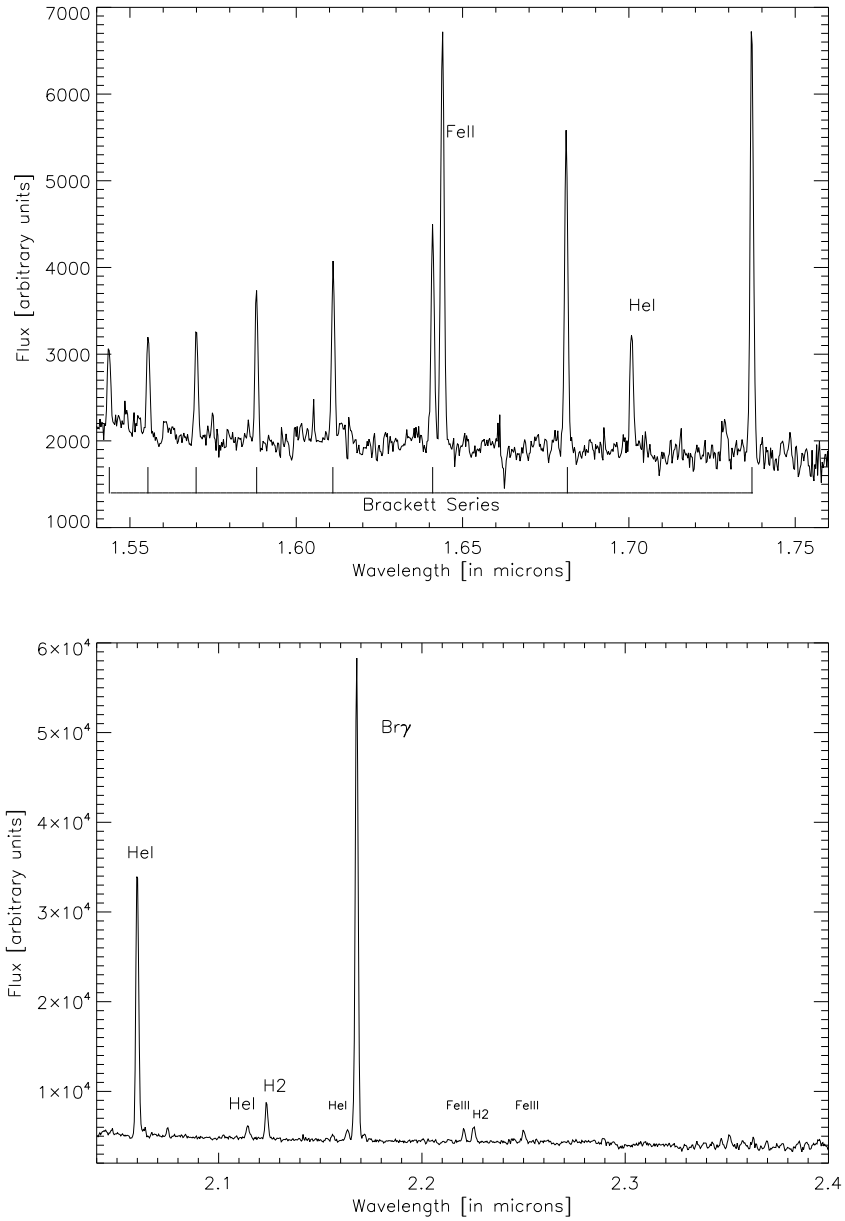

Figure 3.1 NIRSPEC H- and K-band spectrum of Cluster 89/90. Emission lines which are indicative of the youth of the cluster are marked. The data have been shifted to restframe wavelengths. Weak CO(2-0) absorption at 2.29 μm is barely visible at this level.

The reduction of the calibrator stars was carried out in the same manner. To determine the atmospheric calibration we applied template spectra using Meyer et al. (1998) in the H-band and Wallace and Hinkle (1997) in the K-band smoothed to the resolution of our spectra (R $\approx$ 1100 - 1500). The calibrator stars were largely featureless, except for Brγ absorption in the K-band, which was not well matched by the template and removed independently. Stellar absorption centers were measured in both the template and the calibrator spectrum to remove any spectral offset. The H-band template spectra covered the entire wavelength range of the H-band atmospheric calibrator observations; for the K-band, the template spectra ended at 2.4 μm while our observations extended redward to 2.47 μm. We assumed a featureless blackbody for the template spectra from 2.4-2.47 μm. We examined the final telluric spectrum to ensure there were no mismatches between the G2V standard and the solar spectrum particularly around the Mg absorption line at 1.71 μm which could have affected our analysis. The atmospheric calibration was calculated by dividing the calibrator spectrum by the shifted template spectrum and normalizing the result at the center of the band. Any spectral offset between the atmospheric correction and the source spectra were measured by comparing the location of atmospheric absorption features and applying an offset to the atmospheric correction if necessary. Typical offsets were less than 0.1 pixels. The atmospheric correction removes both the effects of the atmosphere and variations in NIRSPEC system throughput as a

[1]See http://www2.keck.hawaii.edu/inst/nirspec/redspec/index.html

function of wavelength. The final spectrum was extracted from the atmospherically calibrated composite exposure with an aperture size of 5 x the seeing. Figure 3.1 shows the final extracted H- and K-band spectrum of cluster 89/90.

3.2 Modeling the Near-Infrared Spectrum of Cluster 89/90

We now model the spectrum of cluster 89/90 comparing the NIRSPEC spectrum to the results of the modeling routine described above. Figure 3.1 shows the H- and K-band spectrum of the cluster with emission lines marked. The absorption lines are barely visible at this scale. Emission lines are not included in our model or our analysis. To model the spectrum of cluster 89/90 we first assume that the cluster represents one co-eval burst of star formation (see 3.4.1) and explore the IMF required to reproduce the spectrum. We also consider two separate bursts as the underlying population to explain the spectrum (see 3.4.2), since i) the spatial scale covered by our spectrum is quite large with $\approx$ 50 % of the clusters in the sample of Christopher (2008) revealed as multiple clusters in HST imaging and ii) the IMF required by a single co-eval burst exceeds the Salpeter slope. Table 3.2 lists the best-fit model parameters for the two approaches. We have adopted solar metallicity for our analysis in the Antennae in accordance with metallicity measurements (Mengel et al. (2001); Christopher (2008)).

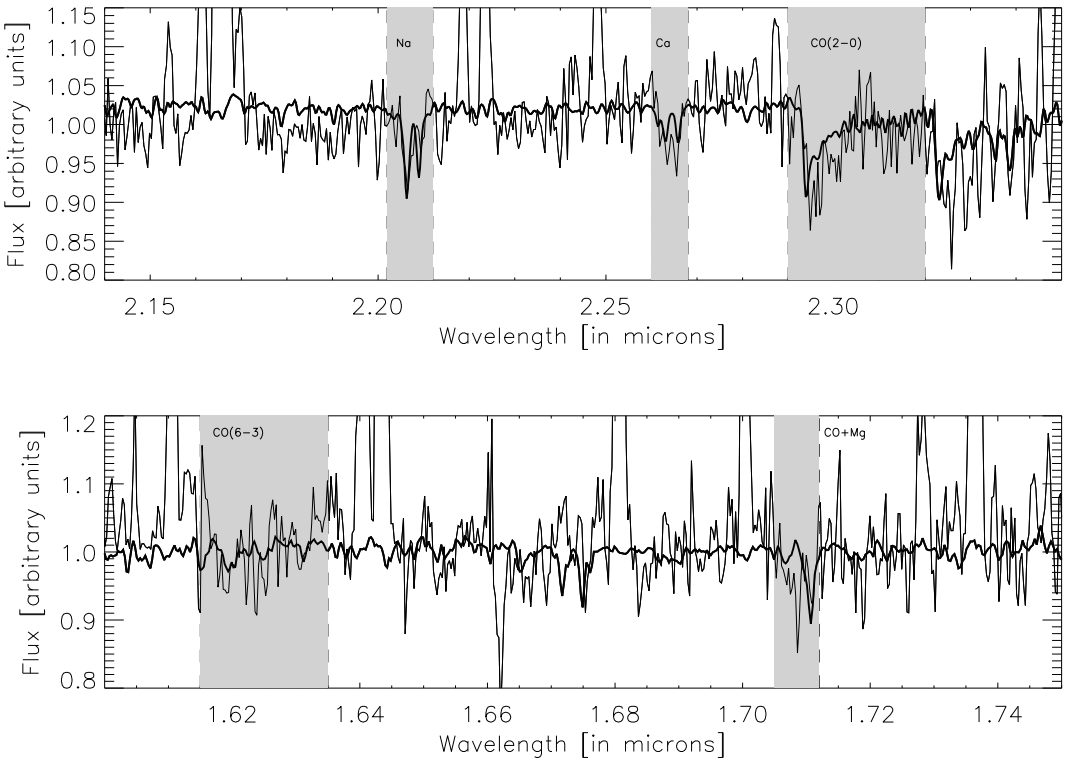

Figure 3.2 Best-fit single age model overlaid over a normalized scaled spectrum of Cluster 89/90. The bands used in our analysis are marked. The emission lines as well as large parts of the continuum were not included in the modeling. The best-fit reduced $\chi^2 = 1.40$.

Table 3.1. Archival data of cluster 89/90

R.A. (J2000.0)	Dec. (J2000.0)	F_{4cm} (μmJy)	[a] F_{6cm} (μmJy)	m_V	[b] m_I	m_J	[c] m_H	[d] m_K
12:01:54.58	-18:53:03.42	1957	2316	19.07	18.40	15.05	14.71	14.27

[a]From Neff and Ulvestad (2000)

[b]From Whitmore and Schweizer (1995)

[c]From Brandl et al. (2005) in the 2MASS system

[d]From 2MASS

3.2.1 Nebular Emission

Cluster 89/90 was observed by Neff and Ulvestad (2000) at 4 and 6 cm (Table 3.1). Using the 4 cm flux, which is less susceptible to non-thermal contamination we estimate the nebular continuum as described in Chapter 2. We assumed a value of 7500 K for T_e which is a 'typical' temperature assumed for Galactic UC HII regions and the same temperature assumed by Neff and Ulvestad (2000). For cluster 89/90 this results in Q_{Lyc} = 8.46 x 10^{52} s^{-1} which corresponds to the equivalent of 2300 O5 stars powering the nebular emission of the cluster. With the assumption of a distance for the Antennae this value can then be directly compared to the measured near-infrared flux for cluster 89/90 in the H-band and the K-band (see Table 1). This results in F_{ffH} = 2.78 x 10^{-13} and F_{ffK} = 1.98 x 10^{-13} erg s^{-1} in cluster 89/90. This corresponds to 19.1 % and 23.5 % of the total H- and K-band flux from the cluster. This is the value we will use for the rest of the analysis as the nebular

percentage contributing to the near-infrared emission in cluster 89/90.

3.2.2 Single-age Burst

To constrain the IMF required in cluster 89/90 if the late-type absorption features are due to a single-age burst we model clusters at ages of 0.3, 1,3 and 5 Myr. Above 6 Myr red supergiants appear in clusters and our single-burst model would no longer be appropriate due to the observed ratios of near-infrared absorption lines in our spectrum (as explained in more detail in the section 3.4.2). We found that the 5 Myr models could not accurate reproduce the observed spectrum because of the rapid dimming of the PMS stars and these models are not included in the two-burst model for that reason. We use a single variable power-law for the IMF with a break-point at 1 $M_{\odot}$ with a variable slope below the break point and a Salpeter (1955) slope (α = 2.35 in linear units) above. We vary the slope below 1 $M_{\odot}$ by 0.5 dex between 0.0 to 4.0. To determine which models best fit the cluster spectrum we performed a χ^2 analysis comparing the model spectrum convolved to the resolution of the data and the data, which has been shifted to restframe wavelengths and normalized by fitting a 5th-order polynomial to the continuum. The nebular emission in the cluster is calculated as given above from the radio data of Neff and Ulvestad (2000) and is independent of these assumptions. We included five spectral regions in our fit, which are marked in Figure 3.2. These five regions include late-type absorption lines that are seen in red supergiants as well as PMS stars. In the H-band there are numerous

^{12}CO transitions which are surface gravity sensitive and strong in red supergiants but weak in main sequence and PMS objects. Of these we include the transitions at 1.62 μm and 1.71 μm in our fit. The CO(2-0) 2.29 μm transition in the K-band is also surface gravity sensitive but is a prominent feature in all late-type objects. The Ca triplet (2.261, 2.263 & 2.117 μm) and the Na doublet (2.206 & 2.208 μm) absorption lines in the K-band are strongest in stars below 3500 K ($\leq$ 0.5 $M_{\odot}$). In addition we included the MgI 1.71 μm feature which is blended with one of the ^{12}CO features at 1.71 μm and is strongest in stars between 0.5 - 1.5 $M_{\odot}$ (3500 - 7000 K).

We then minimize χ^2 of the difference between the model spectrum and the data. Here the goodness of the fit is given by: $\chi^2 = \sum_{i=0}^{n}(d_i - m_i)/\sigma_i^2$, where d_i refers to the ith data pixel and m_i refers to the corresponding model point and σ_i^2 is the signal-to-noise value at the ith pixel. χ^2 is reduced in the standard way by diving by the number of pixels in our absorption bands minus the degrees of freedom in our analysis. This process is described in more detail in the following section.

The best-fit model is plotted in Fig. 3.2 and the model parameters are listed in Table 3.2. This single-age model does not match the depth of the surface gravity sensitive CO features well and the spectrum which best matches the data has dN/dM $\propto m^{-3.0}$ or steeper. As this seems extraordinary, we consider an alternate hypothesis of two separate bursts of star formation at different ages.

3.2.3 Two separate Bursts

We now attempt to reproduce the spectrum given two underlying bursts of star formation. Given that our 1" slit represents a physical scale of $\approx$ 90 pc at the distance of the Antennae this approach seems warranted. We model the spectrum as one young population containing PMS stars (hereafter Population 'A') in addition to an older population containing red supergiants (hereafter Population 'B'). We model these populations separately and then combine the two. Incorporating an older cluster containing supergiants is supported by the fact that the H-band spectrum of cluster 89/90 contains ^{12}CO absorption lines which are much stronger in supergiants than in dwarfs and PMS stars (see Fig. 3.2 & 3.4). However, Figure 3.3 shows that cluster 89/90 lies below supergiant standards when using an index that is surface gravity sensitive as function of temperature. Giants lie between supergiants and dwarfs in this index but are not included in the figure since giants do not appear until ages $\geq$ 100 Myr. This index includes the surface gravity sensitive CO(2-0) 2.29 μm feature as well as the NaI doublet and CaI triplet which are not strongly affected by surface gravity, though the ratio of the lines in the NaI doublet changes with log(g). For reference, supergiant sources have log(g)= 0.0 while dwarfs have log(g)= 5.0 - 5.5. Cluster 89/90 lies close to the dwarf locus in this index which indicates that the late-type absorption features in cluster 89/90 cannot be caused solely by red supergiants, but must have an underlying PMS component. [2]

The presence of a young component is also supported by the emission lines seen in the spectrum of cluster 89/90. The red supergiants have stronger late-type absorption lines but cannot match the observed surface gravity sensitive equivalent width ratios. A combination of red supergiants and late-type dwarfs however can reproduce both the surface gravity index as well as the overall depth of the absorption features. In our best-fit model A and B have a flux ratio of ≈ 7 to 1 which is well reproduced by the location of Cluster 89/90 in Figure 3.3.

There are three variables we consider for each burst: mass, age and IMF. The nebular emission in the cluster is again estimated from the radio data of Neff and Ulvestad (2000). The spectrum of B is modeled using S99, with appropriate standard spectra (Meyer et al. (1998); Wallace and Hinkle (1997)) used for the red supergiants in the spectrum similar to A. The output of S99 includes the number of stars of each spectral type. For each supergiant of a given spectral type and temperature we then use an appropriate spectral standard. The temperature scale used was adapted from the cool supergiant temperature scale by Levesque et al. (2005).

[2]The values measured for Cluster 89/90 for the equivalent widths in Fig. 3.3 are: CO(2-0) = 14.84 $\pm$ 3.29 $\AA$, Ca = 3.30 $\pm$ 0.48 $\AA$ and Na = 4.19 $\pm$ 0.63 $\AA$. The Ca triplet and Na doublet bandpasses were chosen in accordance with Kleinmann and Hall (1986) while the CO(2-0) bandpass was 2.293 - 2.318 μm with the continuum between 2.2887-2.2915 μm.

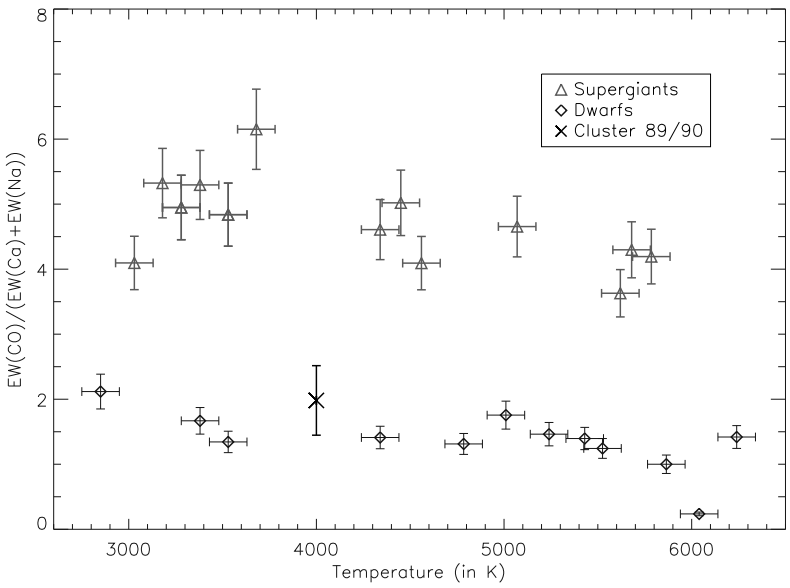

Figure 3.3 Plot of the ratio of equivalent widths of CO(3-1) 2.29 μm, Ca 2.26 μm and Na 2.20 μm absorption features in supergiant and dwarf standards. Overplotted is Cluster 89/90 at an arbitrary temperature. Errors were estimated using standard error propagation. This shows the clear separation between supergiants and dwarfs in this index. Cluster 89/90 lies much closer to the dwarf locus rather than the supergiant locus. This indicates that a supergiant population cannot be solely responsible for the absorption lines present in the spectrum.

3.2.4 Model Parameters

According to S99 the first supergiants in a star cluster appear around 6 Myr though a significant population does not appear before 7 Myr. Late-type supergiants disappear at an age of $\approx$ 30 Myr. Thus we can roughly constrain the age of B to between 7 and 30 Myr. In the H-band, cool stars possess a ^{12}CO absorption line which blends with the 1.71 μm Mg line in the H-band (see Figure 3.2). This CO feature is strongly surface gravity sensitive and very weak in dwarfs. This blend is observed in Cluster 89/90 giving additional credence to the fact that red supergiant features are present in our spectrum. We considered models in 3 Myr steps.

For A the goal was not to constrain the age accurately but to assure that the best fit was consistent across different ages. Changing results with age would have limited the usefulness of our analysis method, since we do not have an independent constraint on the age of A except for an upper limit on the age of $\leq$ 5 Myr. We considered models of 0.3, 1 and 3 Myr.

We vary the mass ratio of the two populations between zero and one in steps of 0.01 below $M_{old}/M_{young} = 0.2$ and in steps of 0.1 above 0.2. We cannot directly constrain the total mass of the cluster, because the overall flux of the spectral model depends on the mass ratio of the best-fit model. After we have determined the best spectral model fit it is possible to constrain the mass through broadband magnitudes. There is no way to directly constrain the IMF of B since we only trace a very small mass range of stars in the population in our spectrum, the red supergiants. Thus

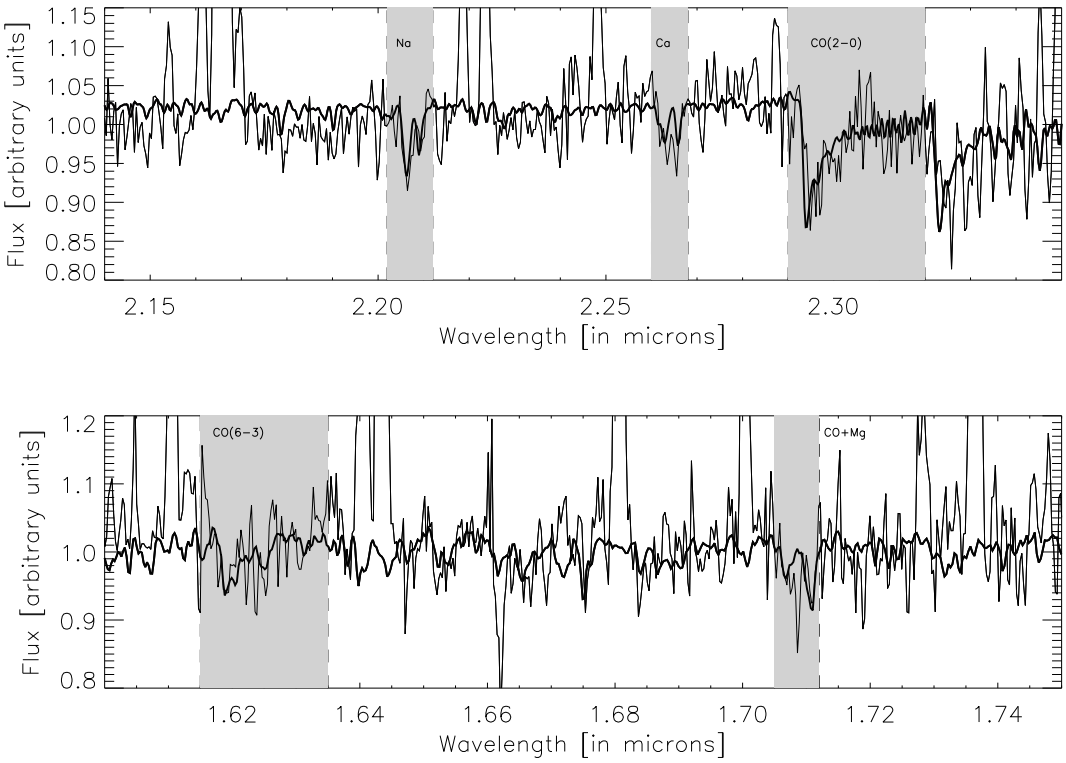

Figure 3.4 Best-fit two-burst model overlaid over a normalized scaled spectrum of Cluster 89/90. The bands used in our analysis are marked. The emission lines as well as large parts of the continuum were not included in the modeling. The best-fit reduced $\chi^2 = 1.23$.

the IMF of B is assumed to be the same as that of A. For A we have allowed the IMF to vary as a broken power-law with a Salpeter slope above 1 $M_{\odot}$ and a varying slope below by 0.5 dex between 0.0 and 2.0 and also including 2.35. We did not attempt varying the break point in the IMF or introduce a low-mass cutoff. There is some evidence that one could expect the Jeans mass to vary in SSCs which would influence the break point of the IMF (Larson, 2005). The limitations of this particular data set, due to a possible overlap of two star clusters, make such a study not feasible.

3.2.5 Analysis

We again perform a χ^2 analysis between the model spectra and the data including the same spectral regions as in 3.4.1. To assess the signal-to-noise ratio (SNR) of the observed spectrum at each spectral region we fit the continuum of the spectrum around each of the absorption bands and measured the RMS noise around the fit. We estimate the average SNR of the spectrum to be ≈ 30. We ran models in all permutations of parameters described in the previous section and determined the best-fit model (with the lowest χ^2) which is shown in Figure 3.4.

Given the large grid of models, we tried to constrain the acceptable range of values for each model parameter in the following way. First we determined the probability of each model given by $P_i \propto e^{-{\chi_i}^2}$ and normalized so that $\sum_{i=0}^{n} P_i = 1$. We then plot the probability separately for each variable (see Figure 5), where each point in the plot represents the sum of the probabilities over the whole

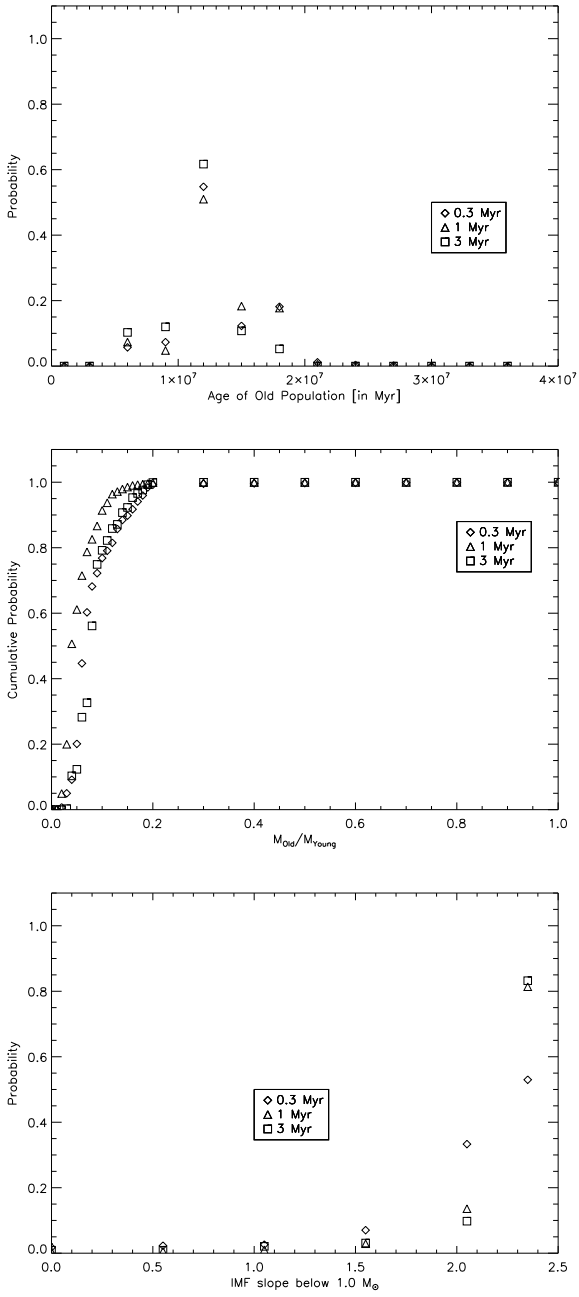

Figure 3.5 Plot of probabilities vs. age of the old population (top), mass ratio (middle) and IMF (bottom) for our models. Each plot includes separate data points for all three young burst ages to make certain that our results are not age dependent. Each plot point in a panel represents a summation over all the values of the other two variables and for each panel the probability has been normalized. For clarity the mass ratio is shown as the cumulative probability. Both the IMF and the age plots show well constrained values at the resolution of the models. The mass ratio is less tightly constrained.

Table 3.2. Best-fit Models

Model prescription	Age(in Myr)	α	[a] M_{old}/M_{young}	$M_{tot}(in M_{\odot})$	[b] Reduced χ^2
Single burst	1	-3.0	..	2 x 10^7	1.40
Two bursts (Population A)	1	-2.35	0.04	1.4 x 10^7	1.23
Two bursts (Population B)	12	-2.35	0.04	1.4 x 10^7	1.23

[a]Power-law slope of the IMF (dN/dm $\propto$ $m^{-\alpha}$)

[b]Flux due to best-fit model as compared with the total K-band flux of cluster 89/90.

range of the other two variables. We also assessed the probabilities in a Monte Carlo way. We added a noise spectrum given by a resampled subtraction of the data and the best-fit model to the cluster spectrum and determined the best fit for each newly realized resampled spectrum. We performed this routine 10000 times and determined the probability a particular set of parameters is determined as the best-fit model. The results from the Monte Carlo simulations agreed well with the probabilities determined from the χ^2 values alone.

3.3 Results

3.3.1 Best-fit Models

We now discuss the implications of the ranges of parameters constrained by our modeling (see Table 3.2). The three plots in Figure 5 show the probability distribution of the age of the old population, mass ratio of the two bursts as well as the

slope of the IMF below 1 $M_\odot$. Each plot shows the probability distribution at the three different ages of A to make sure that the results are consistent over a range of ages. Panel 1 shows that the older population has a most probable age of 12 Myr. Within 90% confidence limits the models are consistent with an age between 6 - 18 Myr for the old population. It should be noted that a population containing no supergiants is ruled out as can be seen by the fact that an age of 1 Myr and 3 Myr for B have zero probability. This coarse age constraint is not surprising since very little differentiates spectra of red supergiants in the near-infrared besides the overall strength of late-type absorption lines.

The plot of mass ratios shows the cumulative probability with respect to $M_{old/young}$. The mass ratio strongly favors A dominating in mass by a factor of $\geq$ five over B. The best-fit model comparison of the K-band flux with the K-band broadband flux of the cluster yields a total mass of 1.4 x 10^7 $M_\odot$ down to the hydrogen burning limit. If we assume that the total mass is 1.4 x 10^7 $M_\odot$ then the total mass of A is $\geq$ 1.2 x 10^7 $M_\odot$, while the mass for B is $\leq$ 2 x 10^6 $M_\odot$. The best-fit indicates a mass of B of 5 $\times$ 10^5 $M_\odot$ and a ratio of $M_{old}/M_{young} = 0.04$. Using the extinction estimate of Christopher (2009) of $A_k = 0.54$ for this region in NGC 4038/39 we can calculate an extinction corrected cluster mass of 1.9 x 10^7 $M_\odot$. The total mass estimates (both extinction and non-extinction corrected) agree well with that calculated by Gilbert et al. (2000) (1.6 x 10^7 $M_\odot$) using the Lyman continuum flux of cluster 89/90 for a Salpeter IMF between 1 and 100 $M_\odot$. Thus

the young component of cluster 89/90 likely is one of the most massive young star clusters which formed in the Antennae galaxies. The 90 % confidence limit for the mass ratio is roughly 0.02 - 0.12 though this value changes slightly between different ages of A. Thus we have clearly detected the PMS in the cluster. A mass ratio of 0 and therefore $M_{old} = 0$ is ruled out as well as a mass ratio ≥ 0.12 and thus no PMS contribution.

Using our best-fit model we can also estimate the number of Lyman continuum photons and compare this to the number estimated through the radio flux by Neff et al. 2000. We find $Q_{Lyc} = 8.05\ ^{+0.58}_{-0.58}$ x $10^{52}\ s^{-1}$ using S99 with our best-fit model parameters which compares well with the value of $Q_{Lyc} = 8.46$ x $10^{52}\ s^{-1}$ derived by Neff et al. 2000.

The probability for the IMF of A rises strongly towards steeper slopes with the probability being highest for a Salpeter slope below 1 $M_{\odot}$. However the spectrum is formally consistent with a slope down to a power-law slope of 1.5 within a 90% confidence limit. This result is consistent across all ages of the young population. A top-heavy IMF weighted more heavily towards high-mass stars than a Kroupa (2001) IMF has often been cited as expected for SSC clusters and the best remaining evidence of an unusual IMF in a SSC (M82-F) indicates a top-heavy IMF. Our result is consistent with a normal Galactic IMF (Covey et al., 2008) as well as a Salpeter IMF down to 0.1 $M_{\odot}$. A low-mass cutoff in this cluster is ruled out since PMS objects in the young burst below 1.0 $M_{\odot}$ are required to produce the observed spectrum.

We did not include any slopes steeper than Salpeter as the goal of this study was not to make claims of extraordinary IMF results within the limited data this cluster offers. In addition, the best-fit model for the two-burst model at a Salpeter slope shown in Figure 3.4 is a very good fit to the data whereas for the single burst even a Salpeter slope did not fit the data well. This is independent of the probability curve which was shown to illustrate the overall trends of the models rather than the quality of the fits. Thus we feel it is reasonable to set the cutoff at the Salpeter slope even though the IMF probability is still rising.

3.3.2 Caveats

Our model has many components and therefore degeneracies exist between its different subsets. One such degeneracy exists between the assumed age of the PMS objects and the IMF slope. Since PMS objects grow fainter as they age one might erroneously assign an IMF that is too flat to a 1 Myr cluster that is really 3 Myr old. However, Figure 3.5 shows that our IMF results are very similar at different assumed ages for the young burst and thus we do not expect this to be a problem. Another concern is that the calculated nebular emission is wrong and this might affect the results of our models. We varied the input nebular continuum by 50% in both directions which did not change our results substantially. We can also use this to understand how sensitive our IMF measurements are to extinction in the region. Varying the nebular continuum in this manner represents an overall change

in the K-band and H-band luminosity of the cluster by ± 11.75 % and ± 9.55 % respectively. This corresponds to an increase or decrease of near-infrared extinction affecting the cluster of $A_k = {}^{+0.13}_{-0.12}$ and $A_h = {}^{+0.11}_{-0.10}$. No direct extinction measurements exist for this cluster though the region of NGC 4038/39 the cluster is located in has been estimated to have an extinction $A_k = 0.54$ by Christopher (2008). Thus the range of extinction covered by our ± 50% variation in nebular emission (A_k = 0.25) is roughly comparable to the overall extinction estimated for the cluster.

In addition there are limits to the inputs of our models. Our standards are field dwarfs with high surface gravity, while PMS objects are young and have lower surface gravity than dwarfs. The surface gravity of PMS objects is generally between log(g) = 3.0 - 4.2 (Gorlova et al., 2003), while dwarfs are generally have log(g) = 5.0 - 5.5. This would increase the depth of the CO absorption features in our spectrum. Obtaining spectral standards of young PMS objects is difficult because the largest nearby sample is found in relatively distant young clusters, making it observationally expensive to obtain a complete high signal-to-noise sample in the near-infrared. Since we used spectral standards to model our spectra rather than synthetic spectra our coverage of individual spectral types is not complete. This might cause errors in the depth of the absorption features of our model spectra due to binning the stars into spectral types for which spectral coverage exists. However, this effect is likely small compared to the error introduced by the usage of dwarf rather than PMS standards. Since synthetic spectra struggle to accurately model low-mass young

PMS stars (Doppmann et al., 2003), currently dwarf standards remain the best option to accurately model the near-infrared spectra of SSC. However, PMS stars generally lie closer to field dwarfs than supergiants in surface gravity (Gorlova et al., 2003) and it is thus likely that even including PMS standards would not remove the need of having a supergiant component in our models. The presence of veiling due to disks around young stars can dilute the absorption features in near-infrared spectra. We do not have an independent method of quantifying the effect veiling has on our data since we are modeling a whole star cluster but we expect the effect to be minimized because since we can expect all our absorption lines to be similarly affected. Finally in some very young objects, CO features can be seen in emission due to the presence of a disk (e.g. Blum and McGregor (2008)). We do not observe evidence for this in our spectrum.

3.4 Discussion

3.4.1 Previous Work

We have shown that it is possible to directly detect PMS stars in unresolved SSC as well as place some constraints on the underlying IMF and age of the cluster. Substantial work has been done studying the IMF of SSC through measurements of mass-to-light ratios, including in the Antennae. Mengel et al. (2002) measured mass-to-light ratios in the K-band for a number of clusters in NGC 4038/9 and found variations indicative of IMF variations in the clusters. To measure mass-to-light

ratios in clusters younger than $\approx$ 30 Myr requires the ability to constrain velocity dispersions through strong CO absorption bands that exist in clusters dominated by red supergiants. Bastian et al. (2006) used UV spectra of clusters in two merger remnants with ages of more than 300 Myr to measure their mass-to-light ratios and found them to be consistent with a Kroupa IMF. Similarly Larsen et al. (2004) and Larsen and Richtler (2004) measured mass-to-light ratios in older clusters through optical spectroscopy and found them to be consistent with a Kroupa IMF. This dichotomy: young clusters with varying mass-to-light ratios and older cluster with mass-to-light ratios consistent with normal IMFs provides evidence that something other than IMF variations are the cause of varying mass-to-light ratios in young SSC or that perhaps SSC with unusual IMFs get disrupted preferentially. This work shows an avenue for providing more concrete measurements of IMFs in SSC.

Work on modeling the integrated spectra of young clusters has up until now been done mostly in the UV and optical (e.g. Tremonti et al. (2001)) because of the strong signatures of massive stars at these wavelengths. The near-infrared is ideally suited to detect the low-mass stellar content of the clusters as well as evolved giants and supergiants. Brandl et al. (2005) attempted to use near-infrared colors of clusters in the Antennae obtained with seeing-limited observations in combination with thermal radio images to constrain their properties and found them to be uncorrelated. However, Antennae are distant enough that multiple stellar populations of different ages may be treated as unresolved point sources. We have shown that it

is possible to constrain the properties of young star clusters through near-infrared spectroscopy. Varying nebular emission due to the ionizing radiation emitted by hot stars provides an additional complication in the understanding of the youngest clusters. The total amount of free-free and free-bound emission in young clusters is easiest to constrain empirically, because it should depend strongly on the formation environment of the cluster. More work is needed studying nearby SSC in the near-infrared to understand whether near-infrared images and spectroscopy can accurately predict the ages and masses of these clusters.

3.4.2 Scales of Star Formation

What can cluster 89/90 tell us about the scales of star formation in the Antennae galaxies as well as locally? The spectrum of our cluster likely contains two separate underlying populations with an age spread between 6-18 Myr and a mass ratio $M_{old}/M_{young} \leq 0.2$. At the distance of the Antennae our 1" slit covers a region of $\approx$ 90 pc. This region likely contains two massive clusters, one with a mass of order 10^7 $M_\odot$ and the other of order 10^6 $M_\odot$. It is possible the older cluster started out at a higher mass and lost a large fraction of its mass due to dynamical evolution. How does this compare to sites of massive star formation we can study in detail?

No young 10^6 $M_\odot$ clusters exist in local group galaxies. However massive sites of star formation (up to roughly 10^5 $M_\odot$) are accessible in both the Milky Way and the LMC. Grebel and Chu (2000) present detailed observations of Hodge 301, a cluster

in the 30 Doradus star forming complex. Hodge 301 is between 20-25 Myr old and lies at a distance of 3' ($\approx$ 44 pc) from the young center of 30 Doradus, R136. It is estimated to have been relatively massive with an initial mass of up to 6000 $M_{\odot}$ though less massive than R136 ($\approx$ 30000 $M_{\odot}$). In the Galaxy, NGC 3603 and the Arches cluster, two of the most massive star forming regions in the Milky Way do not appear to have similar older star formation complexes in their proximity, though both have isolated red supergiants in their younger stellar environments. Melo et al. (2005) found the typical separation of young super-star clusters in M82 to be $\approx$ 12 pc though the equivalent age spread of the clusters is not given. Christopher (2008) found that half of their Antennae NIRSPEC cluster sample with 1" resolution contained more than one star cluster which would indicate a larger typical star cluster separation than in M82. Christopher (2008) also found some sources in their Antennae sample with no obvious cluster superposition which contained emission lines as well as CO bandheads simultaneously. This raises the question whether some SSC have non-instantaneous bursts of star formation over the size of the cluster and about the magnitude of this age spread.

Cluster 89/90 illustrates the need to study massive star forming regions in detail at a distance where the individual cluster complexes can be resolved from each other. Neff and Ulvestad (2000) found radii of $\approx$ 3 pc for the thermal radio sources in NGC 4038/9. This distance corresponds to 0.03" in the Antennae. If we assume a typical star cluster separation of 12 pc, the distance at which a 1" spectrum can resolve this

distance is $\approx$ 2.5 Mpc. More distant galaxies make ideal targets for observations with adaptive optics (AO) equipped with integral field unit (IFU) spectrographs.

CHAPTER 4

APPLICATIONS TO STARBURST NGC 253

We now turn to modeling a young cluster in the starburst NGC 253. NGC 253 is a nearby (d = 3.9 Mpc (Karachentsev et al., 2003), 1" = 19 pc) nearly edge-on spiral galaxy with a star formation rate of 17.4 $M_{\odot}\ yr^{-1}\ kpc^{-2}$ (Kennicutt, 1998) which contains an extremely active nuclear starburst region. Its star formation rate places it in the middle of the starburst sample used by (Kennicutt, 1998) compared to roughly 0.001 - 0.1 $M_{\odot}\ yr^{-1}\ kpc^{-2}$ in normal disk galaxies. The majority of near-infrared emission from the galaxy is emitted by the inner 100 pc (Forbes et al., 2000) indicating the intensity of the starburst occurring in the nucleus of the galaxy. The starburst is thought to be fueled by a bar that conveys gas into the nucleus of the galaxy (Engelbracht et al., 1998). The exact position of the nucleus of NGC 253 remains unclear (Müller-Sánchez et al., 2010). It is either associated with a bright radio source TH2 which is not detected at other wavelengths, which would make it similar to the Galactic Center, or with an X-Ray source separated by $\approx$ 4 pc which would make the nucleus a low luminosity AGN (Müller-Sánchez et al. (2010); Fernández-Ontiveros et al. (2009)).

A number of young star forming regions have been identified in the nuclear region of the galaxy through radio images (Johnson et al., 2001) as well as near-infrared

and mid-infrared imaging and spectroscopy (Alonso-Herrero et al. (2003); Kornei and McCrady (2009); Keto et al. (1999)). Most of the star formation seems to lie on a ring around the nucleus at a distance of $\approx$ 50 pc (Forbes et al., 2000). Johnson et al. (2001) found five massive star clusters in NGC 253 with purely thermal radio emission indicative of an age $\leq$ 3 Myr only one of which is positively associated with a compact optical object. High levels of extinction obscure the other clusters at optical wavelengths. All lie within 150 pc of the nucleus of the galaxy. The cluster population in the nucleus of NGC 253 has also been studied at sub-arcsecond scales with the VLA by Fernández-Ontiveros et al. (2009) who find a total of 37 near-IR sources, most of which are likely star clusters of varying masses and ages. We focus on the brightest near-IR cluster in the galaxy, which is located at a distance of $\approx$ 4" (76 pc) from the kinematic center of NGC 253. .

We obtained spectra of this cluster which is also a thermal radio source estimated to contain up to 319 O7 stars (Johnson et al., 2001). In our analysis we found this object in NGC 253 to have a complex morphology with a young central cluster ($\leq$ 3 Myr) surrounded by an older background population containing red supergiants. Some of this morphology can be seen in near-infrared images of the cluster (e.g. Kornei and McCrady (2009); Fernández-Ontiveros et al. (2009); see also Fig. 4.1). Near-infrared spectra of the same object were also obtained by Kornei and McCrady (2009) though those spectra did not differentiate between background and central cluster spectra due to lower spatial resolution.

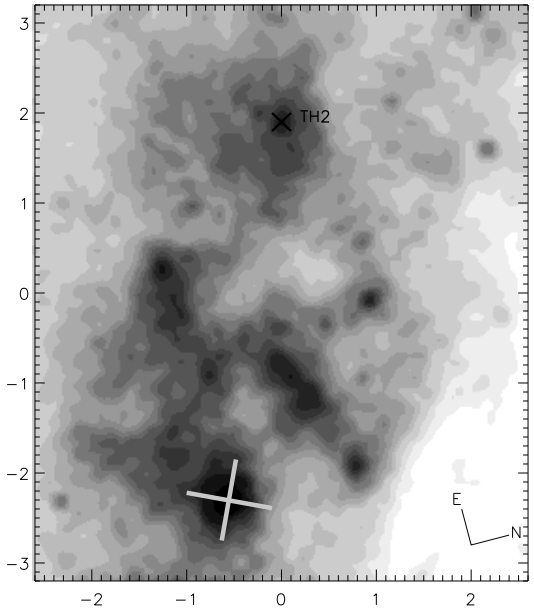

Figure 4.1 Image of the nuclear region of NGC 253 from HST NICMOS in the K-band. The scale of the image is roughly 5.2" X 6.5". The light cross marks the position of the near-infrared peak which coincides with our cluster and shows the two observed spectral orientations as well as indicating the lenth of the slit. The position of TH2, the presumed nucleus of the galaxy, is also marked.

In the following sections we present an analysis of the cluster H- and K-band spectrum similar to that presented in Chaper 3. Section 4.1 describes the observations and data reduction. Section 4.2 describes the modeling details for this cluster. The analysis of the spectrum, which constrains the nature of the cluster, is presented in section 4.3. Section 4.4 puts our results in context with previous work and describes the limitations of the study.

4.1 Observations and Data Reduction

K- and H-band spectra of our source were obtained over two nights (11-21-2007;11-22-2007) with the OSIRIS spectrograph at the 4m SOAR telescope on Cerro Pachon, Chile. The spectra were obtained with the OSIRIS high-resolution longslit which measures 0.42" x 72" with a spectral resolution of R $\approx$ 3000 (2 pixel). The slit was centered on the near-infrared source peak and observations were obtainted in sets of four, offset from each other across the slit by 5". In the K-band, two orientations offset by 90 degrees from each other were taken while only one orientation was obtained in the H-band. The median seeing for both nights was below 1". The two K-band orientations obtained were at PA = +60.9 degrees and PA = +150.9 degrees while the H-band spectra were obtained at PA = +60.9 degrees East of North. See Fig. 4.1 for an image of the nuclear region of NGC 253 from archival HST NICMOS observations with the slit orientations marked.

Total on-source integration in the K-band was 120 min with 60 x 120s exposures. Total on-source integration in the H-band was 80 min with 40 x 120s exposures. Between sets of observations the grating tilt was changed slightly to remove any fringing which can affect high-resolution OSIRIS spectra. Telluric standards were obtained within 30 minutes and 0.1 airmasses of all individual spectra to ensure the best possible correction. An A0V standard was used and a high signal-to-noise spectrum of Vega was used as comparison (see Vacca et al. (2003) for a detailed description of this method). The benefit of using an A0V star is that it is largely

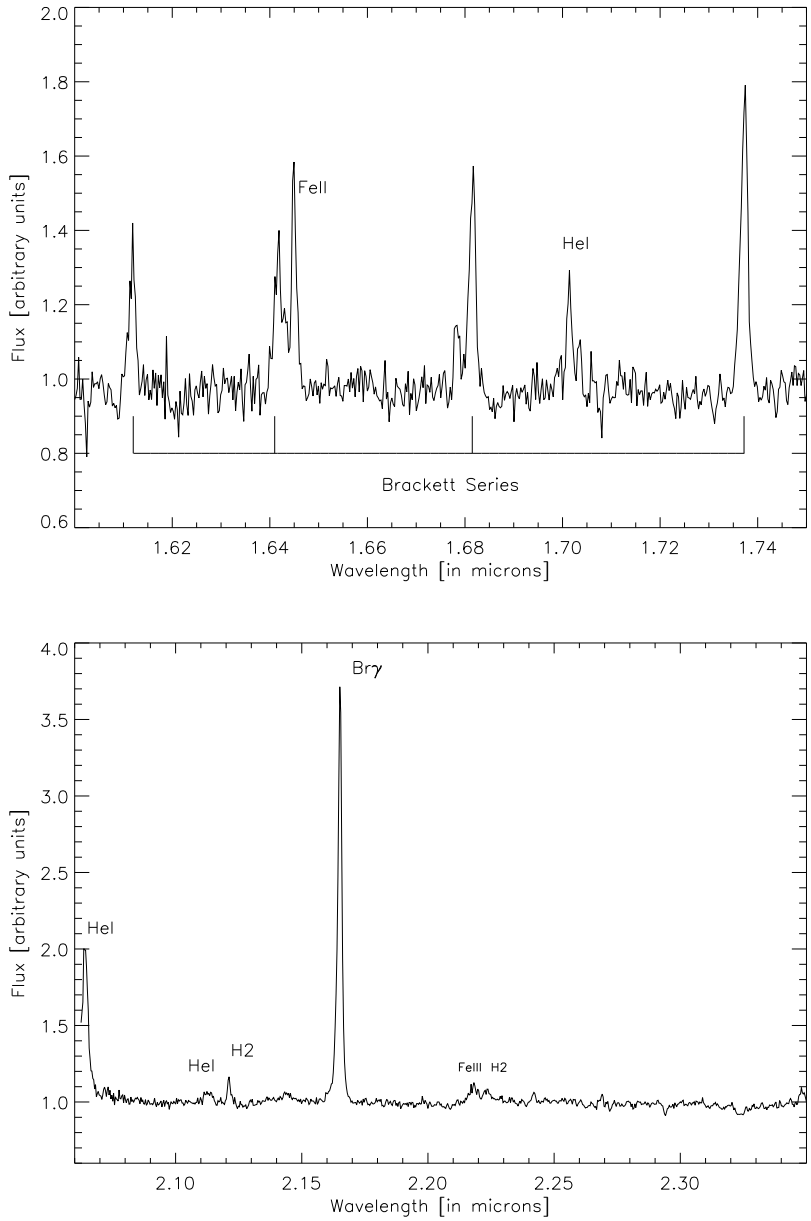

Figure 4.2 Normalized combined OSIRIS H- and K-band cluster spectra. Emission lines which are indicative of the presence of hot stars in the cluster are marked. CO absorption bandheads in the K-band at 2.29 μm are barely visible at this scale.

featureless except for hydrogen absorption lines. These lines are often broadened by rotation however and then need to be adjusted to match the model spectrum of Vega. In our case when comparing our spectrum to the Vega spectrum we found that the hydrogen absorption lines in the telluric standard were extremely well matched in depth and width and did not need to be adjusted. We then divided the telluric standard by the Vega model scaled to match the observed flux of the standard to obtain the telluric spectrum.

The spectra were extracted with a combination of standard IRAF and custom IDL routines. Individual spectra were sky-subtracted by subtracting subsequent observations offset by 5" from each other. The images were then divided by normalized flatfields and finally extracted before being corrected for telluric absorption and summed. The extraction process is described in more detail below. Both spectral orientations in the K- and the single orientation in the H-band showed a remaining galaxian background after sky subtraction most likely due to a population of stars in the region surrounding the central young cluster. Great care was taken to remove this background as it contains CO absorption indicative of the presence of red supergiants and has the potential of contaminating the cluster spectrum which contains the same absorption bands at much weaker levels.

In the K-band the shape of this background varied between the two orientations, one orientation showing a linearly increasing background beneath the cluster peak while the other orientation showed a background well fit by a broad resolved gaussian

distribution. The average flux level of the complex variable background compared to the cluster was $\approx$ 30 %. When fitting this remaining background an important question to answer was whether our limitations in fitting the complex shape of the background dominates the errors or whether the errors are dominated by RMS noise in this background. We found that while errors in fitting the background shape existed, the overall errors in the fit were dominated by RMS noise. The overall level of the two varied between different sets of observations but overall we found that $\leq$ 15 % of the errors in the background fit are generated due to systematic errors in the fit of the shape of the galaxian background while the remaining are due to RMS noise. Thus we conclude that the errors in the fit are dominated by the RMS noise in the background rather than any systematic variations.

In addition we compared the final extracted combined K-band spectra from the two orientations. Any difference in depth of absorption lines beyond that expected from errors in the individual measurements between spectra from the two orientations could indicate issues with the background subtraction. We measured the equivalent widths of these CO absorption lines for both orientations and they agreed to within their errors where the errors are dominated by our ability to fit the continuum around the absorption bands ($EW(CO_1) = 5.2 \pm 0.6$ $\mathring{A}$; $EW(CO_2) = 5.6 \pm 0.7$ $\mathring{A}$). We also found that a difference spectrum constructed by subtracting K-band spectra of the two orientations showed no structure around the CO bandhead at 2.29 μm. The RMS around 2.19 μm of a section of continuum of this

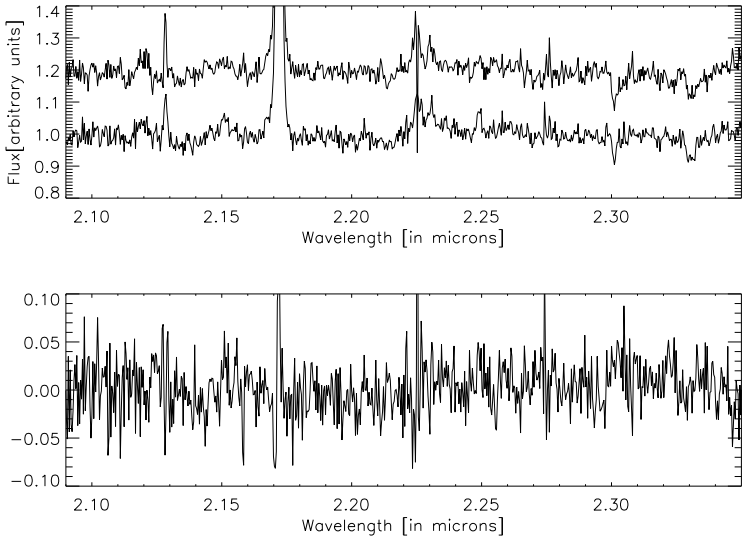

Figure 4.3 Co-added K-band cluster spectra from two positions offset by 90 degrees in the spatial dimension together with a difference spectrum. The RMS of the residuals does not change at the location of the CO(2-0) bandheads indicating no contamination caused by erroneous background subtraction.

difference spectrum was 0.022, while the RMS of the location of the CO bandhead was 0.027 between 2.29-2.32 μm, both of which are consistent, assuming a signal-to-noise rate of ≈ 30 for each individual spectrum. This indicates that background subtraction is consistent for both spectral orientations even though the overall shape of the background varied between the two orientations. We thus conclude that our final extracted K-band spectra of the cluster are not contaminated by the galaxian background.

The final H- and K-band cluster spectra are shown in Figure 4.2, while K-band spectra of the two orientations together with the residual spectrum are shown in Figure 4.3.

4.2 Modeling

4.2.1 Nebular Emission

To estimate the thermal free-free and free-bound emission in the cluster we used the thermal radio data of the cluster obtained by Johnson et al. (2001) (Our cluster is their source 2 in NGC 253). This data can then be used to estimate the contribution of nebular emission to the near-infrared flux. Using the radio flux from the datapoint with the shortest wavelength which is least susceptible to non-thermal emission (1.3 cm) $F_{1.3cm}$ = 33.6 x 10^{24} erg $s^{-1}Hz^{-1}$ and the formula by Condon (1992):

$$Q_{\rm Lyc} \geq 6.3 \times 10^{52} \left(\frac{T_e}{10^4\ {\rm K}}\right)^{-0.45} \times \left(\frac{\nu}{\rm GHz}\right)^{0.1} \times \left(\frac{F_{nebular}}{10^{27}\ {\rm erg\ s^{-1}\ Hz^{-1}}}\right) \tag{4.1}$$

we obtain $Q_{\rm Lyc} \geq$ 3.3 x 10^{51} s^{-1} which corresponds to $\approx$ 100 O5 stars. We believe this value to be consistent with the values derived by Alonso-Herrero et al. (2003) (Q_{Lyc} = 1.4 x 10^{53} s^{-1}) through the Pα flux over an $\approx$ 33" X 53" field of view and Engelbracht et al. (1998) (Q_{Lyc} = 1.0 x 10^{53} s^{-1}) through Brγ narrowband images over a 15" aperture of the nucleus of NGC 253. However, Kornei and McCrady (2009) derive a minimum ionizing flux from the Brγ luminosity of Q_{Lyc} = 1.0 x 10^{53} s^{-1} for this cluster alone. The source of this discrepancy is not clear. We assumed an electron temperature of 7500 K. We then convert this to a nebular flux in the H- and K-band following:

$$F_{nebular} = \left(\frac{c}{\lambda^2}\right) \times \left(\frac{\gamma_{total}}{\alpha_B}\right) \times Q_{Lyc} \tag{4.2}$$

Thus F_{nebK} = 1.88 x 10^{-13} and F_{nebH} = 3.33 x 10^{-13} erg s^{-1} μm^{-1} cm^{-2}. This corresponds to 4.8 % and 10.8 % of the broadband K- and H-band fluxes respectively. When incorporating the nebular flux into our models we adopted these values. We consider these percentage minimum values since the broadband magnitudes may include some background emission and possibly overstate the cluster's nebular emission. However as is detailed in later sections this does not influence our IMF slope determination.

4.3 Analysis

We analyzed three separate sets of spectra: cluster, cluster+background and a set of background spectra. The background spectra were extracted for two reasons. First, to ascertain again that our cluster spectrum was not contaminated by any significant background emission. Second, to understand the nature of the background which can help us understand the star formation history of the larger region.

Four different K-band background spectra were extracted, on either side of the cluster in both orientations. The extracted background spectra were quite different in flux level and they were normalized before combining them into a final background spectrum. We also compared the CO absorption depths of the separate background spectra to make sure they agreed to within the errors and they did. The cluster+background spectrum was extracted in the same manner as the cluster spectrum except with background subtraction turned off. In addition to comparing

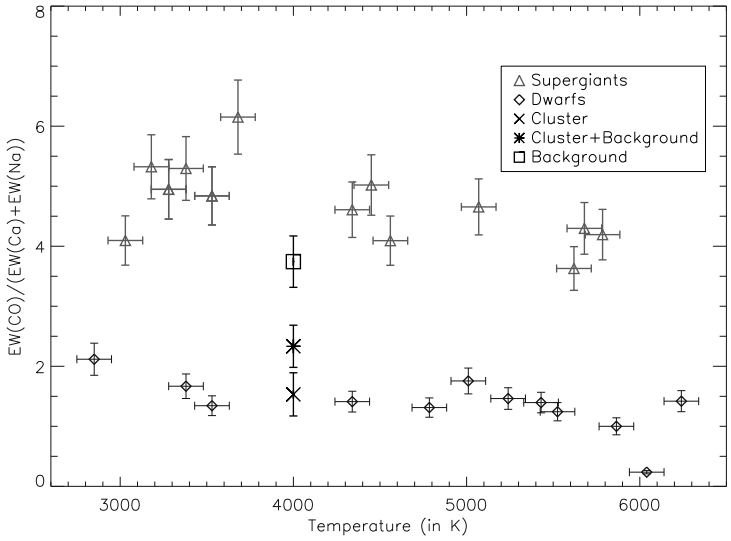

Figure 4.4 Plot of the ratio of equivalent widths of CO(3-1) 2.29 μm divided by the sum of the Ca 2.26 μm and Na 2.20 μm absorption features in supergiant and dwarf standards. A clear separation can be seen between supergiants and dwarfs in this index. Overplotted are cluster, cluster+background and background only spectra at an arbitrary temperature. The cluster spectrum lies on the dwarf locus while the background spectrum fits the supergiant locus and the cluster+background spectrum is in between. This is further indication that we have successfully removed any background contamination in our cluster spectrum.

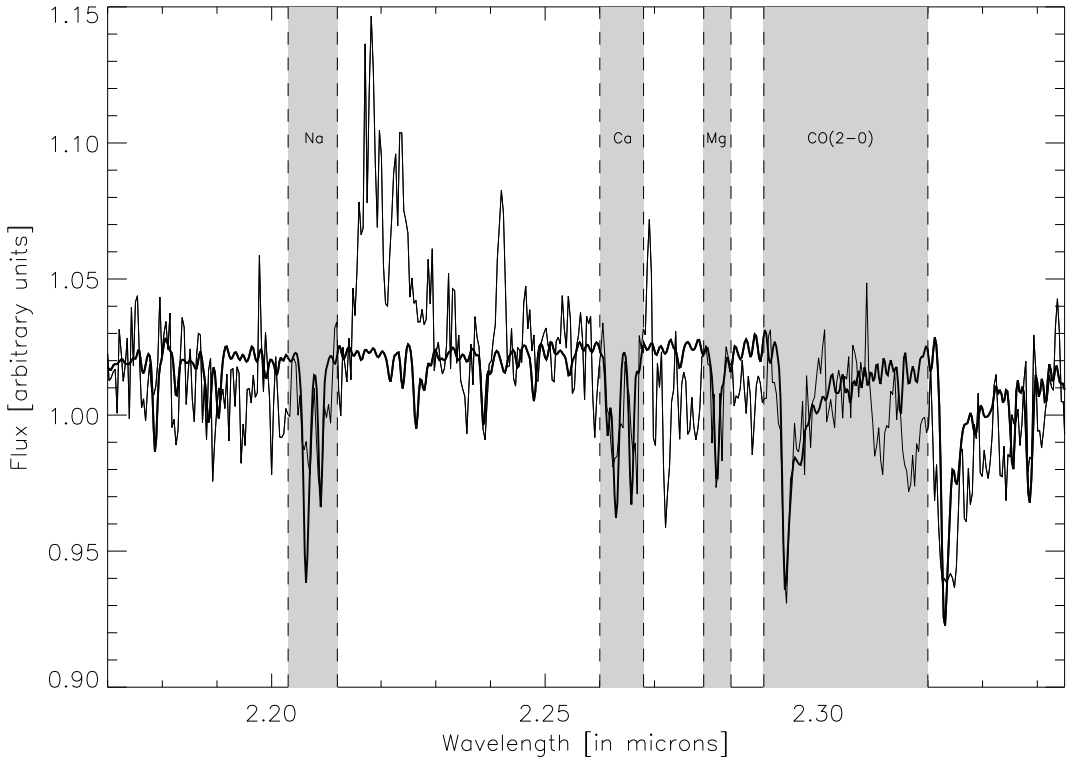

Figure 4.5 Best-fit model overlaid over a normalized scaled cluster spectrum. The bands used in our analysis are marked. The emission lines as well as large parts of the continuum were not included in the modeling. The best-fit reduced $\chi^2 = 1.18$.

spectra obtained at the two different K-band orientations (see Figure 4.3) we examined the surface gravity sensitive index discussed in Chapter 3 for the final cluster, cluster+background and background spectra as an additional safeguard.

This index combines the surface gravity sensitive CO(2-0) line with the Ca and Na lines in the K-band, the depth of which are not surface gravity sensitive (though the ratio of the sodium doublet is surface gravity sensitive). It allows us to differentiate between supergiant dominated older star cluster populations ($\geq$ 6 Myr) and

young clusters dominated by PMS and main sequence stars. Figure 4.4 shows a plot of this index for main sequence and supergiant standards with the computed index for the cluster, cluster+background and background spectra overplotted. The cluster spectrum matches the dwarf locus well while the background spectra agrees well with the supergiant locus. The cluster+background spectrum as would be expected lies in between the two being a mix of a young cluster and older population. Combined with the comparison between the spectra extracted from the two K-band orientations we are convinced that we have properly addressed the background subtraction to the best level possible and in the following sections we attempt to model and derive a best-fit IMF for the cluster spectrum as well as trying to better understand the background population.

4.3.1 Cluster

When determining the IMF in the cluster we rely on absorption lines which are produced by different mass ranges in the cluster. The CO (2-0) line at 2.29 μm, the Ca triplet between 2.26 and 2.27 μm and the Na doublet at 2.21 μm are mainly observed in stars below 0.5 $M_{\odot}$, while the Mg lines at 2.28 μm and 1.71 μm are due to stars between 0.5 - 1.5 $M_{\odot}$. We initially considered both the K-band and H-band spectrum in our analysis. However we could not positively identify the Mg line at 1.71 μm in the H-band spectrum as its signal-to-noise rate is much lower than the K-band spectrum (10-15 vs. 30-40 on average). There is also some evidence of

background contamination in the H-band spectrum not seen in the K-band. The ^{12}CO absorption line at 1.62 μm in the H-band, traces of which are present in our cluster spectrum is surface-gravity sensitive and generally much stronger in the spectra of supergiants than of dwarfs. As we did not observe two spectral orientations in the H-band and since the overall quality of each spectral image was lower we do not have a way to independently assess our background subtraction. Since the 2.28 μm Mg line is clearly present in our K-band spectrum we decided to only include the K-band cluster spectrum in our IMF modeling.

When modeling the cluster spectrum we considered a broken power-law IMF similar to a Kroupa IMF. Similar to both a Chabrier (2003) and Kroupa (2001) IMF we adopted a Salpeter (1955) slope above our break-point. We are not sensitive to massive stars in absorption lines although the emission lines in the cluster are due to ionizing radiation due to hot stars in the cluster. Below the break-point of 1 $M_{\odot}$ we varied the power-law slope between 0.00 and 2.35 in linear units in 0.5 dex steps since our χ^2 analysis shows that we are not sensitive to smaller variations. We considered PMS models of three different ages: 0.3, 1 and 3 Myr. We also varied the break-point of the IMF between 0.25 $M_{\odot}$ and 2 $M_{\odot}$ increasing the break-point by a factor of two in each step. We did not consider ages above 3 Myr as the 3 Myr models were not a good fit for any of the slopes considered and the attenuation of absorption lines above 3 Myr is quite steep as PMS stars are contracting and becoming less luminous. The level of nebular continuum simply attenuates the

absorption lines in our spectrum over the short wavelength range considered. The nebular continuum is thus degenerate with the assumed age for the model. Thus neither can be constrained by our model directly.

We also measured the equivalent widths of the emission lines in our extracted spectra. The cluster alone has a $Br\gamma$ equivalent width of 58.2 $\pm$ 3.2 $\mathring{A}$. The background spectra alone show an average $Br\gamma$ equivalent width of 18.4 $\pm$ 2.3 $\mathring{A}$. Combined with our best-fit model we can use the Brγ equivalent width of the cluster spectrum to infer an age for this cluster in NGC 253 using Starburst99, which generates $Br\gamma$ equivalent widths with respect to age. The age determined through this method is $\approx$ 5 Myr. Possible caveats for this age determination are extinction in the cluster, possible clumpiness of the gas in the cluster as well as uncertainties in the continuum level calculated by S99 in the near-infrared at young ages. Particularly at young ages S99 likely overestimates the level of continuum due to the nebular emission which would make this age an upper limit.

We performed a χ^2 analysis of our model results similar to Chaper 3 and have plotted the best-fit model overlaid over the cluster spectrum in Figure 4.5. The results of our χ^2 analysis as well as corresponding IMF probabilities are plotted in Figure 4.6. We have included only probabilities for models with ages of 0.3 Myr as the overall fit quality was worse for 1 Myr with the best-fit $\chi^2 = 1.40$. The best-fit IMF slope is $1.0\ ^{+0.5}_{-1.0}$ in linear units with a 99 % confidence limit for a model age of 0.3 Myr and for a break-point of 1 $M_{\odot}$. Slopes above 1.5 are ruled out.

We also tried to change the break point between 0.25 and 2 $M_{\odot}$. A lower break point means a cluster contains more low-mass stars compared to a cluster with an IMF with a higher mass breakpoint assuming the slope is kept constant. For 2 $M_{\odot}$ we found that 1.5 $^{+0.5}_{-0.5}$ (99 % confidence) in linear units becomes the best-fit slope. By shifting the break point to 0.5 $M_{\odot}$ (the same as a Kroupa IMF) we found we required a more shallow IMF slope to produce an adequate fit with a best-fit slope of 0.5 $^{+1.0}_{-0.5}$ (99 % confidence) in linear units.

The best-fit IMF slopes of 0.5 and 1.0 for breakpoints of 0.5 and 1 $M_{\odot}$ respectively contain a factor of 33 % and 50 % fewer low-mass stars than a Kroupa IMF (where a low-mass star is defined as an object with m $\leq$ 0.5 $M_{\odot}$). Though our IMF results are broad, an IMF with a slope steeper than 2.0 in linear units below the break-point is excluded for all IMF breakpoints. Based on these results dense nuclear starburst environments appear capable of producing a normal IMF.

4.3.2 Nature of the Background

To understand the formation history of this region in NGC 253 we also modeled the cluster+background spectrum in a simple way. We combined the best-fit cluster model with an older supergiant dominated cluster model at a varying mass ratio. The best-fit model is plotted in Figure 4.7. We did not attempt to conduct a detailed analysis: we more interested in qualitative than quantitative results since it is unclear whether the region surrounding our young cluster is a coherent population

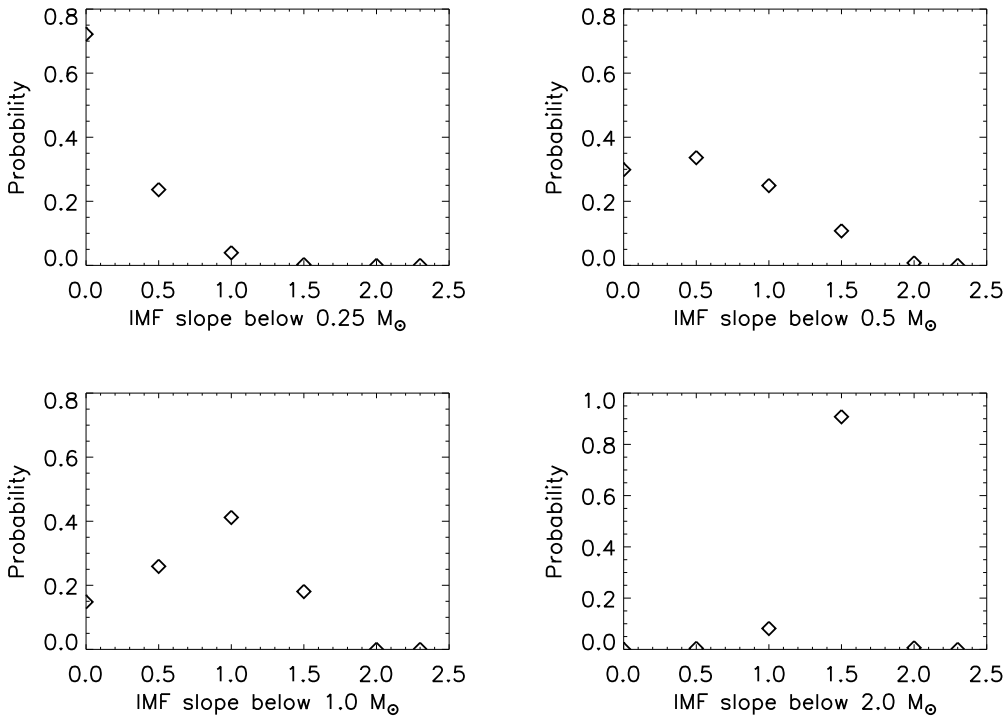

Figure 4.6 Plot of probabilities vs. IMF for 0.3 Myr and breakpoints between 0.25 - 2 $M_{\odot}$. Older models provided worse fits and are not included. As the IMF breakpoint decreases flatter IMF slopes become more likely.

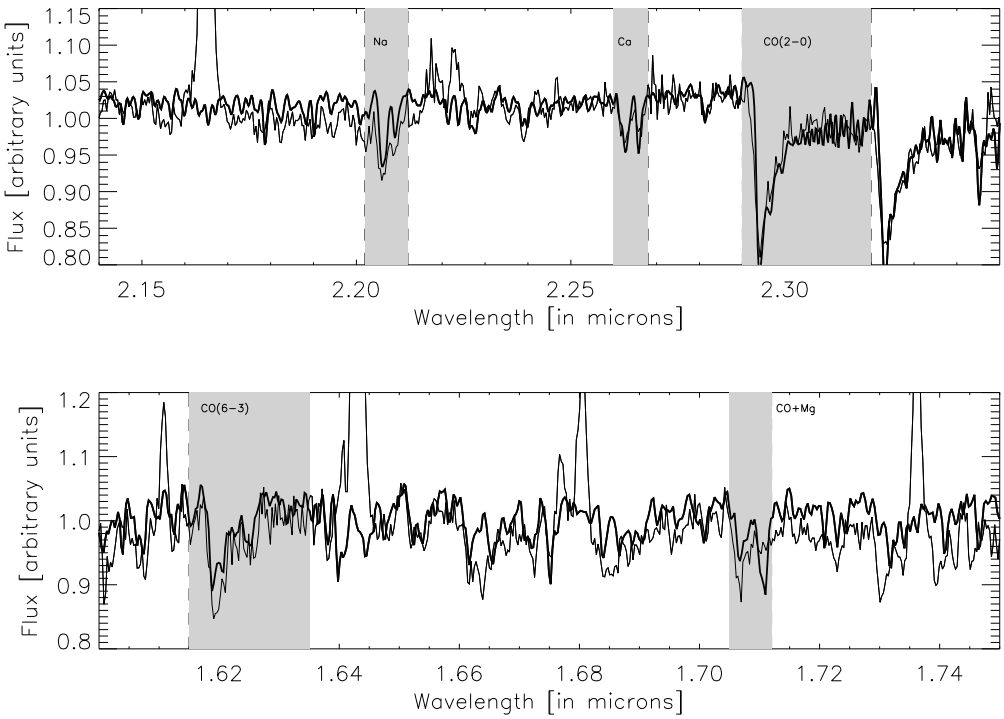

Figure 4.7 Best-fit model of a supergiant population plus a young cluster with the properties described in the text. Overplotted is the extracted cluster+background spectrum. Note the presence of surface gravity sensitive CO absorption bands in the H-band, which are well matched by a population of red supergiants with an age of 12 Myr.

or perhaps successive star formation events. The pure background spectra show that some emission lines are still present in this background region. Specifically the H2 line at 2.12 μm present in the cluster+background spectrum is equally strong in the background population and the cluster population as indicated by the equivalent width of the line in both the cluster spectrum and the background spectrum. The He I line at 2.05 μm is present in both cluster and background spectra though at reduced strength in the background, similar to $Br\gamma$. All three lines are produced by ionizing radiation due to massive stars and their presence in the background spectrum indicates that massive stars are still be present in this region. This may be an indication either that there are multiple generations of star formation present in the background population or that stars have been forming in this region continuously over several Myr. The best-fit simple population model for the background cluster has an age of 12 Myr. As is evident from Figure 6 the H-band spectrum is not a good fit to the model, particularly around the 1.71 μm Mg line, possibly indicating a more complicated star formation history than we model here, though the Mg line in the K-band is quite well matched.

4.3.3 Caveats

Similar caveats exist for our results with regard to NGC 253 as with regard to NGC 4038/39 presented in Chapter 3. We are limited by the stellar library of field dwarfs we use to model the spectra of PMS stars with lower surface gravity. The use of a

stellar library also limits our spectral coverage. Because we have limited information about the cluster we are trying to model it is possible that we may have assigned an erroneous age or nebular flux contribution. As in Chapter 3 we tried varying the nebular contribution by by 50% and found no significant effect on our results. Varying the nebular continuum in this manner represent an overall change in the K-band and H-band luminosity of the cluster by ± 2.4 % and ± 5.4 % respectively. This corresponds to an increase or decrease of near-infrared extinction affecting the cluster of $A_k = ^{+0.018}_{-0.017}$ and $A_h = ^{+0.059}_{-0.058}$. Kornei et al. (2009) estimated an extinction for this cluster of $A_k = 1.57$ using Fe 1.64 μm to Fe 1.64 μm line ratios while Alonso-Herrero et al. (2003) estimate $A_k = 0.4$ - 1.0 for the central region of NGC 253 using a H-K color map. Thus the range of extinction covered by our ± 50% variation in nebular emission ($A_k = 0.25$) exceeds the change in extinction estimated by the variation of ± 50% of nebular emission. Though ages older than 1 Myr provided bad fits to the cluster spectra we also tried models with ages between 0.3 and 1 Myr and found that while 0.3 Myr models provided the overall best fit the IMF, results returned by older models matched well with those of the 0.3 Myr models indicating that errors in age assumptions are not a dominant issue.

Since we performed a background subtraction which contains the same absorption lines as those which are used in our analysis it is possible that we have affected our results by imperfect background subtraction. We found no evidence in our surface gravity analysis or comparing spectra of different orientations of any systematic

contamination. Should there be any contamination it could cause us to either over- or under-subtract the background. Thus this could lead us to both over- and underestimate the absorption lines in our analysis. In particular the CO absorption line would be affected since the underlying contamination would be through a population of supergiants. Thus this would shift our IMF results erroneously towards steeper slopes.

4.4 Discussion

What can the IMF results in this cluster in NGC 253 tell us about the shape of the IMF in general and in this galaxy specifically? The only previous measurements of an IMF in the central region of NGC 253 have come from Engelbracht et al. (1998) who constrained the IMF in NGC 253 using near-infrared images and spectra combined with evolutionary synthesis models to derive an IMF overabundant in high-mass stars compared to a Basu and Rana (1992) IMF. Similarly to the results discussed for M82 in Chapter 1, this IMF is skewed towards low-mass stars more strongly than a Chabrier or Kroupa IMF and the IMF they derive is in reasonable agreement with a Kroupa or Chabrier IMF. It should be noted that their spectra targeted the near-infrared peak of NGC 253 which likely refers to the same cluster which is described in this chapter but over a much larger region ($\approx$ 12" aperture) than we study here. However that paper was focused on the overall properties of the galaxy rather than a specific cluster and for the photometry large apertures were used.

Our results come from a very different set of measurements. Since we focus on tracing stars just above and below the breakpoint in the IMF below 1 $M_{\odot}$ our measurements are in many ways complementary to those by Engelbracht et al. (1998) who are tracing mainly the output of massive stars. Given that our results are perfectly compatible with a Chabrier or Kroupa IMF we consider this an indication that a normal IMF is possible in nuclear super-star clusters such as this object in NGC 253.

Any indirect IMF measurements such as those presented in this chapter will always be prone to some modeling degeneracies. If IMF variations in this cluster compared to the field were present in the shape of an IMF breakpoint shifted to higher masses as well as a steeper slope below the breakpoint we would not be able to distinguish this from a lower mass breakpoint and a shallower slope. This is a shortcoming in using integrated spectra since the assumption of a variation in the IMF breakpoint with perhaps a simultaneous slope change is likely if the breakpoint is somehow correlated to the thermal Jeans mass in star forming clouds. We may be able to break this degeneracy by using a larger set of absorption lines not present in H- and K-band spectra which trace different mass ranges to give our measurements finer mass bins.

With mounting evidence that statistically significant IMF variations if they exist are modest a reasonable approach is to assume a "normal" IMF unless strong evidence presents itself that proves otherwise (Bastian et al., 2010). As such, more

measurements of the IMF in extreme regions of metallicity or star formation environment are needed which span a broad range of stellar masses.

This star forming region in NGC 253 appears to have a complex formation history with the presence of red supergiants as well as PMS stars over a 20 pc region though line-of-sight effects cannot be ruled out particularly because of the large inclination of NGC 253 which increases line-of-sight issues. The young cluster could be superimposed on a background of a larger diffuse region old enough to contain red supergiants. Since we can clearly distinguish the young cluster and the older (12 Myr) population in our spectra we can rule out a cluster with a continuous burst of star formation over several Myr. It is possible that this cluster is similar to the nuclear cluster in NGC 4244 (Seth et al., 2008) which has two distinct stellar populations though this cluster in NGC 253 is at a distance of roughly 80 pc from the presumed nucleus of the galaxy. If dynamical friction is one of the methods by which nuclear clusters are created as has been proposed in the past (Tremaine et al. (1975); Milosavljevic and Agarwal (2009)) then if our cluster remains bound it may end up in as part of a nuclear star cluster in NGC 253. If it disperses its stars may either disperse into the field of NGC 253 or also be accreted onto a nuclear star cluster.

CHAPTER 5

CONCLUSIONS: IMPLICATIONS FOR THE IMF AND CLUSTER FORMATION

5.1 Summary of Results

In this study we have constructed models of young super-star clusters using a combination of the pre-existing Starburst99 population synthesis models as well as a suite of our own models adapted to young clusters with the inclusion of pre-main sequence tracks. The primary purpose of these models is to constrain the IMF as well as the star formation history in young super-star clusters through comparison with near-IR spectra. To test our models on real datasets we obtained spectra of young super-star clusters in the merger NGC 4038/39 (the "Antennae") and the nuclear starburst NGC 253. Both systems were selected because of previous reports of unusual IMF measurements and because their properties (mass, environment etc.) make them good candidates in the search for IMF variations.

5.1.1 PMS Starburst Models

Our models are a combination of the population synthesis code Starburst99 and our own models which integrate treatment of pre-main sequence evolution. Pre-main sequence stars can have a significant influence on the flux of a super-star cluster at

ages younger than 6 Myr as discussed in Chapter 2 and their inclusion is important if one wants to study the properties of clusters younger than this age.

Our approach utilizes analysis of stellar absorption bands in the H- and K-band originating from different stellar mass ranges ($\leq$ 0.5 $M_{\odot}$; 0.5 - 1.5 $M_{\odot}$) to constrain the IMF. We generate integrated synthetic cluster spectra using a library of near-infrared spectra which can then be compared to observations to determine a best-fit IMF. Though our model is optimized for young clusters it can also generate synthetic spectra of older clusters dominated by red supergiants. We demonstrate that for clusters with an age younger than 3 Myr it is possible to detect IMF variations down to $\pm$ 0.25 dex in linear units depending on the signal-to-noise of the data and the accuracy to which the age of the cluster is known.

Our target selection is currently limited to clusters with available radio data which present the best and easiest way to detect young clusters unambiguously. Other corresponding multi-wavelength data is often not present or not cohesive. Since different wavelengths generally trace different stellar populations, more readily available multiwavelength datasets would improve age constraints on young clusters and give insight into star formation histories of individual clusters.

5.1.2 NGC 4038/4039

Our first target was a massive young cluster in the overlap region of the Antennae (d = 19.2 Mpc). The H- and K-band spectra of the cluster (Cluster 89/90 in Whitmore

and Schweizer (1995)) contain both emission lines indicative of young hot stars as well as late-type absorption lines. However these absorption lines show evidence of the presence of both PMS stars as well as red supergiants. Due to the distance of the Antennae the obtained spectrum covers a large region of physical space ($\approx$ 90 pc) and we interpret the spectrum as being due to two separate star clusters of different ages.

Our models indicate the presence of a young ($\leq$ 3 Myr) massive star forming region that dominates in mass (by a factor of five) a second stellar population (12 $^{+6}_{-6}$ Myr within 90 % confidence) old enough to contain red supergiants. Comparing these models to the K-band magnitude of the region we derive a total mass of 1.4 x 10^7 $M_\odot$ (extinction corrected: 1.9 x 10^7 $M_\odot$). We also derive limits on the IMF of the young cluster and find the IMF to be consistent with a Chabrier or Kroupa IMF though the best-fit IMF is a Salpeter slope down to 0.1 $M_\odot$. We derive slopes of 1.5 - 2.35 within 90 % confidence. We rule out a low-mass cutoff in this cluster in the Antennae.

5.1.3 NGC 253

The second cluster studied in this work is a massive young cluster (Cluster 2 in Johnson et al. (2001)) in the nuclear region of the spiral galaxy NGC 253. Due to the galaxy's proximity (d = 3.9 Mpc), the cluster's brightness in the near-infrared, as well as its location near the nucleus of NGC 253 this target is ideal to search for

IMF variations. We find that our spectra are best explained as a young cluster (≤ 3 Myr) sitting in front of a background of older stars which contains red supergiants. After carefully subtracting this background and performing several tests to quantify residual errors we find that the young cluster shows clear evidence of the presence of PMS stars.

We modeled the cluster properties as was done for the cluster in the Antennae and found a best-fit IMF slope below 1.0 $M_{\odot}$ of $\alpha = 1.0\ ^{+0.5}_{-1.0}$ within 99 % confidence which is consistent with a Chabrier IMF. Note that all IMF slopes quoted in this section are in linear units. We found similar results for an IMF breakpoint of 0.5 $M_{\odot}$ though the best-fit slope in this case was $\alpha = 0.5\ ^{+1.0}_{-0.5}$ within 99 % confidence compared to a Kroupa IMF with a slope of 1.3 below 0.5 $M_{\odot}$. Thus there is slight evidence that this cluster in NGC 253 may have an IMF deficient in low-mass stars compared to a Kroupa IMF though the IMF slopes allowed by our models are quite broad. Both a Kroupa and a Chabrier IMF are consistent with out results. An additional measurement of a second cluster in NGC 253 with a higher signal-to-noise level would be very useful in refining our results.

5.2 Discussion

5.2.1 Implications for the Shape of the Low-Mass IMF

Our technique has allowed us to detect directly low-mass stars in two super-star clusters and thus for the first time provide measurements of the low-mass IMF in

such objects. In this section we discuss the implications our results in NGC 253 and NGC 4038/39 have for the shape of the low-mass IMF in extreme regions of star formation in combination with previous work. It is important to remember that previous work on the IMF in unresolved super-star clusters has come mostly through analysis of the integrated properties of the cluster stellar population such as mass-to-light ratios (e.g. Bastian et al. (2006)). Those studies do provide a host of information that is complementary to our work such as dynamical mass estimates and independent age estimates. In contrast our work can trace two distinct mass ranges which allows for a much more robust IMF measurement even if the errors on derived slopes remain large.

Since our study uses high signal-to-noise spectroscopy it is observationally expensive and we are limited to studying a small sample of clusters younger than 3 Myr. Compared to photometric studies (e.g. Whitmore et al. (1999)) which study cluster populations over whole galaxies we will always have smaller samples. We require the starburst in the galaxy to be ongoing so that massive young clusters are present and the greater the distance the more massive and thus brighter the cluster must be. Despite the small sample, the targets that are accessible are generally objects in which a search for IMF variations is warranted. However we are left with trying to draw conclusions about global IMF properties from a small sample.

With the caveat of a small sample to bear in mind, the IMF results from our two targets indicate that low-mass stars can form with the same frequency in super-star

clusters as in local star forming regions in the Milky Way. Since our IMF diagnostics trace objects below 0.5 $M_{\odot}$ we in effect rule out a low-mass stellar cutoff in both of our targets though we have no information below the hydrogen burning limit. The results from NGC 253 indicate that super-star clusters with solar metallicity in the intense radiation environment of a galactic nucleus produce an IMF that is consistent with that measured in the field of the Milky Way. Combined with other evidence on the universality of the IMF above 1 $M_{\odot}$ in extreme regions of star formation such as R136 (Andersen et al., 2009), the Arches (Espinoza et al., 2009) and Westerlund 1 (Brandner et al., 2008) our results seem to indicate that no large IMF variations exist in SSC though smaller variations in the low-mass IMF are not ruled out by our results. More data in other super-star clusters would be very valuable in confirming these results in particular with respect to metallicity since both of our targets have solar metallicity.

And yet claims remain that it is possible to change the conditions for star formation enough that the IMF changes. The first stars are thought to have formed with an IMF with an overabundance of massive stars compared to the present-day form due to inefficient cooling of gas by molecular hydrogen (e.g. Tumlinson et al. (2004)) though recent improvements in measurements of the cooling behavior of metal-free gas may challenge these results (Kreckel et al., 2010). Observational evidence supports this assertion due to the non-detection of Population III stars as well as the predictions of an IMF skewed towards high-mass stars due to properties of

low metallicity stars in the Galactic halo (Tumlinson, 2006). The theoretical predictions as well as the observation evidence remain the single strongest argument that IMF variations are possible. The question remains at what metallicity the shape of the IMF begins to change (Omukai et al. 2005) and whether an object such as SBS 0335-052 can be studied in enough detail to investigate the IMF of its massive young clusters with our technique. It is important to note that there are also simulations of Population III stars which indicate that metallicity is not the deciding factor in causing a changing IMF even at very low metallicities (Jappsen et al., 2009) and instead suggest that other factors such as dust cooling (which may be present down to $10^{-6}Z_{\odot}$) play a more important role in shaping the IMF of the first stars.

5.2.2 Thoughts on Cluster Formation and Evolution

Both regions in this study appear to have a complicated star formation history over modest spatial scales. In NGC 253 a young cluster sits in front of a background population of older stars which contains red supergiants and thus implies a minimum age of ≈ 6 Myr (Leitherer et al., 1999). However emission lines are present in both the older background as well as the young cluster possibly indicating the presence of young massive stars in both. The young cluster shows late-type absorption lines due to low-mass PMS stars and must thus be younger than 3 Myr. Kornei and McCrady (2009) find a similarly complex star formation history for our source in NGC 253 due to the fact that their near-infrared spectra, which do not separate the young

cluster and background population show both strong CO absorption bandheads and recombination lines due to massive young stars in the cluster. Multiple generations of star formation have now been observed in several nuclear star clusters (e.g. Seth et al. (2008); Walcher et al. (2006)). There are several proposed theoretical formation mechanisms for nuclear clusters with multiple age populations. Seth et al. (2008) prefer a scenario where nuclear star clusters form through accretion of either gas or already formed young star clusters.

We also found a similar result for the young object in NGC 4038/39 though the greater distance to the Antennae does not allow us to separate the populations as the physical resolution of our spectra is $\approx$ 90 pc. As discussed in Chapter 3, 30 Doradus shows a similar age spread as our target with the young R136 at the center of the star forming region and an old cluster Hodge 301 (20 - 25 Myr) (Grebel and Chu, 2000) within 45 pc. In NGC 4038/39, Christopher (2008) found approximately half of their sample of 100 clusters in the Antennae showed indication of multiple sources over spatial resolutions of 90 pc while Mengel et al. (2005) estimate that less than 5 % of their targets are superpositions of clusters. However Christopher (2008) also found clusters which show evidence of hydrogen emissions and CO bandheads but which are not resolved into multiple clusters based on HST imaging. They interpret this as indication that these clusters may be single objects which could have formed over a timescale of multiple Myr in a long duration burst.

Both these targets, though forming in a very different environment thus combine

an older and a younger star forming region in close proximity. What conclusions do these similarities allow us to draw? The age spread in both targets is the same though the ages of the older stellar components are not well constrained. While we do not know the exact spatial extent of the older cluster in NGC 4038/39 or the spatial separation of the two populations, our 1" (90 pc) resolution provides an upper limit. Given the high infant mortality of SSC it seems quite possible that this older population is similarly diffuse to that of NGC 253. Using our spectra we can estimate the spatial extent of the older background population to be $\approx$ 3" (60 pc) (though the background is not symmetric in both spectral directions). Thus the physical scales may actually be quite similar. We do not have an exact constraint on the mass of this population in NGC 253 but given the flux ratio between background population and young cluster it is likely that these populations are comparable in mass rather than the situation in NGC 4038/39 where the younger population dominates in mass by a factor of 10. It is tempting to try to look for an association between the two star forming events in both targets. The physical scales associated with the clusters in NGC 253 ($\approx$ 20 pc) and NGC 4038/39 ($\approx$ 90 pc) make triggering of the younger component by the older population feasible. Triggered star formation should proceed at roughly the sounds speed of an HII region ($\approx$ 10 km s^{-1}) which would imply a timescale of roughly 5 Myr to cover 50 pc. Thus a 90 pc box certainly makes a triggered event for the younger cluster a possibility and since the age of the older population is ill constrained in NGC 253 this is not ruled out.

Since mergers and nuclear starbursts are two of the most common formation scenarios for super-star clusters we may need to consider the possibility of multiple generations of star formation in close proximity whether due to multiple star clusters forming in distinct star forming events or due to star formation over long time scales in a single molecular cloud. Recently some globular clusters have also been found to contain multiple populations of main-sequence stars indicating that it is possible to create bound entities with wide age spreads (Portegies Zwart et al., 2010) though we have no indication that this is occuring in our NGC 253 source. Since our spectra are still not sensitive to scales finer than 10 pc an integral field unit spectrograph such as NIFS may be the perfect instrument to explore the complex star formation history of NGC 253 and NGC 4038/39 and other SSC in greater detail.

5.3 Future Directions

Apart from the two galaxies studied in this work there remain several interesting targets containing SSC that are accessible with current observational capabilities. Targets with metallicities different from solar as well as dwarf starbursts would be prime targets to investigate IMF variations. In particular the dwarf starburst NGC 5253 with subsolar metallicity which hosts two very young SSC in close spatial proximity (Tremonti et al., 2001) and which is at a distance similar to NGC 253 is an excellent target. We obtained near-infrared spectra of these young SSC with OSIRIS on SOAR and detected CO absorption in the spectra. The quality of the data was

not good enough for inclusion in this thesis. However there appears to be no contamination issues by red supergiants in this galaxy. Within a 10 Mpc volume there are several other starbursts with relatively well studied young SSC populations, such as He 2-10 and NGC 4449 which make worthwile targets. The most tantalizing target remains SBS 0335-052 because of its extremely low metallicity ($Z=Z_{\odot}/40$ (Izotov et al., 1990)) and high star formation rate. It contains several clusters younger than 3 Myr (Johnson et al., 2009) with masses of $\approx 10^6$ $M_{\odot}$. Its large distance of 55.7 Mpc (Hunt et al., 2005) makes observations of individual star clusters extremely challenging with current observational capabilities (0.1" = 27 pc). However future IFUs on the next generation of ground based AO enabled telescopes should be able to resolve individual star cluster spectra in this galaxy.

This thesis encountered two main limitations when trying to apply our models to real cluster data. Both of our targets had issues with background contamination and spatial resolution. This is likely to also plague any future investigations especially for more distant targets. There are a limited number of starburst galaxies with massive clusters and good radio observations available at distances where seeing limited observations can resolve small enough spatial scales that contamination of stellar populations can be minimized. Even for targets at a few Mpc spatial scales accessible with seeing limited observations of 0.5" scales correspond to tens of parsecs. SSC are generally measured to have radii of 3 -4 parsecs (Neff and Ulvestad, 2000). Thus even for nearby clusters AO observations are critical and for more distant objects

which may be interesting to investigate in the future such as He 2-10 (d = 9 Mpc; (Vacca and Conti, 1992)) they are essential to minimize background contamination. Using AO IFU spectrographs with a resolution of 0.1" or less would mean that we could have resolved the target in NGC 253 to a resolution of $\approx$ 2 pc and even the object in the Antennae to scales of less than 10 pc. The second limitation we face is a more fundamental one. Even spectra of a S/N of 120 can only resolve IMF slope differences of $\pm$ 0.25 dex in linear units. Any IMF variations smaller than this will not be discernible even under optimal conditions. It is possible that including a wider array of absorption lines (such as those present in the J-band) could improve this detection limit or increase the mass range traced by our methodology.

5.3.1 Near-IR Population Synthesis Modeling

Many challenges remain in trying to accurately model spectra of star clusters in the near-infrared in particular where clusters including red supergiants are involved. Model atmospheres of red supergiants remain uncertain and evolutionary tracks in this phase are also still subject to some refinement. For our technique in particular, as also discussed in more detail Chapter 2.5, we are limited by the accuracy of the PMS tracks we use as well as our spectral library which is comprised of solar metallicity main sequence stars as opposed to PMS stars which have lower gravity. It would be interesting to explore what effects incorporating other pre-main sequence tracks or model spectra for PMS stars would have on our model predictions. It may

also be worthwile to attempt to construct a stellar library of PMS stars which could produce model spectra with appropriate gravities.

Any photometric and spectroscopic studies of unresolved star clusters rely on the availability of accurate population synthesis models. At present many modeling suites exist (e.g. Bruzual and Charlot (2003); Vázquez and Leitherer (2005)) though these models in general do not incorporate high resolution near-infrared libraries. Efforts to accurately reproduce near-infrared high resolution spectra of star clusters remain challenging. Lançon et al. (2008) found that accurate age determination was difficult based on a sample of medium age star clusters in M82 and were only able to derive quite broad age ranges. However more study is required to see how accurately near-infrared population synthesis can constrain cluster properties such as age, mass or ionizing radiation. The launch of JWST will make it possible to conduct diffraction-limited spectroscopic surveys of a large population of star clusters in the near-infrared simultaneously. If accurate age determinations are possible with near-infrared population synthesis models, JWST as well as other future infrared instruments will enable determination of star formation histories in starburst galaxies in detail.

5.3.2 IMF studies

Despite the difficulty involved in measuring IMFs both in resolved clusters and unresolved star forming regions and galaxies and despite the scarcity of evidence for

variations uncovered thus far, the challenge remains worthwile. We have presented the first direct evidence of a normal low-mass IMF in unresolved super-star clusters in this work. However a larger sample is needed to support this result, especially in starburst galaxies which have been reported to have an unusual IMF in the past, such as M82.

It is also important to remember that we do not have as of yet direct data on stars below the breakpoint of the IMF in any SSC or even any massive star forming region in the Milky Way. Of particular interest remain clusters in the LMC and the SMC, due to their low metallicities, where the next generation of telescopes should be able to uncover stars down to a few tenths of $M_{\odot}$ (Bastian et al., 2010). There are compelling theoretical arguments that the location of the IMF break point as well as star counts above and below this breakpoint are the ideal location to search for IMF variations if different star formation regimes dominate above and below this mass. Measurements of an IMF comparable to the field below the breakpoint in these regions would be the strongest evidence yet for a universal IMF. The improvement of current observational capabilities and a new generation of telescopes will bring such surveys within our reach. The next generation of ground based telescopes as well as the launch of JWST will be invaluable in this respect. While the capabilities of JWST and telescopes such as the GMT will likely be comparable in the near-infrared, both being able to study massive star forming regions in the Milky Way down to the hydrogen burning limit, JWST will

far exceed any ground based capabilities in the mid and far-IR. In conjunction with such observatories as the Herschel Space Telescope it will thus make it possible to study the core mass function in more detail and trace star formation activity at the youngest ages out to further distances than presently possible. First results from Herschel are already showing a direct connection between the CMF and the IMF at much higher statistical significance than before (André et al., 2010).

The question about the IMF extrema: the maximum stellar mass as well as the minimum mass for gravitational fragmentation also remains. There is reason to believe that both the minimum (Whitworth et al., 2007) and maximum stellar mass (Zinnecker and Yorke, 2007) could be influenced by environmental conditions and could thus help understand star formation properties. New discoveries of very low-mass members of nearby star forming regions down to a few M_{Jup} (e.g. Lafrenière et al. (2008); Chauvin et al. (2004)) are pushing the boundaries on the minimum mass object formed through gravitational collapse though their number counts remain few. JWST should make it possible to conduct surveys down to a few M_{Jup} in nearby star forming regions helping us understand the frequency of such very low mass objects. The next generation of telescopes will help us study star clusters at an unprecedented level of detail beyond the Milky Way and in conjunction with robust statistical techniques help us measure the IMF over orders of magnitude in mass in a wide range of star forming environments.

5.4 Conclusions

We have demonstrated that is is possible to constrain the low-mass IMF in unresolved SSC with our technique. Our results add an important datapoint to a growing body of evidence towards a universal stellar IMF though more clusters with higher signal-to-noise spectra would narrow the range of IMF slopes allowed. However, we cannot detect variations in the slope smaller than $\pm$ 0.25 dex in linear units and contamination of populations containing red supergiants appears to be a serious issue. We also demonstrate the importance of studying SSC with detailed near-infrared spectroscopy to help understand their star formation histories which may be more complex than the single age starburst often assumed. Understanding how common bound clusters of multiple bursts of star formation are could be important in understanding star formation in giant molecular clouds as well as shedding insight on the formation of globular clusters with multiple age populations.

REFERENCES

Abel, T., G. L. Bryan, and M. L. Norman (2002). The Formation of the First Star in the Universe. *Science*, **295**, pp. 93–98. doi:10.1126/science.1063991.

Adams, F. C. and M. Fatuzzo (1996). A Theory of the Initial Mass Function for Star Formation in Molecular Clouds. *ApJ*, **464**, pp. 256–+. doi:10.1086/177318.

Alonso-Herrero, A., C. W. Engelbracht, M. J. Rieke, G. H. Rieke, and A. C. Quillen (2001). NGC 1614: A Laboratory for Starburst Evolution. *ApJ*, **546**, pp. 952–965. doi:10.1086/318282.

Alonso-Herrero, A., G. H. Rieke, M. J. Rieke, and D. M. Kelly (2003). The [Fe II] 1.644 Micron Emission in M82 and NGC 253: Is It a Measure of the Supernova Rate? *AJ*, **125**, pp. 1210–1225. doi:10.1086/367790.

Anders, P., N. Bissantz, U. Fritze-v. Alvensleben, and R. de Grijs (2004a). Analysing observed star cluster SEDs with evolutionary synthesis models: systematic uncertainties. *MNRAS*, **347**, pp. 196–212. doi:10.1111/j.1365-2966.2004.07197.x.

Anders, P., R. de Grijs, U. Fritze-v. Alvensleben, and N. Bissantz (2004b). Star cluster formation and evolution in the dwarf starburst galaxy NGC 1569. *MNRAS*, **347**, pp. 17–28. doi:10.1111/j.1365-2966.2004.07171.x.

Andersen, M., M. R. Meyer, J. Greissl, and A. Aversa (2008). Evidence for a Turnover in the Initial Mass Function of Low-Mass Stars and Substellar Objects: Analysis from an Ensemble of Young Clusters. *ApJ*, **683**, pp. L183–L186. doi:10.1086/591473.

Andersen, M., H. Zinnecker, A. Moneti, M. J. McCaughrean, B. Brandl, W. Brandner, G. Meylan, and D. Hunter (2009). The Low-Mass Initial Mass Function in the 30 Doradus Starburst Cluster. *ApJ*, **707**, pp. 1347–1360. doi:10.1088/0004-637X/707/2/1347.

Ando, M., T. Nagata, S. Sato, N. Mizuno, A. Mizuno, T. Kawai, H. Nakaya, and I. S. Glass (2002). Near-Infrared and CO (J=1-0) Observations of Photodissociation Regions in M17. *ApJ*, **574**, pp. 187–197. doi:10.1086/340922.

André, P., A. Men'shchikov, S. Bontemps, V. Könyves, F. Motte, N. Schneider, P. Didelon, V. Minier, P. Saraceno, D. Ward-Thompson, J. di Francesco, G. White, S. Molinari, L. Testi, A. Abergel, M. Griffin, T. Henning, P. Royer,

B. Merín, R. Vavrek, M. Attard, D. Arzoumanian, C. D. Wilson, P. Ade, H. Aussel, J. Baluteau, M. Benedettini, J. Bernard, J. A. D. L. Blommaert, L. Cambrésy, P. Cox, A. di Giorgio, P. Hargrave, M. Hennemann, M. Huang, J. Kirk, O. Krause, R. Launhardt, S. Leeks, J. Le Pennec, J. Z. Li, P. G. Martin, A. Maury, G. Olofsson, A. Omont, N. Peretto, S. Pezzuto, T. Prusti, H. Roussel, D. Russeil, M. Sauvage, B. Sibthorpe, A. Sicilia-Aguilar, L. Spinoglio, C. Waelkens, A. Woodcraft, and A. Zavagno (2010). From filamentary clouds to prestellar cores to the stellar IMF: Initial highlights from the Herschel Gould Belt Survey. *A&A*, **518**, pp. L102+. doi:10.1051/0004-6361/201014666.

Bastian, N. (2008). On the star formation rate - brightest cluster relation: estimating the peak star formation rate in post-merger galaxies. *MNRAS*, **390**, pp. 759–768. doi:10.1111/j.1365-2966.2008.13775.x.

Bastian, N., K. R. Covey, and M. R. Meyer (2010). A Universal Stellar Initial Mass Function? A Critical Look at Variations. *ArXiv e-prints*.

Bastian, N., M. Gieles, H. J. G. L. M. Lamers, R. A. Scheepmaker, and R. de Grijs (2005). The star cluster population of M 51. II. Age distribution and relations among the derived parameters. *A&A*, **431**, pp. 905–924. doi:10.1051/0004-6361:20041078.

Bastian, N., R. P. Saglia, P. Goudfrooij, M. Kissler-Patig, C. Maraston, F. Schweizer, and M. Zoccali (2006). Dynamical mass estimates for two luminous star clusters in galactic merger remnants. *A&A*, **448**, pp. 881–891. doi:10.1051/0004-6361:20054177.

Basu, S. and N. C. Rana (1992). Multiplicity-corrected mass function of main-sequence stars in the solar neighborhood. *ApJ*, **393**, pp. 373–384. doi:10.1086/171511.

Baumgardt, H., P. Kroupa, and G. Parmentier (2008). The influence of residual gas expulsion on the evolution of the Galactic globular cluster system and the origin of the Population II halo. *MNRAS*, **384**, pp. 1231–1241. doi:10.1111/j.1365-2966.2007.12811.x.

Blum, R. D. and P. J. McGregor (2008). The Ionizing Stars of the Galactic Ultra-Compact H II Region G45.45+0.06. *AJ*, **135**, pp. 1708–1717. doi:10.1088/0004-6256/135/5/1708.

Brandl, B. R., D. M. Clark, S. S. Eikenberry, J. C. Wilson, C. P. Henderson, D. J. Barry, J. R. Houck, J. C. Carson, and T. L. Hayward (2005). Deep Near-Infrared Imaging and Photometry of the Antennae Galaxies with WIRC. *ApJ*, **635**, pp. 280–289. doi:10.1086/497357.

Brandner, W., J. S. Clark, A. Stolte, R. Waters, I. Negueruela, and S. P. Goodwin (2008). Intermediate to low-mass stellar content of Westerlund 1. *A&A*, **478**, pp. 137–149. doi:10.1051/0004-6361:20077579.

Bressan, A., F. Fagotto, G. Bertelli, and C. Chiosi (1993). Evolutionary sequences of stellar models with new radiative opacities. II - Z = 0.02. *A&AS*, **100**, pp. 647–664.

Briceño, C., K. L. Luhman, L. Hartmann, J. R. Stauffer, and J. D. Kirkpatrick (2002). The Initial Mass Function in the Taurus Star-forming Region. *ApJ*, **580**, pp. 317–335. doi:10.1086/343127.

Brodie, J. P. and J. Strader (2006). Extragalactic Globular Clusters and Galaxy Formation. *ARA&A*, **44**, pp. 193–267. doi:10.1146/annurev.astro.44.051905.092441.

Bruzual, G. and S. Charlot (2003). Stellar population synthesis at the resolution of 2003. *MNRAS*, **344**, pp. 1000–1028. doi:10.1046/j.1365-8711.2003.06897.x.

Carpenter, J. M., M. R. Meyer, C. Dougados, S. E. Strom, and L. A. Hillenbrand (1997). Properties of the Monoceros R2 Stellar Cluster. *AJ*, **114**, pp. 198–221. doi:10.1086/118465.

Chabrier, G. (2003). Galactic Stellar and Substellar Initial Mass Function. *PASP*, **115**, pp. 763–795. doi:10.1086/376392.

Charbonnel, C., G. Meynet, A. Maeder, G. Schaller, and D. Schaerer (1993). Grids of Stellar Models - Part Three - from 0.8 to 120-SOLAR-MASSES at Z=0.004. *A&AS*, **101**, pp. 415–+.

Chauvin, G., A. Lagrange, C. Dumas, B. Zuckerman, D. Mouillet, I. Song, J. Beuzit, and P. Lowrance (2004). A giant planet candidate near a young brown dwarf. Direct VLT/NACO observations using IR wavefront sensing. *A&A*, **425**, pp. L29–L32. doi:10.1051/0004-6361:200400056.

Christopher, M. H. (2008). *Young, Massive Star Clusters in the Antennae*. Ph.D. thesis, California Institute of Technology, Pasadena, United States – California.

Condon, J. J. (1992). Radio emission from normal galaxies. *ARA&A*, **30**, pp. 575–611. doi:10.1146/annurev.aa.30.090192.003043.

Covey, K. R., S. L. Hawley, J. J. Bochanski, A. A. West, I. N. Reid, D. A. Golimowski, J. R. A. Davenport, T. Henry, A. Uomoto, and J. A. Holtzman (2008). The Luminosity and Mass Functions of Low-Mass Stars in the Galactic Disk. I. The Calibration Region. *AJ*, **136**, pp. 1778–1798. doi:10.1088/0004-6256/136/5/1778.

Doppmann, G. W., D. T. Jaffe, and R. J. White (2003). Stellar Properties of Pre-Main-Sequence Stars from High-Resolution Near-Infrared Spectra. *AJ*, **126**, pp. 3043–3057. doi:10.1086/378958.

Engelbracht, C. W., M. J. Rieke, G. H. Rieke, D. M. Kelly, and J. M. Achtermann (1998). The Nuclear Starburst in NGC 253. *ApJ*, **505**, pp. 639–658. doi:10.1086/306176.

Espinoza, P., F. J. Selman, and J. Melnick (2009). The massive star initial mass function of the Arches cluster. *A&A*, **501**, pp. 563–583. doi:10.1051/0004-6361/20078597.

Fagotto, F., A. Bressan, G. Bertelli, and C. Chiosi (1994a). Evolutionary sequences of stellar models with new radiative opacities. III. Z=0.0004 and Z=0.05. *A&AS*, **104**, pp. 365–376.

Fagotto, F., A. Bressan, G. Bertelli, and C. Chiosi (1994b). Evolutionary sequences of stellar models with new radiative opacities. IV. Z=0.004 and Z=0.008. *A&AS*, **105**, pp. 29–38.

Fall, S. M. (2006). Relations between the Luminosity, Mass, and Age Distributions of Young Star Clusters. *ApJ*, **652**, pp. 1129–1132. doi:10.1086/508404.

Fall, S. M. and Q. Zhang (2001). Dynamical Evolution of the Mass Function of Globular Star Clusters. *ApJ*, **561**, pp. 751–765. doi:10.1086/323358.

Ferland, G. J. (1980). Hydrogenic emission and recombination coefficients for a wide range of temperature and wavelength. *PASP*, **92**, pp. 596–602. doi:10.1086/130718.

Fernández-Ontiveros, J. A., M. A. Prieto, and J. A. Acosta-Pulido (2009). The nucleus of NGC 253 and its massive stellar clusters at parsec scales. *MNRAS*, **392**, pp. L16–L20. doi:10.1111/j.1745-3933.2008.00575.x.

Figer, D. F., S. S. Kim, M. Morris, E. Serabyn, R. M. Rich, and I. S. McLean (1999). Hubble Space Telescope/NICMOS Observations of Massive Stellar Clusters near the Galactic Center. *ApJ*, **525**, pp. 750–758. doi:10.1086/307937.

Forbes, D. A., E. Polehampton, I. R. Stevens, J. P. Brodie, and M. J. Ward (2000). A multiwavelength view at the heart of the superwind in NGC253. *MNRAS*, **312**, pp. 689–697. doi:10.1046/j.1365-8711.2000.03120.x.

Gallagher, J. S. and L. J. Smith (2004). Environments of Super Star Clusters. In H. J. G. L. M. Lamers, L. J. Smith, & A. Nota (ed.) *The Formation and Evolution of Massive Young Star Clusters*, volume 322 of *Astronomical Society of the Pacific Conference Series*, pp. 149–+.

Gilbert, A. M., J. R. Graham, I. S. McLean, E. E. Becklin, D. F. Figer, J. E. Larkin, N. A. Levenson, H. I. Teplitz, and M. K. Wilcox (2000). Infrared Spectroscopy of a Massive Obscured Star Cluster in the Antennae Galaxies (NGC 4038/9) with NIRSPEC. *ApJ*, **533**, pp. L57–L60. doi:10.1086/312599.

Girardi, L., A. Bressan, G. Bertelli, and C. Chiosi (2000). Evolutionary tracks and isochrones for low- and intermediate-mass stars: From 0.15 to 7 M_{sun}, and from Z=0.0004 to 0.03. *A&AS*, **141**, pp. 371–383. doi:10.1051/aas:2000126.

Goodwin, S. P. and N. Bastian (2006). Gas expulsion and the destruction of massive young clusters. *MNRAS*, **373**, pp. 752–758. doi:10.1111/j.1365-2966.2006.11078.x.

Goodwin, S. P., D. Nutter, P. Kroupa, D. Ward-Thompson, and A. P. Whitworth (2008). The relationship between the prestellar core mass function and the stellar initial mass function. *A&A*, **477**, pp. 823–827. doi:10.1051/0004-6361:20078452.

Gorlova, N. I., M. R. Meyer, G. H. Rieke, and J. Liebert (2003). Gravity Indicators in the Near-Infrared Spectra of Brown Dwarfs. *ApJ*, **593**, pp. 1074–1092. doi:10.1086/376730.

Goudfrooij, P., F. Schweizer, D. Gilmore, and B. C. Whitmore (2007). Dynamical Evolution of Globular Cluster Systems Formed in Galaxy Mergers: Deep Hubble Space Telescope Advanced Camera for Surveys Imaging of Old and Intermediate-Age Globular Clusters in NGC 3610. *AJ*, **133**, pp. 2737–2751. doi:10.1086/516634.

Grebel, E. K. and Y. Chu (2000). Hubble Space Telescope Photometry of Hodge 301: An "Old" Star Cluster in 30 Doradus. *AJ*, **119**, pp. 787–799. doi:10.1086/301218.

Greissl, J., M. R. Meyer, M. H. Christopher, and N. Z. Scoville (2010). Star Formation History of a Young Super-Star Cluster in NGC 4038/39: Direct Detection of Low-Mass Pre-Main Sequence Stars. *ApJ*, **710**, pp. 1746–1754. doi:10.1088/0004-637X/710/2/1746.

Harris, W. E. (1991). Globular cluster systems in galaxies beyond the Local Group. *ARA&A*, **29**, pp. 543–579. doi:10.1146/annurev.aa.29.090191.002551.

Hillenbrand, L. A. (1997). On the Stellar Population and Star-Forming History of the Orion Nebula Cluster. *AJ*, **113**, pp. 1733–1768. doi:10.1086/118389.

Hillenbrand, L. A., A. Bauermeister, and R. J. White (2008). An Assessment of HR Diagram Constraints on Ages and Age Spreads in Star-Forming Regions and Young Clusters. In G. van Belle (ed.) *14th Cambridge Workshop on Cool Stars, Stellar Systems, and the Sun*, volume 384 of *Astronomical Society of the Pacific Conference Series*, pp. 200–+.

Hillenbrand, L. A. and R. J. White (2004). An Assessment of Dynamical Mass Constraints on Pre-Main-Sequence Evolutionary Tracks. *ApJ*, **604**, pp. 741–757. doi:10.1086/382021.

Hunt, L., S. Bianchi, and R. Maiolino (2005). The optical-to-radio spectral energy distributions of low-metallicity blue compact dwarf galaxies. *A&A*, **434**, pp. 849–866. doi:10.1051/0004-6361:20042157.

Hunt, L. K., L. Vanzi, and T. X. Thuan (2001). The deeply embedded starburst in SBS 0335-052. *A&A*, **377**, pp. 66–72. doi:10.1051/0004-6361:20011088.

Hunter, D. A., E. J. Shaya, J. A. Holtzman, R. M. Light, E. J. O'Neil, Jr., and R. Lynds (1995). The Intermediate Stellar Mass Population in R136 Determined from Hubble Space Telescope Planetary Camera 2 Images. *ApJ*, **448**, pp. 179–+. doi:10.1086/175950.

Indebetouw, R., B. A. Whitney, K. E. Johnson, and K. Wood (2006). Three-dimensional Models of Embedded High-Mass Stars: Effects of a Clumpy Circumstellar Medium. *ApJ*, **636**, pp. 362–380. doi:10.1086/497886.

Ivanov, V. D., M. J. Rieke, C. W. Engelbracht, A. Alonso-Herrero, G. H. Rieke, and K. L. Luhman (2004). A Medium-Resolution Near-Infrared Spectral Library of Late-Type Stars. I. *ApJS*, **151**, pp. 387–397. doi:10.1086/381752.

Izotov, I. I., N. G. Guseva, V. A. Lipovetskii, A. I. Kniazev, and J. A. Stepanian (1990). Unusually low heavy-element abundance found in the blue compact dwarf galaxy SBS0335-052. *Nature*, **343**, pp. 238–240. doi:10.1038/343238a0.

Jappsen, A., R. S. Klessen, S. C. O. Glover, and M. Mac Low (2009). Star Formation at Very Low Metallicity. IV. Fragmentation does not Depend on Metallicity for Cold Initial Conditions. *ApJ*, **696**, pp. 1065–1074. doi:10.1088/0004-637X/696/2/1065.

Johnson, K. E. (2005). Probing the birth of super star clusters: Implications for massive star formation. In R. Cesaroni, M. Felli, E. Churchwell, & M. Walmsley (ed.) *Massive Star Birth: A Crossroads of Astrophysics*, volume 227 of *IAU Symposium*, pp. 413–422. doi:10.1017/S1743921305004825.

Johnson, K. E., L. K. Hunt, and A. E. Reines (2009). Probing Star Formation at Low Metallicity: The Radio Emission of Super Star Clusters in SBS 0335-052. *AJ*, **137**, pp. 3788–3799. doi:10.1088/0004-6256/137/4/3788.

Johnson, K. E., H. A. Kobulnicky, P. Massey, and P. S. Conti (2001). A Sample of Clusters of Extragalactic Ultracompact H II Regions. *ApJ*, **559**, pp. 864–877. doi:10.1086/322335.

Karachentsev, I. D., M. E. Sharina, A. E. Dolphin, and E. K. Grebel (2003). Distances to nearby galaxies around IC 342. *A&A*, **408**, pp. 111–118. doi: 10.1051/0004-6361:20030912.

Kennicutt, R. C., Jr. (1998). The Global Schmidt Law in Star-forming Galaxies. *ApJ*, **498**, pp. 541–+. doi:10.1086/305588.

Kenyon, S. J. and L. Hartmann (1995). Pre-Main-Sequence Evolution in the Taurus-Auriga Molecular Cloud. *ApJS*, **101**, pp. 117–+. doi:10.1086/192235.

Keto, E., J. L. Hora, G. G. Fazio, W. Hoffmann, and L. Deutsch (1999). A Super-Star Cluster in NGC 253: Mid-Infrared Properties. *ApJ*, **518**, pp. 183–189. doi: 10.1086/307246.

Kleinmann, S. G. and D. N. B. Hall (1986). Spectra of late-type standard stars in the region 2.0-2.5 microns. *ApJS*, **62**, pp. 501–517. doi:10.1086/191149.

Kornei, K. A. and N. McCrady (2009). A Young Super Star Cluster in the Nuclear Region of NGC 253. *ApJ*, **697**, pp. 1180–1186. doi:10.1088/0004-637X/697/2/1180.

Kreckel, H., H. Bruhns, M. Cizek, G. S. C. O., K. A. Miller, X. Urbain, and D. W. Savin (2010). Experimental Results for H2 Formation from H and H and Implications for First Star Formation. *Science*, **329**, pp. 69–71.

Kroupa, P. (2001). On the variation of the initial mass function. *MNRAS*, **322**, pp. 231–246. doi:10.1046/j.1365-8711.2001.04022.x.

Lafrenière, D., R. Jayawardhana, and M. H. van Kerkwijk (2008). Direct Imaging and Spectroscopy of a Planetary-Mass Candidate Companion to a Young Solar Analog. *ApJ*, **689**, pp. L153–L156. doi:10.1086/595870.

Lançon, A., J. S. Gallagher, III, M. Mouhcine, L. J. Smith, D. Ladjal, and R. de Grijs (2008). Near-infra-red spectroscopic ages of massive star clusters in M 82. *A&A*, **486**, pp. 165–176. doi:10.1051/0004-6361:200809439.

Lançon, A. and P. R. Wood (2000). A library of 0.5 to 2.5 mu m spectra of luminous cool stars. *A&AS*, **146**, pp. 217–249. doi:10.1051/aas:2000269.

Larsen, S. S. (2002). The Luminosity Function of Star Clusters in Spiral Galaxies. *AJ*, **124**, pp. 1393–1409. doi:10.1086/342381.

Larsen, S. S., J. P. Brodie, and D. A. Hunter (2004). Dynamical Mass Estimates for Five Young Massive Stellar Clusters. *AJ*, **128**, pp. 2295–2305. doi:10.1086/424538.

Larsen, S. S. and T. Richtler (2004). Dynamical mass estimates for two luminous young stellar clusters in ¡ASTROBJ¿Messier 83¡/ASTROBJ¿. *A&A*, **427**, pp. 495–504. doi:10.1051/0004-6361:20040547.

Larson, R. B. (2005). Thermal physics, cloud geometry and the stellar initial mass function. *MNRAS*, **359**, pp. 211–222. doi:10.1111/j.1365-2966.2005.08881.x.

Leitherer, C. (2001). Star Formation in Starbursts and Active Galactic Nuclei. In J. H. Knapen, J. E. Beckman, I. Shlosman, & T. J. Mahoney (ed.) *The Central Kiloparsec of Starbursts and AGN: The La Palma Connection*, volume 249 of *Astronomical Society of the Pacific Conference Series*, pp. 457–+.

Leitherer, C., D. Schaerer, J. D. Goldader, R. M. González Delgado, C. Robert, D. F. Kune, D. F. de Mello, D. Devost, and T. M. Heckman (1999). Starburst99: Synthesis Models for Galaxies with Active Star Formation. *ApJS*, **123**, pp. 3–40. doi:10.1086/313233.

Levesque, E. M. (2010). The Physical Properties of Red Supergiants. In C. Leither, P. Bennet, P. Morris, & J. van Loon (ed.) *Astronomical Society of the Pacific Conference Series*, volume 425 of *Astronomical Society of the Pacific Conference Series*, pp. 103–+.

Levesque, E. M., P. Massey, K. A. G. Olsen, B. Plez, E. Josselin, A. Maeder, and G. Meynet (2005). The Effective Temperature Scale of Galactic Red Supergiants: Cool, but Not As Cool As We Thought. *ApJ*, **628**, pp. 973–985. doi:10.1086/430901.

Luhman, K. L., P. R. Allen, C. Espaillat, L. Hartmann, and N. Calvet (2010). The Disk Population of the Taurus Star-Forming Region. *ApJS*, **186**, pp. 111–174. doi:10.1088/0067-0049/186/1/111.

Luhman, K. L., E. E. Mamajek, P. R. Allen, and K. L. Cruz (2009). An Infrared/X-Ray Survey for New Members of the Taurus Star-Forming Region. *ApJ*, **703**, pp. 399–419. doi:10.1088/0004-637X/703/1/399.

Luhman, K. L., G. H. Rieke, C. J. Lada, and E. A. Lada (1998). Low-Mass Star Formation and the Initial Mass Function in IC 348. *ApJ*, **508**, pp. 347–369. doi:10.1086/306393.

Mac Low, M. and R. S. Klessen (2004). Control of star formation by supersonic turbulence. *Reviews of Modern Physics*, **76**, pp. 125–194. doi:10.1103/RevModPhys.76.125.

Massey, P. and D. A. Hunter (1998). Star Formation in R136: A Cluster of O3 Stars Revealed by Hubble Space Telescope Spectroscopy. *ApJ*, **493**, pp. 180–+. doi:10.1086/305126.

McCrady, N., J. R. Graham, and W. D. Vacca (2005). Mass Segregation and the Initial Mass Function of Super Star Cluster M82-F. *ApJ*, **621**, pp. 278–284. doi: 10.1086/427487.

McCrady, N. T. (2005). *The super star cluster population of the M82 nuclear starburst*. Ph.D. thesis, University of California, Berkeley, United States – California.

McLean, I. S., E. E. Becklin, O. Bendiksen, G. Brims, J. Canfield, D. F. Figer, J. R. Graham, J. Hare, F. Lacayanga, J. E. Larkin, S. B. Larson, N. Levenson, N. Magnone, H. Teplitz, and W. Wong (1998). Design and development of NIRSPEC: a near-infrared echelle spectrograph for the Keck II telescope. In A. M. Fowler (ed.) *Society of Photo-Optical Instrumentation Engineers (SPIE) Conference Series*, volume 3354 of *Society of Photo-Optical Instrumentation Engineers (SPIE) Conference Series*, pp. 566–578.

Melo, V. P., C. Muñoz-Tuñón, J. Maíz-Apellániz, and G. Tenorio-Tagle (2005). Young Super Star Clusters in the Starburst of M82: The Catalog. *ApJ*, **619**, pp. 270–290. doi:10.1086/426421.

Mengel, S., M. D. Lehnert, N. Thatte, and R. Genzel (2002). Dynamical masses of young star clusters in NGC 4038/4039. *A&A*, **383**, pp. 137–152. doi:10.1051/0004-6361:20011704.

Mengel, S., M. D. Lehnert, N. Thatte, and R. Genzel (2005). Star-formation in NGC 4038/4039 from broad and narrow band photometry: cluster destruction? *A&A*, **443**, pp. 41–60. doi:10.1051/0004-6361:20052908.

Mengel, S., M. D. Lehnert, N. Thatte, L. E. Tacconi-Garman, and R. Genzel (2001). K-Band Spectroscopy of Compact Star Clusters in NGC 4038/4039. *ApJ*, **550**, pp. 280–286. doi:10.1086/319704.

Meyer, M. R., F. C. Adams, L. A. Hillenbrand, J. M. Carpenter, and R. B. Larson (2000). The Stellar Initial Mass Function: Constraints from Young Clusters, and Theoretical Perspectives. *Protostars and Planets IV*, pp. 121–+.

Meyer, M. R., S. Edwards, K. H. Hinkle, and S. E. Strom (1998). Near-Infrared Classification Spectroscopy: H-Band Spectra of Fundamental MK Standards. *ApJ*, **508**, pp. 397–409. doi:10.1086/306402.

Meyer, M. R. and J. Greissl (2005). Constraining the Initial Mass Function in Extreme Environments: Detecting Young Low-Mass Stars in Unresolved Starbursts. *ApJ*, **630**, pp. L177–L180. doi:10.1086/491647.

Meynet, G., A. Maeder, G. Schaller, D. Schaerer, and C. Charbonnel (1994). Grids of massive stars with high mass loss rates. V. From 12 to 120 M_{sun} at Z=0.001, 0.004, 0.008, 0.020 and 0.040. *A&AS*, **103**, pp. 97–105.

Miller, G. E. and J. M. Scalo (1979). The initial mass function and stellar birthrate in the solar neighborhood. *ApJS*, **41**, pp. 513–547. doi:10.1086/190629.

Milosavljevic, M. and M. Agarwal (2009). Nuclear Star Clusters in Spheroidal and Late-Type Disk Galaxies. In S. Jogee, I. Marinova, L. Hao, & G. A. Blanc (ed.) *Astronomical Society of the Pacific Conference Series*, volume 419 of *Astronomical Society of the Pacific Conference Series*, pp. 46–+.

Mirabel, I. F., L. Vigroux, V. Charmandaris, M. Sauvage, P. Gallais, D. Tran, C. Cesarsky, S. C. Madden, and P. Duc (1998). The dark side of star formation in the Antennae galaxies. *A&A*, **333**, pp. L1–L4.

Moraux, E., J. Bouvier, J. R. Stauffer, and J. Cuillandre (2003). Brown dwarfs in the Pleiades cluster: Clues to the substellar mass function. *A&A*, **400**, pp. 891–902. doi:10.1051/0004-6361:20021903.

Müller-Sánchez, F., O. González-Martín, J. A. Fernández-Ontiveros, J. A. Acosta-Pulido, and M. A. Prieto (2010). The Stellar Kinematic Center and the True Galactic Nucleus of NGC 253. *ApJ*, **716**, pp. 1166–1177. doi:10.1088/0004-637X/716/2/1166.

Neff, S. G. and J. S. Ulvestad (2000). VLA Observations of the Nearby Merger NGC 4038/4039: H II Regions and Supernova Remnants in the "Antennae". *AJ*, **120**, pp. 670–696. doi:10.1086/301503.

Omukai, K., T. Tsuribe, R. Schneider, and A. Ferrara (2005). Thermal and Fragmentation Properties of Star-forming Clouds in Low-Metallicity Environments. *ApJ*, **626**, pp. 627–643. doi:10.1086/429955.

Portegies Zwart, S., S. McMillan, and M. Gieles (2010). Young massive star clusters. *ArXiv e-prints*.

Rebull, L. M., D. L. Padgett, C. McCabe, L. A. Hillenbrand, K. R. Stapelfeldt, A. Noriega-Crespo, S. J. Carey, T. Brooke, T. Huard, S. Terebey, M. Audard, J. Monin, M. Fukagawa, M. Güdel, G. R. Knapp, F. Menard, L. E. Allen, J. R. Angione, C. Baldovin-Saavedra, J. Bouvier, K. Briggs, C. Dougados, N. J. Evans, N. Flagey, S. Guieu, N. Grosso, A. M. Glauser, P. Harvey, D. Hines, W. B. Latter, S. L. Skinner, S. Strom, J. Tromp, and S. Wolf (2010). The Taurus Spitzer Survey: New Candidate Taurus Members Selected Using Sensitive Mid-Infrared Photometry. *ApJS*, **186**, pp. 259–307. doi:10.1088/0067-0049/186/2/259.

Rieke, G. H., K. Loken, M. J. Rieke, and P. Tamblyn (1993). Starburst modeling of M82 - Test case for a biased initial mass function. *ApJ*, **412**, pp. 99–110. doi:10.1086/172904.

Salpeter, E. E. (1955). The Luminosity Function and Stellar Evolution. *ApJ*, **121**, pp. 161–+. doi:10.1086/145971.

Satyapal, S., D. M. Watson, J. L. Pipher, W. J. Forrest, M. A. Greenhouse, H. A. Smith, J. Fischer, and C. E. Woodward (1997). The Intrinsic Properties of the Stellar Clusters in the M82 Starburst Complex: Propagating Star Formation? *ApJ*, **483**, pp. 148–+. doi:10.1086/304214.

Schaerer, D., C. Charbonnel, G. Meynet, A. Maeder, and G. Schaller (1993a). Grids of Stellar Models - Part Four - from 0.8-SOLAR-MASS to 120-SOLAR-MASSES at Z=0.040. *A&AS*, **102**, pp. 339–+.

Schaerer, D., G. Meynet, A. Maeder, and G. Schaller (1993b). Grids of stellar models. II - From 0.8 to 120 solar masses at Z = 0.008. *A&AS*, **98**, pp. 523–527.

Schaller, G., D. Schaerer, G. Meynet, and A. Maeder (1992). New grids of stellar models from 0.8 to 120 solar masses at Z = 0.020 and Z = 0.001. *A&AS*, **96**, pp. 269–331.

Seth, A. C., R. D. Blum, N. Bastian, N. Caldwell, and V. P. Debattista (2008). The Rotating Nuclear Star Cluster in NGC 4244. *ApJ*, **687**, pp. 997–1003. doi:10.1086/591935.

Shu, F. H., Z. Li, and A. Allen (2004). Does Magnetic Levitation or Suspension Define the Masses of Forming Stars? *ApJ*, **601**, pp. 930–951. doi:10.1086/380602.

Siess, L., E. Dufour, and M. Forestini (2000). An internet server for pre-main sequence tracks of low- and intermediate-mass stars. *A&A*, **358**, pp. 593–599.

Sirianni, M., A. Nota, C. Leitherer, G. De Marchi, and M. Clampin (2000). The Low End of the Initial Mass Function in Young Large Magellanic Cloud Clusters. I. The Case of R136. *ApJ*, **533**, pp. 203–214. doi:10.1086/308628.

Smith, L. J. and J. S. Gallagher (2001). M82-F: a doomed super star cluster? *MNRAS*, **326**, pp. 1027–1040. doi:10.1046/j.1365-8711.2001.04627.x.

Smith, V. V. (1999). Stellar Metallicities in the Megellanic Clouds. In Y.-H. Chu, N. Suntzeff, J. Hesser, & D. Bohlender (ed.) *New Views of the Magellanic Clouds*, volume 190 of *IAU Symposium*, pp. 259–+.

Snijders, L., P. P. van der Werf, B. R. Brandl, S. Mengel, D. Schaerer, and Z. Wang (2006). Subarcsecond Resolution Mid-Infrared Observations of Super Star Clusters in the Antennae (NGC 4038/4039). *ApJ*, **648**, pp. L25–L28. doi:10.1086/507424.

Steidel, C. C., M. Giavalisco, M. Dickinson, and K. L. Adelberger (1996). Spectroscopy of Lyman Break Galaxies in the Hubble Deep Field. *AJ*, **112**, pp. 352–+. doi:10.1086/118019.

Thompson, R. I., M. Sauvage, R. C. Kennicutt, Jr., C. W. Engelbracht, and L. Vanzi (2006). Delayed Photoionization Feedback in a Super Star Cluster in SBS 0335-052E. *ApJ*, **638**, pp. 176–182. doi:10.1086/498743.

Toomre, A. (1977). Mergers and Some Consequences. In B. M. Tinsley & R. B. Larson (ed.) *Evolution of Galaxies and Stellar Populations*, pp. 401–+.

Tremaine, S. D., J. P. Ostriker, and L. Spitzer, Jr. (1975). The formation of the nuclei of galaxies. I - M31. *ApJ*, **196**, pp. 407–411. doi:10.1086/153422.

Tremonti, C. A., D. Calzetti, C. Leitherer, and T. M. Heckman (2001). Star Formation in the Field and Clusters of NGC 5253. *ApJ*, **555**, pp. 322–337. doi:10.1086/321436.

Tumlinson, J. (2006). Chemical Evolution in Hierarchical Models of Cosmic Structure. I. Constraints on the Early Stellar Initial Mass Function. *ApJ*, **641**, pp. 1–20. doi:10.1086/500383.

Tumlinson, J. (2007). Carbon-enhanced Hyper-Metal-poor Stars and the Stellar IMF at Low Metallicity. *ApJ*, **665**, pp. 1361–1370. doi:10.1086/519917.

Tumlinson, J., A. Venkatesan, and J. M. Shull (2004). Nucleosynthesis, Reionization, and the Mass Function of the First Stars. *ApJ*, **612**, pp. 602–614. doi:10.1086/422571.

Vacca, W. D. and P. S. Conti (1992). Optical spectrophotometry of Wolf-Rayet galaxies. *ApJ*, **401**, pp. 543–558. doi:10.1086/172085.

Vacca, W. D., M. C. Cushing, and J. T. Rayner (2003). A Method of Correcting Near-Infrared Spectra for Telluric Absorption. *PASP*, **115**, pp. 389–409. doi:10.1086/346193.

van Dokkum, P. and C. Conroy (2010). A Substantial Population of Low Mass Stars in Luminous Elliptical Galaxies. *ArXiv e-prints*.

Vázquez, G. A. and C. Leitherer (2005). Optimization of Starburst99 for Intermediate-Age and Old Stellar Populations. *ApJ*, **621**, pp. 695–717. doi:10.1086/427866.

Vesperini, E. and S. E. Zepf (2003). Effects of the Dissolution of Low-Concentration Globular Clusters on the Evolution of Globular Cluster Systems. *ApJ*, **587**, pp. L97–L100. doi:10.1086/375313.

Walcher, C. J., T. Böker, S. Charlot, L. C. Ho, H. Rix, J. Rossa, J. C. Shields, and R. P. van der Marel (2006). Stellar Populations in the Nuclei of Late-Type Spiral Galaxies. *ApJ*, **649**, pp. 692–708. doi:10.1086/505166.

Wallace, L. and K. Hinkle (1997). Medium-Resolution Spectra of Normal Stars in the K Band. *ApJS*, **111**, pp. 445–+. doi:10.1086/313020.

Wallace, L., M. R. Meyer, K. Hinkle, and S. Edwards (2000). Near-Infrared Classification Spectroscopy: J-Band Spectra of Fundamental MK Standards. *ApJ*, **535**, pp. 325–337. doi:10.1086/308835.

Wang, Z., G. G. Fazio, M. L. N. Ashby, J. Huang, M. A. Pahre, H. A. Smith, S. P. Willner, W. J. Forrest, J. L. Pipher, and J. A. Surace (2004). The Off-Nuclear Starbursts in NGC 4038/4039 (The Antennae Galaxies). *ApJS*, **154**, pp. 193–198. doi:10.1086/423205.

Whitmore, B. C. and F. Schweizer (1995). Hubble space telescope observations of young star clusters in NGC-4038/4039, 'the antennae' galaxies. *AJ*, **109**, pp. 960–980. doi:10.1086/117334.

Whitmore, B. C., Q. Zhang, C. Leitherer, S. M. Fall, F. Schweizer, and B. W. Miller (1999). The Luminosity Function of Young Star Clusters in "the Antennae" Galaxies (NGC 4038-4039). *AJ*, **118**, pp. 1551–1576. doi:10.1086/301041.

Whitworth, A., M. R. Bate, Å. Nordlund, B. Reipurth, and H. Zinnecker (2007). The Formation of Brown Dwarfs: Theory. *Protostars and Planets V*, pp. 459–476.

Zepf, S. E., K. M. Ashman, J. English, K. C. Freeman, and R. M. Sharples (1999). The Formation and Evolution of Candidate Young Globular Clusters in NGC 3256. *AJ*, **118**, pp. 752–764. doi:10.1086/300961.

Zhang, Q., S. M. Fall, and B. C. Whitmore (2001). A Multiwavelength Study of the Young Star Clusters and Interstellar Medium in the Antennae Galaxies. *ApJ*, **561**, pp. 727–750. doi:10.1086/322278.

Zinnecker, H. and H. W. Yorke (2007). Toward Understanding Massive Star Formation. *ARA&A*, **45**, pp. 481–563. doi:10.1146/annurev.astro.44.051905.092549.